

Computational Analysis of Critical Gusset Plate Connections in Steel Bridges

by
Francisco Del Valle-Roldán

A thesis submitted in partial fulfillment of the requirements for the degree of
MASTER OF SCIENCE
in
CIVIL ENGINEERING

UNIVERSITY OF PUERTO RICO
MAYAGÜEZ CAMPUS
2012

Approved by:

Luis E. Suarez, Ph.D.
Member, Graduate Committee

Date

Daniel Wendichansky, Ph.D.
Member, Graduate Committee

Date

Genock Portela, Ph.D.
President, Graduate Committee

Date

Edgardo Lorenzo, Ph.D.
Representative of Graduate Studies

Date

Ismael Pagán Trinidad, MSCE.
Chairperson of the Department

Date

ABSTRACT

An existing steel truss bridge located in Missouri was selected to determine the critical connections based on the loads criteria established in the Manual for Bridge Evaluation. The selected connections were typically used in steel truss bridges. A Finite Element Analysis (FEA) of critical connections was performed in order to: i) study the stress distribution in the elements, rivets, and gusset plates, ii) compare Finite Element Model (FEM) techniques used to study steel gusset plates, iii) study the Load Rating results in gusset plates based on the Federal Highway Administration (FHWA) Load Rating Guidance for Truss Bridges, iv) validate the methods used for tension capacity in gusset plates, v) study the corrosion effects and loss of rivets, vi) study the effect of thickness reductions and increments of unbraced length in the gusset plates buckling capacity, and vii) compare the methods used to determine the buckling capacity and the FEA results. Results demonstrated that the simplified FEM using the fastener technique in Abaqus to simulate rivets provides comparable results with the 3-D deformable solid rivets. However, it cannot be used to study in detail the stress concentration generated around the rivet holes and the rivets. The stresses generated due to tension loads in the FEA are in accordance with the equations used to determine the tension capacity. A 6 % of rivet diameter loss due to corrosion effects generated a reduction strength capacity of approximately 7%. Otherwise, the instability study demonstrated that for a thickness reduction of 15 % of its original thickness and an increment of 30 % of its unbraced length, the gusset plate have a structural reduction capacity of 20% and 6%, respectively. Finally, according to the FEA, results showed that the Thornton method used in the FHWA guidance leads to highly conservative results. The Yoo method is in very close agreement to the FEA, and this study recommends its use instead of Thornton method.

RESUMEN

Un puente existente localizado en Missouri fue seleccionado en esta investigación en donde se seleccionaron las conexiones críticas basado en el Manual de Evaluación de Puentes MBE. Las configuraciones de las conexiones críticas seleccionadas en este estudio son comunes en los puentes de acero. Un análisis de elementos finitos (FEA, por sus siglas en inglés) de las conexiones críticas fue desarrollado para: i) estudiar la distribución de esfuerzos en los elementos, remaches y placas de refuerzo, ii) comparar los resultados generados por un modelo de elementos finitos (FEM, por sus siglas en inglés) bien detallado y uno simplificado que se usa comúnmente en las investigaciones, iii) estudiar los resultados de “Load Rating” en las placas de refuerzo basado en la guía para determinar el “Load Rating” de placas de refuerzo desarrollado por la Administración Federal de Carreteras (FHWA, por sus siglas en inglés) iv) validar los métodos utilizados para determinar la capacidad en tensión de las placas de refuerzo, v) estudiar los efectos de corrosión y el efecto de pérdida de remaches en la conexión, vi) estudiar el efecto en capacidad de pandeo ocasionado por la reducción de espesor de las placas debido a corrosión y el incremento en el largo sin confinar y vii) comparar los métodos usados para determinar capacidad de pandeo con los resultados obtenidos de los modelos de elementos finitos. Los resultados de esta investigación demuestran que los modelos de elementos finitos simplificados (FEM) usando la técnica de “fastener” disponible en el programa Abaqus para simular remaches y tornillos presenta resultados similares al modelo detallado el cual tiene los pernos como sólidos deformables en tres dimensiones. Por otro lado, el modelo simplificado no puede ser utilizado para estudiar en detalle las concentraciones de esfuerzos generadas en los huecos de los remaches ni en los pernos. Los esfuerzos generados por cargas en tensión presentan una buena correlación con las ecuaciones usadas para determinar la capacidad en tensión. La pérdida de 6%

de diámetro de los tornillos como consecuencia del efecto de corrosión ocasiona una reducción en capacidad de aproximadamente 7%. Por otro lado, la inestabilidad de las placas de refuerzo es otro factor importante y los resultados demuestran que una reducción en espesor de 15% y un incremento de hasta 30% del largo sin confinar podría generar una reducción de su capacidad estructural de 20% y 6% respectivamente. Finalmente, los resultados del análisis de elementos finitos demuestran que el método de Thornton usado en la guía de FHWA presenta resultados muy conservadores. El método de Yoo presenta resultados similares al del análisis de elementos finitos por lo que este estudio sugiere su uso en vez del método de Thornton.

© Francisco Del Valle-Roldán 2012

DEDICATION

I want to dedicate the effort of this project to my family, especially my mother and my father since without them, I could not have the most precious gift that they can give me, that is life. They are my inspiration to succeed, to improve each day and to make the best of me in every aspect of my life.

ACKNOWLEDGEMENT

I want to say thanks first to God for blessing me during my life. He is with me every time, every moment. Thanks to my family for giving me the support during all my steps in life. My mother was the last month of this journey with me, cooked me every lunch and dinner, and watching me while I was hours in front of my computer working hard. Thanks to my friends, for giving me support and motivation during my graduate studies.

My special thanks to my advisor Dr. Genock Portela, for giving me the opportunity to work with him, trust in me, and helping me in the completion of this thesis. Thanks to my graduate committee Dr. Luis E. Suarez and Dr. Daniel Wendichansky. Thanks to all the professors of the Jose Rosario and Maria Cruz Buitrago schools and the University of Puerto Rico at Mayaguez for teaching and bringing me one the most important tools that a human could have: knowledge. Finally, thanks to Gerardo Velazquez, Edgardo Ruiz, and the U.S. Army Engineer Research and Development Center in Vicksburg, Mississippi for gave me the tools, the support, and guidelines to perform this thesis.

TABLE OF CONTENTS

Abstract	ii
Resumen	iii
Dedication	vi
Acknowledgement	vii
Table of Contents	viii
List of Figures	xi
List of Tables	xv
Chapter 1	1
1. Introduction	1
1.1. General Background	1
1.2. Scope of the Research.....	2
1.3. Objectives	3
1.4. Methodology	4
1.5 Contents of this Thesis.....	6
Chapter 2	7
2. Literature Review	7
2.1. Previous Research on Structural Performance of Gusset Plate Connections.....	7
2.1.1. Early Studies	7
2.1.2. Recent Studies.....	12
2.2. Bridge Cases Studies.....	13
2.2.1. Silver Bridge, 1967 (Report NTSB 1971).....	14
2.2.2. Suspended Span Bridge, 1983 (Report NTSB 1984).....	15
2.2.3. Highway Bridge on the I-35W, 2007 (Report NSTB 2008)	16
2.3. Finite Element Method.....	17
2.3.1. General Static Analysis.....	17
2.3.2. Eigenvalue Buckling Analysis	19
2.3.3. Riks Analysis	20

2.4.	Load Rating Guidance for Riveted Gusset Plates in Truss Bridges.....	23
Chapter 3	27
3.	Computational Model of the Bridge.....	27
3.1.	Target Bridge Description.....	27
3.1.1.	Bridge Material Properties.....	30
3.1.2.	Bridge Section Properties and Dimensions.....	31
3.2.	Bridge Model Description.....	36
3.2.1.	Loads Considered in the Analysis.....	37
Chapter 4	41
4.	Localized FEA of Critical Connections.....	41
4.1.	Critical Connections Selection.....	41
4.2.	Finite Element Model Description.....	41
4.3.	Loading, Boundary Conditions, and Material Properties.....	45
4.4.	Mesh Refinement.....	47
4.4.1.	Mesh Refinement Across Gusset Plate Thickness.....	47
4.4.2.	Mesh Refinement Throughout X-Y Plane.....	48
Chapter 5	52
5.	Analysis and Results.....	52
5.1.	Introduction.....	52
5.2.	Computational Study of the Target Bridge.....	53
5.3.	Deterministic Load-Induced Fatigue Analysis.....	57
5.4.	Modeling Techniques.....	59
5.4.1.	3-D Deformable Contact Rivet Technique.....	59
5.4.2.	Fastener Technique.....	60
5.4.3.	Comparison of Model Techniques.....	60
5.5.	FEA of Critical Connection J-6.....	68
5.6.	Nonlinear Tensile Analysis.....	75
5.7.	Rivet Analysis.....	78
5.7.1.	Rivets Diameter Loss due to Corrosion Effect.....	78
5.7.2.	Loss of Rivets.....	86
5.8.	Nonlinear Buckling Analysis.....	89

5.8.1. Thickness Variation	92
5.8.2. Unbraced Length Variation.....	100
Chapter 6	108
6. Conclusion and Recommendations.....	108
6.1. Summary	108
6.2. Conclusions.....	108
6.3. Recommendations.....	110
References.....	111
Appendix A. Load Rating of Critical Gusset Plates.....	114
Appendix B. Hand Calculations Examples for the Three Methods used to Determine Buckling Capacity of Gusset Plate Connections.....	137

LIST OF FIGURES

Figure 1: Whitmore Effective Width.	8
Figure 2: Three Methods Established to Predict Buckling Capacity: a) Thornton Method, b) Modified Thornton Method, and c) Yoo Method.	11
Figure 3: Silver Bridge Collapse (The Herald-Dispatch)	14
Figure 4: Mianus River Bridge Collapse (http://35wbridge.pbworks.com/w/page/900718/Mianus%20River%20Bridge%20Collapse)	15
Figure 5: I-35 Bridge Collapse (http://www.ptank.com/blog/2007/08/i-35w-bridge-collapse-in-minneapolis/).....	16
Figure 6: Target Bridge.....	28
Figure 7: Top View of the Bridge.....	28
Figure 8: Plan View of Steel Truss Bridge Span.	29
Figure 9: Cross Section of the R.C. slab.	29
Figure 10: Components of Truss Sections: a) Elements, b) Joints.	33
Figure 11: Floor Components: a) Elements, b) Joints.....	34
Figure 12: Global Model: a) Steel Floor Elements, b) Concrete Decks.	36
Figure 13: Dimensions of Concrete Barriers and Railing.....	39
Figure 14: Design Truck HS-44. Obtained from LRFD 3.6.1.2.2	39
Figure 15: LRFD Tandem Loading. Obtained from Varela (2006).....	40
Figure 16: LRFD Lane Loading.....	40
Figure 17: General J-6 Connection Model.....	43
Figure 18: Kinematic Coupling Constrain Between Solid and Beam Elements.....	44
Figure 19: Rivets Interacting with the Perimeter of Rivet Holes.....	44
Figure 20: Forces Direction for Each Member.	46
Figure 21: Steel True Stress-Strain Curve (Non-linear Regime)	46
Figure 22: Three different through the thickness elements quantities: a) two elements, b) three elements, and c) five elements.	48

Figure 23: Points selected in the gusset plate.	49
Figure 24: Three different mesh refinement, a) 20,847 elements, b) 56,601 elements, c) 81,480 elements, d) 100,200 elements.	49
Figure 25: Final FE model.	51
Figure 26: Bridge Posting Sign.	54
Figure 27 : Two modeling techniques: a) 3-D Deformable Rivets and b) Fastener Rivets.	62
Figure 28: Von Mises Stress Distribution of the two Techniques (ksi): a) 3-D Deformable Rivets and b) Fastener Rivets.	63
Figure 29: Von Mises Stress Distribution for the Gusset Plates (ksi): a) 3-D Deformable Rivets and b) Fastener Rivets.	64
Figure 30: 3-D View and Mesh Illustration of both techniques: a) 3-D Fastener b) 3-D Rivets.	65
Figure 31: Shear Stress Distribution Comparison (ksi): a) Fastener and b) 3-D Rivets.	66
Figure 32: Diagonal D-9 Local Stress Distribution (ksi): a) 3-D Rivet and b) Fasteners.	67
Figure 33. General von Mises stress (ksi) distribution in Connection J-6.	70
Figure 34. Von Mises stress (ksi) distribution of elements.	70
Figure 35: Von Mises stress and Equivalent Plastic Strain (PEEQ) distribution for the Rivet Hole.	71
Figure 36. Von Mises stress (ksi) distribution of gusset plates in Connection J-6.	72
Figure 37. Shear stress (ksi) distribution of gusset plates in Connection J-6.	73
Figure 38. Von Mises stress (ksi) of rivets in Connection J-6.	73
Figure 39. Von Mises and shear stress (ksi) distribution in the critical rivet (Connection J-6).	74
Figure 40: Gusset Plate of Connection J-6.	76
Figure 41: Maximum Principal Stress Distribution in the Element D-13 Region.	77
Figure 42: Local Stress Distribution in the Element D-13 Region.	77
Figure 43: General FE model for Connection J-2.	81
Figure 44: von Mises Stress Distribution (ksi) for: a) no reduction in diameter and b) 6% reduction in diameter.	82
Figure 45: Shear Stress Distribution (ksi) for: a) no reduction in diameter and b) 6% reduction in diameter.	83

Figure 46. Shear stress, von Mises Stress and FHWA Shear Rivet Equation Percentage Difference Results due to a Rivet Diameter Reduction.	84
Figure 47: Shear Stress vs. % Rivet Diameter Reduction.....	85
Figure 48: Connection J-2.....	87
Figure 49: Sub-model of Connection J-2.....	87
Figure 50: Shear Stress Variation for Case a.	88
Figure 51: Shear Stress Variation for Case b.	88
Figure 52: General FEM of Connection J-6.....	90
Figure 53: Sub-model of Connection J-6.....	91
Figure 54: Mesh Representation for J-6 FE Sub-model.....	91
Figure 55: Buckling Mode for Thickness Case1.....	94
Figure 56: Load-Displacement Curve for Thickness Case 1.	94
Figure 57: Buckling Mode for Thickness Case2.....	95
Figure 58: Load-Displacement Curve for Thickness Case 2.	95
Figure 59: Buckling Mode for Thickness Case3.....	96
Figure 60: Load-Displacement Curve for Thickness Case 3.	96
Figure 61: Buckling Mode for Thickness Case 4.....	97
Figure 62: Load-Displacement Curve for Thickness Case 4.	97
Figure 63: Load-Displacement for the four Thickness Cases.....	98
Figure 64: Maximum Load for each Case number.	99
Figure 65: Unbraced length and length increment location for the J-6 Sub-Model.....	101
Figure 66: Buckling Mode for Unbraced Case 1.	102
Figure 67: Load-Displacement Curve for Unbraced Case 1.....	102
Figure 68: Buckling Mode for Unbraced Case 2.	103
Figure 69: Load-Displacement Curve for Unbraced Case 2.....	103
Figure 70: Buckling Mode for Unbraced Case 3.	104
Figure 71: Load-Displacement Curve for Unbraced Case 3.....	104

Figure 72: Buckling Mode for Thickness Case 4.....	105
Figure 73: Load-Displacement Curve for Unbraced Case 4.....	105
Figure 74: Load-Displacement for the four Unbraced Cases.....	106
Figure 75: Maximum Load vs Length Increment.	107

LIST OF TABLES

Table 1: K Values FHWA (2009).....	26
Table 2: General Bridge Data.	30
Table 3: Bridge Material Properties.....	31
Table 4: Element Dimensions.	35
Table 5: Elements Sections Properties.....	35
Table 6: Percentage Differences between Elements across the Thickness.	48
Table 7: Stresses results for the different models.	50
Table 8: Stress percentage differences between models.	50
Table 9: Envelope forces for HS20-44 loading.....	54
Table 10: Envelope forces for MLC-8 loading.	55
Table 11: Envelope forces for half-scaled Type 3 (12.5 Tons) legal notional truck.....	55
Table 12: Envelope forces for half-scaled Type 3S2 (18 Tons) legal notional truck.	56
Table 13: Envelope forces for half-scaled Type 3-3 (20 Tons) legal notional truck.	56
Table 14. Fatigue check criteria to determine possible fatigue conditions.	58
Table 15: Factored Redistribution Load.	69
Table 16: Load Rating Results for Connections J-6 and J-2.....	74
Table 17: Shear Stress Reduction.	84
Table 18: Shear Load Capacity, Max. von Mises ans Max. Shear Stress Results.	85
Table 19: Percentage Difference of critical load Between Hand Calculations and FEM (Thickness Variation).....	98
Table 20: Maximum Critical Loads and their Ratio with Respect to the FEA Results for Thickness Variation.	99
Table 21: Length Values for the Different Cases.....	101
Table 22: Percentage Difference in critical load Between Hand Calculations and FEM (Unbraced length Variation).....	106

Table 23: Maximum Critical Loads and their Ratio with Respect to the FEA Results for Unbraced length Variation. 107

CHAPTER 1

1. INTRODUCTION

1.1. GENERAL BACKGROUND

Structural steel has many advantages when compared with other construction materials. Some of the benefits are ductility, strength and fast construction processes. Structural steel has the strength to cost ratio in tension and the stiffness to weight ratio higher than concrete. Conversely, it exhibits a lower strength to cost ratio in compression than concrete. At the end of 1800's and at the beginning of 1900's, steel bridges have been an innovative solution principally for long span bridges. The construction of steel bridges in the U.S. began in the 1870's. In the present days, the most common types of structural systems consist of girder bridges, rigid frame bridges, arch bridges, cable stayed bridges, suspension bridges, and trusses bridges. Most of the existing bridges carry vehicular, truck and train traffic loads higher than the original design loads. After 1960's, many steel bridges have developed cracks due to lack of adequate design details, overloading, and repeated loading effects. The results of these effects reflect as structural instabilities. Regrettably, some of these steel bridges have collapsed as a result of shear overstress, fatigue and buckling, questioning the economical and reliable reputation of steel bridges.

According to the Federal Highway Administration, 11,424 steel truss bridges are in service today in the US and its territories. Some of these bridges are non-load path redundant, i.e., the failure of member or connections could cause the collapse of the whole structure. Many steel truss bridges have members connected together by gusset plate connections using bolts or rivets. The design of these connections follows simplified methods made by Whitmore (1952), Hardash and Bjorhovde (1985) and Thornton (1984). Many inspection reports reveal loosen rivets and

bolts in critical connections. These effects are aggravated by exposition to environmental attacks, although there are some methods recently used to preserve the original mechanical properties of the structural components like inhibitive coating systems and weathering steel. The conditions described in US infrastructure reports evidence that large numbers of bridges in the United States are not being adequately maintained, having uncertain conditions.

After the collapse of the I-35 Bridge in Minnesota, there was a great interest in studying gusset plate connections. There were some experimental and analytical investigations to study the behavior of gusset plate connection (GPC) under tension and compression loads. The Federal Highway Administration (FHWA 2009) has developed guidelines to evaluate GPC. The incorporation of connections in load-ratings is very important for bridge engineers, but this represents a real challenge due the complexity of the analysis and inspection of a large amount of connections in their inventories. In addition, there were some studies demonstrating the conservative equations used in the guidelines especially for shear capacity of rivets and compressive instability evaluation. This study aims to contribute in the understanding of the structural behavior of selected steel connections focused in buckling behavior, tensile and shear strength of elements in typical steel gusset plate connections. The analysis uses the FEM to simplify and discretize in finite elements the continuous domain of forces, displacements, stresses and strains. These analyses corresponded to computational models involving two general steps: i) the global bridge behavior and ii) specific sub-model representations of critical connections.

1.2. SCOPE OF THE RESEARCH

Previous studies do not account for military loading characteristics, which are different to those of civilian vehicles. Furthermore, most of these studies concentrate on gusset plate

connections represented by simplified models excluding the interaction between different elements in tension and compression, as well as the real representation of rivets in direct contact with the elements and the plate. This study aims to analyze and rate an existing bridge subjected to civilian and military vehicles. The results obtained from detailed FEA of all components in the critical connections will be compared to those recommended by FHWA guide (FHWA 2009).

A 3-D FEA will be performed to the critical connections of an in service bridge of the US Army garrisons. FEA is used to develop models that present complex geometry and loading conditions, non-linear material behavior and contact interactions. The Static-Riks module will be used to evaluate the buckling capacity of the connections. Sub-models will be extracted from the whole gusset plate connection to obtain in detail the effects of gusset plate (GP) buckling and rivets diameter reduction. As mentioned before, those results are compared to FHWA guide (FHWA 2009) equations.

1.3. OBJECTIVES

The main objective of this research is to develop finite element models of typical steel bridge GPC to study the states of stress and strain and to perform a buckling sensitivity analysis.

- Develop a three-dimensional (3-D) finite element model of the critical connections obtained from the global model of the bridge. The finite element analysis will be performed using the commercial software Abaqus CAE.
 - Analyze stress in the connection.
 - Identify the highest stress concentration regions.
- Compare modeling techniques commonly used to study gusset plates.
- Study the corrosion effect of rivets.
- Study the effects of missing rivets in critical connections.

- Perform a buckling sensitivity analysis of compression zones in the gusset plates:
 - Effect of thickness reduction and increase in unbraced length.
 - Compare the critical load obtained from FEA and the hand calculations.

1.4. METHODOLOGY

Numerous researches have been developed to understand the structural capacity of steel connections in order to avoid and diminished catastrophic events due to the collapse of bridges. Gusset plate connections are difficult to study because of its complex geometry, boundary conditions, loads conditions, large geometries and contact interactions. The challenge in model connections containing rivets or bolts are the possible local instabilities developed when the rivets or bolts interact with the gusset plates and the truss elements. In addition, the connection must be in equilibrium to execute the analysis without convergence problems. Experimental tests on small-scale connections composed of single braced member subjected to monotonic axial tension or compression have been studied in previous researches. To supplement the experimental results and validate it, FEA has been a reliable technique to implement in such cases. FEA has been used to study the causes of the I-35 bridge collapsed (Minmao Liao et al. 2010) to conduct parametric studies, and to study the stresses and strains of gusset plates. The use of FEA has been a powerful tool in structural engineering applications. Knowing the reliability of FEA and using previous experimental and analytical investigations, this research plans to study an in service steel truss bridge focusing on its critical connections. However, even though the target connections are obtained from a constructed in-service bridge, there are many other bridges with similar geometrical, material, and loading parameters. Therefore, the results obtained in this study will be of general interest to designers and inspectors evaluating existing bridges with similar characteristics.

The first step is to conduct a literature review of previous research and literature related to connections, steel material behavior, FEA, fracture mechanics, imperfections in connections, and structural instability. Numerous papers and thesis were found related to the development of FEA of connections, the use of fracture mechanics to study life predictions of connections, and buckling sensitivity analysis of shells and plates. The commercial FEA software Abaqus CAE is used to develop and analyze the critical connections. FEA techniques used in previous research were adopted as starting point to obtain reliable results. Based on the literature review, the FEM presented in this study has been the most detailed and realistic model developed in the study of gusset plates. All parts of the connection (gusset plates, elements, rivets) are presented as 3-D deformable solid elements interacting together. This model has the capability to determine the stress distribution in the elements, rivets, and gusset plates.

This study uses an in-service steel truss bridge located in Missouri. It consists of four spans, but this study emphasizes the second one, from west to east direction. As an initial step, the bridge will be modeled using the computer-aided software SAP2000 (2009) to study its structural condition. A moving load analysis will be conducted to obtain the most critical loads and consequently the most critical connections of the bridge. Connections with the highest load in compression and tension will be selected. A three dimensional (3-D) finite element model will be developed in Abaqus to study in detail the critical connections. 3-D contact modeling using solid representation of the gusset plate, rivets and members will be incorporated in the models, to represent in detail the load transfer from elements to plates throughout rivets bearing contact. In addition, sub-models were developed to study the effects of rivets corrosion, loss of rivets, and buckling instability. A super computer located in the Information Technology Laboratory (ITL) of the U.S. Army Research and Development Center (ERDC) was used for the analyses.

Appropriate boundary conditions, material properties, mesh refinement, part interactions, and stability analysis are some of the challenges to overcome in the highly complex solid models.

1.5 CONTENTS OF THIS THESIS

This thesis is subdivided into the following parts:

- Chapter 2 shows a literature review with previous analytical and experimental investigations of gusset plates. Then, three bridge case studies of collapse are presented. A summary of the finite element method algorithm used in Abaqus for general static, eigenvalue, and Riks analyses is presented after the bridge case section. Finally, a summary of the load rating for connections is explained to demonstrate the development and how to use this methodology.
- Chapter 3 shows a brief description of the bridge to be analyzed (material properties, elements dimensions, and loads conditions).
- Chapter 4 explained the critical connections to be analyzed (loads, boundary condition, mesh refinement and material properties).
- Chapter five shows the analysis and results of the present study. These include the following:
i) target bridge analysis results, ii) fatigue analysis of the bridge, iii) modeling techniques of connections, iv) FEA of critical connection J-6, v) nonlinear tension analysis, vi) rivet analysis, and vii) nonlinear buckling analysis of GPC.
- The conclusions and recommendations based on the results are presented in the last chapter and the load rating and buckling capacity example calculations are shown in the appendix.

CHAPTER 2

2. LITERATURE REVIEW

2.1. PREVIOUS RESEARCH ON STRUCTURAL PERFORMANCE OF GUSSET PLATE CONNECTIONS

2.1.1. EARLY STUDIES

Whitmore (1952) is one of the pioneers studying and modifying the analysis and design philosophy of gusset plate connections. In his study he addressed the maximum stress location, distribution and intensity of a Warren truss gusset plate connection. Whitmore developed a method to determine the maximum stress of a gusset plate based what became known as the Whitmore effective width. This effective width is defined as the length of a line in the bottom row of bolts that are perpendicular to the member longitudinal axis intersecting two lines drawn 30° from the outer row of bolts (see Figure 1). Whitmore concluded that the maximum compressive and tensile stresses in gusset plates are located at the end of each diagonal member. These maximum stresses in the members are calculated by multiplying the axial load by the thickness of the plate and the Whitmore effective width at the end of each diagonal. Nowadays, this concept is used for the design of gusset plate connections. Irvan (1957) conducted experimental studies of general stress distribution in a double plate Pratt truss. His findings were very similar to Whitmore's results, except that he modified the Whitmore effective width by extending the 30° lines from the center of gravity of the bolt groups to the bottom row of bolts. The pioneers in the implementation of the finite element method (FEM) to analyze gusset plate connections were Davis (1967) and Vasarhelyi (1971). Davis validated Whitmore's work by analytical analysis. Davis conducted analytical studies and experimental tests for a bottom chord of a simple Warren truss. Davis suggested that Whitmore method is appropriate to determine the

magnitude of the maximum stress, but the location of those maximum stresses may change depending on the load condition of the connection.

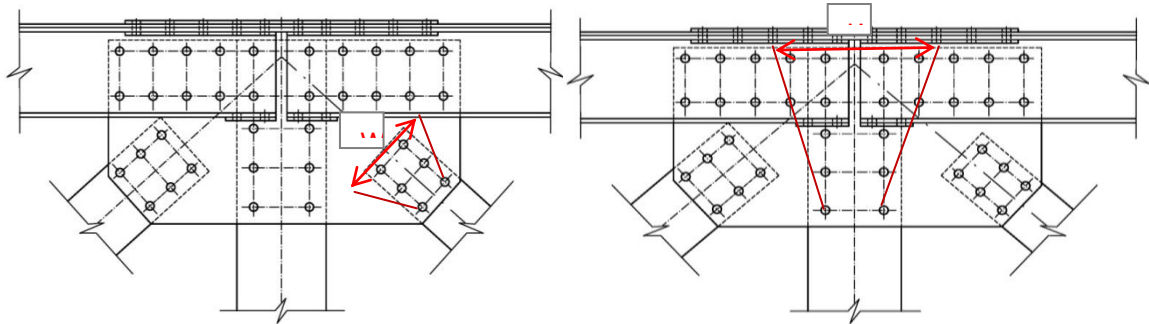


FIGURE 1: WHITMORE EFFECTIVE WIDTH.

The first method to estimate the buckling strength of gusset plates was implemented by Thornton (1984). He suggested that treating the unbraced length (average L_1 , L_2 and L_3) and the Whitmore effective width of a gusset plate as an imaginary column the standard buckling equations can be used to determine the gusset plate buckling capacity (see Figure 2 a). Bjorhovde and Chakrabarti (1985) conducted full-scale gusset plate connection tests to study the behavior and ultimate strength of gusset plate connections in tension. Six different specimens were tested varying the thickness and the angles of bracing. The results demonstrated that gusset plates failed due to tearing in the last row of bolts of the bracing members. Bjorhovde and Chakrabarti suggested that Whitmore effective width concept is applicable for gusset plates in braced frames and also confirmed that the method can be effectively used to predict net section fracture. Richard et al. (1983) performed a FEA to study the diagonal bracing used in the experimental tests of Bjorhovde. They reported very similar strains between the analytical and experimental tests for low strain gradients. However, a large difference in results was obtained in the analytical results compared with test results for high strain gradients. This was attributed to the mesh size used in the FE-discretization.

Hu and Cheng (1987) studied the buckling capacity in the elastic range (material) of steel gusset plates. The effect of thickness, boundary conditions, eccentricity and edge stiffening reinforcement of gusset plate connections were evaluated. Results showed that the primary failure mode was elastic buckling in the longest free edge of the gusset plate using concentric loads. Otherwise, cases of eccentric loading showed that failure occurred at the splice member due to excessive yielding. The experimental results also showed that thin gusset plates buckle at load levels (elastic buckling) smaller than those of Whitmore's effective width approach. Furthermore, the FEA demonstrated that the elastic buckling strength is affected by the rotational restraint from the boundary elements, the bending stiffness of the splice plates and the distance between the end of the splice plate and the beam-column boundaries. Yamamoto *et al.* (1988) conducted an experimental study of a full-scale gusset plate Warren truss joints taking in consideration the development of plastic zones, local buckling strength, and ultimate strength. They proposed an equation to obtain the gusset plate thickness and their safety factor. Local buckling failure located in the compression diagonal was observed in the experiment. They concluded that when the ratio of ultimate load vs. design load is in the range between 2.5 and 3.8, an extra strength after local buckling occurs.

Yam and Cheng (1993) performed experimental tests of gusset plates to investigate its compressive behavior. Nineteen specimens were tested varying the gusset plate thickness, plate sizes, brace angle, beam and column moment, out of plane loading eccentricity, and out-of-plane restrain boundary conditions. The results of the experimental tests demonstrated that ultimate load capacities of gusset plates depend on the plate thickness and plate size. The ultimate load capacity is directly proportional to the increase in thickness. On the other hand, ultimate load capacity decreases as the gusset plate size increase. Sway buckling was the principal failure

mode on gusset plates without out-of-plane restraint while local buckling was observed for gusset plates with out-of-plane restraint. In addition, Yam and Cheng concluded that the Whitmore method predicts a conservative strength for plates that shows significant yielding prior to inelastic buckling. However, for slender plates the Whitmore method for calculating the plate's strength could be unconservative. In addition, Yam and Cheng (1994) through their analytical investigations of steel gusset plates under compressive loads proposed a Modified Thornton Method changing the dispersion angle to 45° instead of 30° . It used an unbraced length that extends from the centroid of the brace at the last row of rivet holes to the first intersection of any gusset plate support, as shown in Figure 2 b. This modified method takes into account the load redistribution caused by yielding prior to stability failure.

Gross (1990) performed an experimental study of gusset connections for lateral bracing systems in buildings. Three full-scaled specimens were tested in order to determine the behavior and strength of the connection influenced by the frames, the effect of bracing member eccentricity on gusset plate capacity, and study the difference in performance between the gusset plate connected to the column flange and the gusset plate connected to the column web. Gross showed that for strong-axis columns with no eccentricity and eccentric configurations, buckling of the diagonal member in compression controlled the failure mode of gusset plates. Tearing of the gusset plate failure occurred for the weak-axis column connection. Gross suggested to use an effective length factor of $k=0.65$ to determine the buckling capacity instead of $k=0.5$, because the latter gives a conservative value in gusset plate connections. Kulak and Grondin (2001) performed an experimental study to verify the LRFD block shear equations from the AISC. From the study, it seems that the LRFD block shear equations give conservative gusset plate capacities and nominal ultimate tensile capacity equation (Hardish and Bjorhovde) present better

estimations for tensile capacity. Roeder et al. 2005 and Yoo (2006) during their investigations of seismic design and performance of steel frame connections and braced frame respectively, proposed a new method to predict gusset plate buckling capacity by combining the Thornton and Modified Thornton Methods. The method, known as the Yoo Method, uses the 45° dispersion angle suggested by Yam and Cheng and the average of unbraced length suggested by Thornton as shown in Figure 2 c.

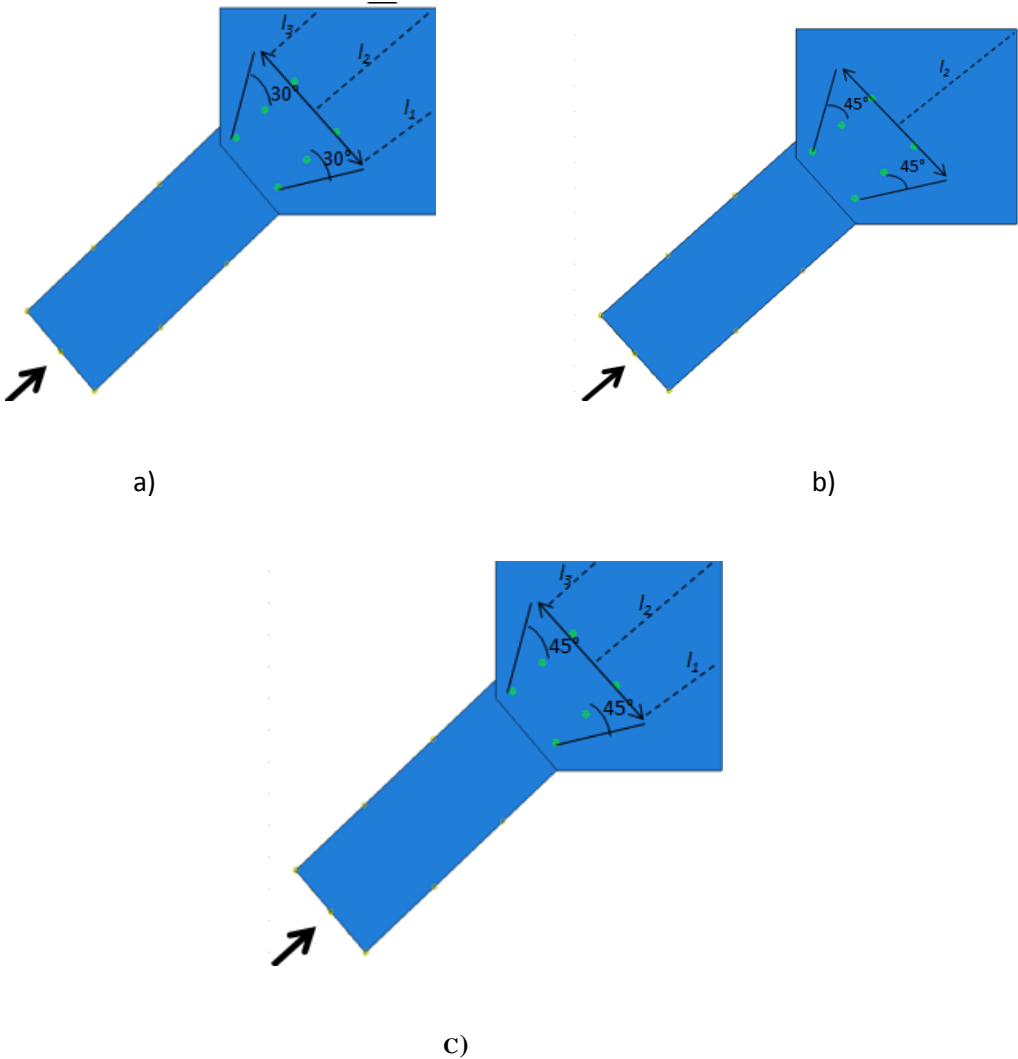


FIGURE 2: THREE METHODS ESTABLISHED TO PREDICT BUCKLING CAPACITY: A) THORNTON METHOD, B) MODIFIED THORNTON METHOD, AND C) YOO METHOD.

2.1.2. RECENT STUDIES

During the last years, FEA has been frequently applied in structural engineering applications. Researchers calibrating FEA with experimental studies have demonstrated that analytical results using computer-aided software, such as Abaqus CAE, produce economical and reliable results. Without underestimating the importance of experimental tests to study the structural performance of real engineering systems, the costs involved in experimental programs (equipment, instrumentation, materials, technicians, etc.) are surpassed by time-consuming FE computational analyses. However, it is always beneficial to conduct experimental and analytical studies to provide a complete outlook of the case studied. Walbridge et al. 2005 performed an analytical study to understand the behavior of gusset plates under monotonic tension, monotonic compression, and cyclic loading. The nonlinear FEM analysis of the gusset plate was validated using experimental results from studies conducted by Yam and Cheng (1993) and Rabinovitch and Cheng (1993). The FEA was developed using Abaqus to study the effects of framing member stiffness, nonlinear material behavior, initial imperfections, and bolt slippage. The gusset plate, beam and column were modeled using shell element S4R while the bolt was developed using Abaqus SPRING2 elements. The results predicted very well the buckling and post-buckling load resistance under cyclic loading.

There are several studies focused on the causes of the I-35W bridge collapse that occurred in 2007 in Minnesota. One of these studies conducted by Liao et al. 2010 developed an analytical investigation on the condition of one of the gusset plates at the time of the bridge collapse. Forces obtained from available information of the bridge were placed in a detailed nonlinear, three-dimensional FE model to calculate stress and strain states in the gusset plates. C3D8 elements, 16 elements surrounding the bolt holes, two elements across the thickness, and elasto-

plastic steel properties were used to model the connection. The results of the study revealed that some gusset plate regions yield at the time of collapse as a consequence of smaller thickness dimensions of gusset plates and due to increment of bridge's weight at the time of the collapse. In addition, from their results it seems that compression and shear interactions play an important role in the gusset plate mode failure.

Otherwise, the Triage Evaluation of Steel Gusset Plate Connections TEGP (2010) developed a Triage Evaluation Procedure (TEP) capable of evaluating more rapidly gusset plate connections than the current FHWA recommendations. Analytical methods using FEM of different gusset plate connections were conducted in the study. The TEP procedure contains three main checks: i) gusset plate yielding, ii) gusset plate buckling, and iii) fastener strength. The research concluded that TEP is safe and conservative for bridge load ratings when compared to the FHWA recommendations.

Kay (2011) performed a numerical analysis of steel gusset plates. The goals of this research were to study the stresses and ultimate strength limit states, compare different bolt modeling techniques and determine the effectiveness of these in the study of the buckling loads and stress distributions. The elastic stress analysis showed negligible variations in the results obtained varying the bolt modeling technique. The differences in the computational and experimental buckling loads were in the order of 10%, while for tension members the difference is in the order of 7%.

2.2. BRIDGE CASES STUDIES

The US National Transportation Safety Board documented some catastrophic bridge accidents that have been reported in the US in the last 60 years. Unfortunately, many of these

accidents involved human fatalities. Casualties are the main reason to better understand the behavior of gusset plate connections, in addition to prevent future collapses. The following subsections describe some of the events, its causes and consequences.

2.2.1. SILVER BRIDGE, 1967 (REPORT NTSB 1971)

The Silver Bridge has been one of the reported bridge collapses in the US (December 15, 1967). According to the report (NTSB 1971), forty-six people died, nine were injured, and thirty-one vehicles fell down from the bridge (Figure 3). The reason for the collapse according to the safety board investigation was initiated by a cleavage fracture in a lower member followed by a ductile fracture in an upper member in the same connection. Those fractures were originated by development of critical size flaw due to stress corrosion and corrosion fatigue. It seems that the crack rapidly propagated by lack of maintenance, stress corrosion, and corrosion fatigue design considerations. The problem was compound by the flaw location, i.e., an area inaccessible to inspectors.



FIGURE 3: SILVER BRIDGE COLLAPSE (THE HERALD-DISPATCH)

2.2.2. SUSPENDED SPAN BRIDGE, 1983 (REPORT NTSB 1984)

Figure 4 shows a bridge collapse in the Mianus River in Greenwich, Connecticut, USA on June 28, 1983. An over 100-foot-long suspended span collapsed, falling into the river. Three people were wounded and three other died. Pin and hanger assemblies connected the suspended span that collapsed. Before the collapse, the inner hanger of one of the hangers released the lower pin. As a result, a fatigue crack was developed in one of the upper pins generating failure in the pin and the hanger of that span. The investigation concluded that the reason for the collapse was the result of an undetected lateral displacement in one pin-hanger suspension assembly caused by corrosion. Bridges with structural systems that depend on hangers are of great concern to their owners due to fracture critical conditions, i.e., failure of this element represent a bridge collapse. Non-destructive testing (NDT) programs are currently established to physically inspect these bridges.



FIGURE 4: MIANUS RIVER BRIDGE COLLAPSE

([HTTP://35WBRIDGE.PBWORKS.COM/W/PAGE/900718/MIANUS%20RIVER%20BRIDGE%20COLLAPSE](http://35wbridge.pbworks.com/w/page/900718/Mianus%20River%20Bridge%20Collapse))

2.2.3. HIGHWAY BRIDGE ON THE I-35W, 2007 (REPORT NSTB 2008)

The collapse of the I-35W Bridge in Minneapolis, Minnesota has been one of the largest bridge catastrophes in the US highway history (Figure 5). The collapse happened in a rush hour (6:05 pm) on August 2, 2007 as a result of failure in the main span of the deck truss. Thirteen people died and 145 were injured. The I-35W bridge had design and inspection issues contributing to the collapse, namely: i) insufficient bridge design firm quality control; ii) exclusion of gusset plates in bridge load rating guidance; iii) lack of inspection guidance for conditions of gusset plates distortion; and iv) inadequate use of technologies for accurately assessing the condition of gusset plates on deck truss bridges (Highway Accident Report NTSB/HAR-08/03, 2007). However, contrary to what originally was speculated, forensic evidence of the I-35W bridge suggests that the failure initiated by buckling of gusset plates connecting top chord elements in the truss.



FIGURE 5: I-35 BRIDGE COLLAPSE ([HTTP://WWW.PTANK.COM/BLOG/2007/08/I-35W-BRIDGE-COLLAPSE-IN-MINNEAPOLIS/](http://www.ptank.com/blog/2007/08/i-35w-bridge-collapse-in-minneapolis/))

2.3. FINITE ELEMENT METHOD

Courant first introduced the finite element method (FEM) in 1943 to find solutions for problems of equilibrium and vibrations using the Ritz method. Its origins were to solve structural engineering problems, however, nowadays the method is used in many other disciplines capable of solving problems with complex geometries and continuous domains. The method is used as a computer-based capable to analyze engineering problems. The FEM is a numerical technique that uses integral formulations to perform a system of algebraic equations assuming a continuous function for each element. The systematic process of the FEM divides a domain into discretized subdomains (elements), and analyzes each element. The result is an approximate solution of the exact differential equation.

The modeling of a domain with a FE program involves three parts: i) preprocessor, ii) processor, and iii) postprocessor. The preprocessor is the first step, in which the user draws the geometry, inputs the data related to the problem, generates the finite element mesh and indicates the type of analysis to be performed. The processor consists in the steps generated to solve the finite element problem. Finally, the postprocessor represents is the output data (results) commonly shown in tabular and/or graphical forms.

The computer software Abaqus (2011) uses the finite element method with a mathematical technique, in which the solution depends on the convergence level of the mesh density and other input parameters in the preprocessor step.

2.3.1. GENERAL STATIC ANALYSIS

A general static analysis is one of the analysis procedures that can be done with Abaqus (2011). This static stress analysis is used for problems in which the inertia effects are neglected and for linear or nonlinear response (material and geometrical) problems. Some stability

problems could occur in the analysis due to the following reasons: i) buckling, ii) collapse, or iii) local instabilities. The Newton's method is used for solving nonlinear equilibrium equations. The discrete virtual work equilibrium equation is as follows:

$$F^N(u^M) = 0$$

where:

F^N = Force component of the N^{th} variable.

u^M = Displacement value of the M^{th} variable.

Assuming an initial iteration i , an approximation value of u_i^M is obtained and a correction factor c_{i+1}^M is inserted to reach equilibrium as follows:

$$F^N(u_i^M + c_{i+1}^M) = 0$$

Expanding the previous equation into a Taylor series expansion for an approximate value of u_i^M :

$$F^N(u_i^M) + \frac{\partial F^N}{\partial u^P}(u_i^M)c_{i+1}^P + \dots = 0$$

If the u_i^M value is close to the exact solution, then c_{i+1}^M will be small and the above equation will become a linear system of equation:

$$K_i^{NP} c_{i+1}^P = - (F^N(u_i^M))_i^N$$

where,

$$K_i^{NP} = \frac{\partial F^N}{\partial u^P}(u_i^M) = \text{Jacobian matrix.}$$

The next approximation will be:

$$u_{i+1}^M = u_i^M + c_{i+1}^M$$

The iteration continues until convergence is reached (i.e, F_i^N and c_{i+1}^N are neglected).

2.3.2. EIGENVALUE BUCKLING ANALYSIS

The eigenvalue analysis is one of the methods used to study the instability of structures. This analysis consists in a linear perturbation procedure used to obtain the critical load when the structure bifurcates. It is commonly used in stiff structures where a linear behavior is observed or nonlinear behavior is minimal before buckling. Mathematically, the analysis finds the singularities of the model stiffness matrix. For structures where inelastic behavior will occur before bending, this method can estimate the buckling mode shape of the structure. The critical load for inelastic structures may be lower than the critical load obtained in the eigenvalue analysis.

The eigenvalue problem consists of finding the values of λ (eigenvalues) that makes null the determinant of the matrix presented below. The lowest value of λ is named the critical eigenvalue (λ_{cr}) and is selected to find the critical buckling load. The buckling mode shapes ($\{V\}$) are normalized vectors and represent the actual magnitudes of deformation at critical buckling loads. As mentioned before, eigenvalue method can be used to predict the failure mode of the structure.

$$([K_o] + \lambda[\Delta K])\{V\} = \{0\}$$

where:

$[K_o]$ = stiffness matrix;

$[\Delta K]$ = differential initial stress and load stiffness matrix;

$\{V\}$ = buckling mode shapes; and

λ = eigenvalues.

In ABAQUS (2011), the critical load is obtained from:

$$P_0 + \lambda_{cr}\Delta P$$

where:

P_0 = dead load of the structure;

λ_{cr} = critical eigenvalue; and

ΔP = incremental loading pattern.

Abaqus (2011) has two eigenvalue extraction methods. These are the subspace iteration method (Bathe 1996) and the iteration method with Lanczos transformation (Lanczos 1950). Both methods work extracting a selected set of eigenvalues and eigenvectors.

2.3.3. RIKS ANALYSIS

For cases where the structure presents large geometric changes prior to buckling during static loads, material nonlinearity, or unstable postbuckling response, a nonlinear analysis must be performed to investigate the structure. The modified Riks algorithm is the most popular method used to study this kind of structural problems and it is employed in Abaqus (2011). This method searches for the static equilibrium of a structure implementing an incremental load to find the displacements that provide equilibrium by an iterative process. An arc length parameter is measured to obtain the static equilibrium path in a load-displacement space regardless the structure response is stable or unstable. The method uses the load magnitude as an unknown variable and it solves simultaneously for loads and displacement.

The following paragraphs describe the algorithm used by Abaqus (2011) to incorporate the Riks method to the solution of problems involving nonlinear conditions. Using P^N as the loads applied to the structure in any degree of freedom and λ as the load magnitude parameter, the load increment in the analysis is λP^N and the respective displacement is u^N . Abaqus scales the solution using the maximum absolute displacement \bar{u} in the initial iteration (lineal). The scalar space is represented by:

$$\lambda \tilde{P}^N = \frac{\lambda P^N}{\bar{P}}$$

$$\tilde{u}^N = \frac{u^N}{\bar{u}}$$

where:

$$\bar{P} = (P^N P^N)^{1/2}$$

Using the points of the vector $(\tilde{u} ; \lambda)$, the solution path achieving equilibrium is constructed.

Starting from a point $A^0 = (\tilde{u}_0^N ; \lambda_0)$, the tangent stiffness (K_o^{NM}) is obtained to solve:

$$K_o^{NM} v_o^M = P^N$$

After this step, an increment point (A^1) is calculated using $\Delta\lambda$ obtained with $\tilde{u}_o^N = \frac{u_o^N}{\bar{u}}$ and a specific path length Δl specified by the user.

$$\Delta\lambda_o = \pm \frac{\Delta l}{(\tilde{v}_o^N \tilde{v}_o^N + 1)^{1/2}}$$

The sign of the previous equation is selected so that the dot product of the vector $\Delta\lambda_o(\tilde{v}_o^N ; 1)$ is positive.

$$\Delta\lambda_o(\Delta\lambda_o(\tilde{v}_o^N ; 1)) > 0$$

At this step, point A^1 has coordinates $(\tilde{u}_o^N + \Delta\lambda_o \tilde{v}_o^N, \lambda_o + \Delta\lambda_o)$. The solution is corrected onto an orthogonal plane $(\tilde{v}_o^N ; 1)$ passing through point A^1 following the algorithm presented below.

- 1) Initialize the proportionally load factor increment and its response,

$$\Delta\lambda_i = \Delta\lambda_o, \Delta u_i^N = \Delta\lambda_o v_o^N \text{ for } i=1, 2, 3, 4,..$$

- 2) Calculate the internal forces and the tangent stiffness matrix at nodes with coordinates

$$(u_o^N + \Delta u_i^N, \lambda_o + \Delta\lambda_i),$$

$$I^N = \int_V \beta^N \sigma dV$$

$$K^{MN} = \frac{\partial I^N}{\partial u^M}$$

- 3) Verify equilibrium in the system. If the residual load is sufficiently small, the system has converged, if not the program makes iterations until equilibrium is reached.

$$R_i^N = (\lambda_o + \Delta\lambda_i)P^N - I^N$$

- 4) Solve simultaneously for P^N , R^N , v_i^N , and c_i^N in the following equation,

$$K^{NM}\{v_i^N; c_i^M\} = \{P^N, R_i^N\}$$

- 5) The projection of the scaled residual forces onto \tilde{P}^N is:

$$\rho_i = R_i^N \frac{P^N}{\bar{P}^2}$$

- 6) Adding $(\tilde{c}_i^N; \rho_i)$ into the scaled vector $(\tilde{v}_i^N; 1)$, we move A^i to A^{i+1} in the orthogonal plane $(\tilde{v}_0^N; 1)$ obtained the following equation (simplified):

$$\mu = -\frac{\tilde{c}_i^N \tilde{v}_0^N}{\tilde{v}_i^N \tilde{v}_0^N + 1}$$

- 7) The solution of point A^i now is:

$$(u_0^N + \Delta u_i^N + c_i^N + \mu v_i^N; \lambda_o + \Delta\lambda_i + \mu)$$

- 8) Return to step 2 until the system converge.

$$\Delta u_{i+1}^N = \Delta u_i^N + c_i^N + \mu v_i^N$$

$$\Delta \lambda_{i+1} = \Delta \lambda_i + \mu$$

$$i = i + 1$$

2.4. LOAD RATING GUIDANCE FOR RIVETED GUSSET PLATES IN TRUSS BRIDGES

This guidance is mainly focused in the evaluation of connecting plates and fasteners of gusset plate connections for non-load-path-redundant truss bridges (FHWA, 2009). It is in accordance with AASHTO LRFD, Load and Resistance Factor Rating Method (LRFR) and Load Factor Rating Method (LFR). A summary below presents the strength limit states used for the evaluation of connections based on LRFR method.

Rivets are evaluated to prevent shear and plate bearing failures at the strength limit states. The latter failure verification shall be following AASHTO Article 6.13.2.9 (LRFD 2007) for bearing resistance at bolt holes. The rivet factored shear resistance is verified using the following equation. For rivets greater than 50 in. in length, the guidance suggests that the following equation shall be multiplied by 0.80.

$$\phi R = \phi F m A_r$$

where:

ϕR = shear capacity;

ϕF = factored shear strength of one rivet;

m = number of shear planes; and

A_r = cross-sectional area of the rivet before driving.

Gusset plates subjected to axial tension shall be evaluated for the following cases: yield on the gross section, fracture on the net section, and block shear rupture. The smallest value obtained in the previous cases will be the factored resistance. Gross section yielding resistance and net section fracture resistance are verified using the following equations. The gross and net section areas use the Whitmore effective width.

$$P_r = \phi_y F_y A_g$$

$$P_r = \phi_u F_u A_n U$$

where:

ϕ_y = resistance factor for tension yielding = 0.95;

ϕ_u = resistance factor for tension fracture = 0.80;

A_n = net cross-sectional area of the plates as specified in AASTHO LRFD Article 6.8.3.;

A_g = gross cross-sectional area of the plates;

F_y = yield strength of the plates;

F_u = tensile strength of the plates; and

U = reduction factor to account for shear lag = 1.0 for gusset plates.

Otherwise, block shear rupture resistance take into account axial tension and shear.

If $A_m \geq 0.58A_{vn}$, then,

$$P_r = \phi_{bs} (0.58F_y A_{vg} + F_u A_n)$$

Otherwise,

$$P_r = \phi_{bs} (0.58F_u A_{vn} + F_y A_{tg})$$

where:

ϕ_{bs} = resistance factor for block shear = 0.80;

A_{vg} = gross area along the plane resisting shear stress;

A_{tg} = gross area along the plane resisting tension stress;

A_{vn} = net area along the plane resisting shear stress;

A_{tn} = net area along the plane resisting tension stress;

F_y = minimum yield strength of the plate; and

F_u = minimum tensile strength of the plate.

The factored shear resistance for gusset plates subjected to shear is evaluated taking the lesser value of the shear yield and the fracture resistance showed in the following equations.

$$V_r = \phi_{vy} (0.58F_y A_g \Omega)$$

$$V_r = \phi_{vu} (0.58F_u A_n)$$

where:

ϕ_{vy} = resistance factor for shear yielding on the gross section = 0.95;

ϕ_{vu} = resistance factor for shear fracture on the net section = 0.80;

A_g = gross area of the plates resisting shear;

A_n = net area of the plates resisting shear;

F_y = minimum yield strength of the plate;

F_u = minimum tensile strength of the plate; and

Ω = 1 for ample stiffness or 0.74 in the absence of a more rigorous analysis.

Idealized members in compression were developed in AASTHO LRFD Articles 6.9.2.1 and 6.9.4 to determine the gusset plate's buckling resistance.

Evaluating,

$$\lambda = \left(\frac{kL}{r_s \pi} \right)^2 \frac{F_y}{E}$$

For $\lambda \leq 2.25$, then

$$P_r = \phi_c 0.66^\lambda F_y A_s = \phi_c 0.66^\lambda F_y w_l t$$

Otherwise:

$$P_r = \frac{\phi_c 0.88 F_y A_s}{\lambda} = \frac{\phi_c 0.88 F_y w_l t}{\lambda}$$

where:

k = effective length factor;

L = Whitmore effective length;

r_s = Radius of gyration = $\sqrt{I_g/A_g}$;

w_l = Whitmore effective width; and

ϕ_c = resistance factor for member in compression = 0.9.

The selection of the effective length factor k depends on the gusset plate's boundary condition (sway or non-sway conditions exist). For lateral sway conditions, cases (d), (e), or (f) may be taken from Table 1. Otherwise, cases (a), (b), or (c) are used.

TABLE 1: K VALUES FHWA (2009).

	(a)	(b)	(c)	(d)	(e)	(f)
Buckled shape						
Theoretical K value	0.5	0.7	1.0	1.0	2.0	2.0
Design K value	0.65	0.80	1.0	1.2	2.1	2.0

CHAPTER 3

3. COMPUTATIONAL MODEL OF THE BRIDGE

3.1. TARGET BRIDGE DESCRIPTION

The target bridge used in this study was constructed in 1958 and is located in Missouri, USA (Figure 6). The bridge consists of four spans; however this study is focused on the second one, from west to east direction as illustrated in Figure 7 (red rectangle). The second span of the target bridge is evaluated using the existing structural bridge conditions obtained from the CAD drawings, physical inspections, and details provided by construction documents.

The simply-supported bridge (second span) is 90 ft long. It was originally constructed with a deck consisting of laminated timber. The deck is supported by I-shaped steel stringers and lateral floor beams interconnected by diagonal cross bracings (Figure 8). Twenty six years after its construction (i.e., 1984) the timber deck was replaced by a 9.75 *in.* thick reinforced concrete (R.C.) slab (Figure 9). Concrete Jersey barriers with 3 *in.* inside diameter round-tubular steel railing rest on the lateral sides of the slab. Table 2 shows general data of the bridge.



FIGURE 6: TARGET BRIDGE.

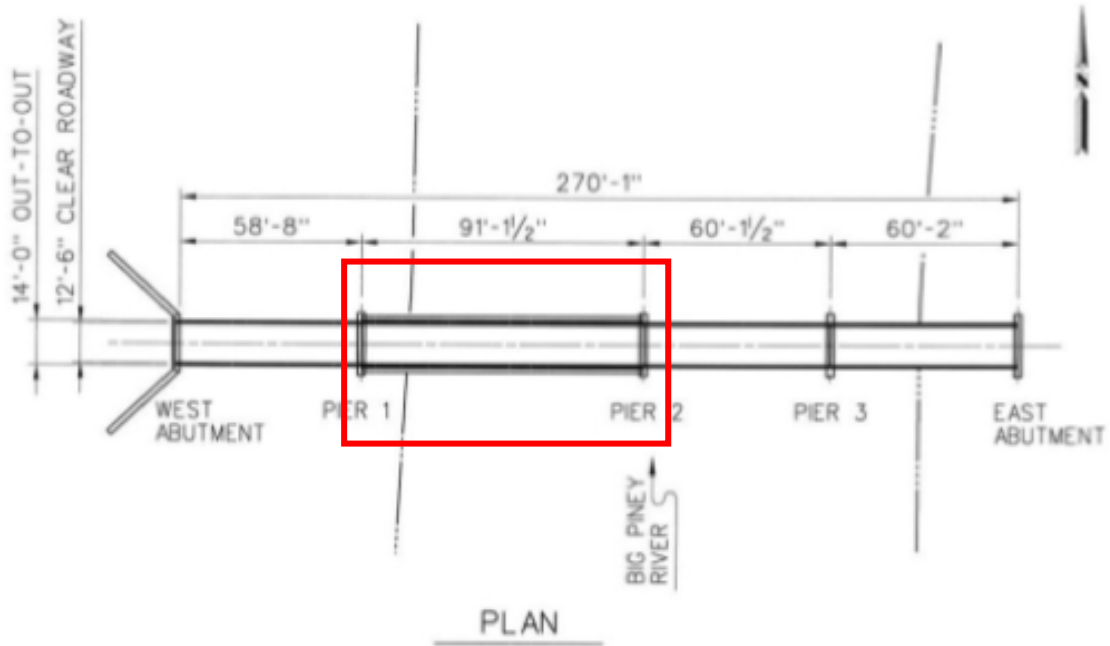


FIGURE 7: TOP VIEW OF THE BRIDGE.



FIGURE 8: PLAN VIEW OF STEEL TRUSS BRIDGE SPAN.

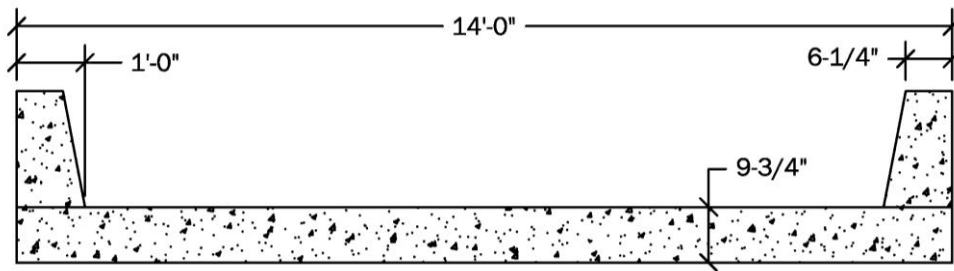


FIGURE 9: CROSS SECTION OF THE R.C. SLAB.

TABLE 2: GENERAL BRIDGE DATA.

Description	Date or Quantity
Date of construction	1958
Date of deck replacement	1984
Date of last inspection	2008
Number of traffic lanes	1
ADT	115
Clear span length [ft]	90
Effective width of bridge B_{eb} [ft]	44
Roadway width [ft]	12.5
Thickness of concrete Slab [in.]	9.75
Number of trusses	2
Skew [degrees]	0

3.1.1. BRIDGE MATERIAL PROPERTIES

The bridge was constructed of steel and concrete materials. All members and connections are made of steel whereas the slab and barriers are made of concrete. The concrete compressive strength of the slab is unknown. For cases in which the year of construction of the bridge is known but the compressive strength of concrete is unknown, Table 6-7 of MBE (2011) can be used to estimate a minimum value. For a slab built on 1984, it represents a value of 3 *ksi*. The elastic modulus of normal weight concrete can be estimated as $E_c = 33,000 \cdot (W_c)^{1.5} \cdot \sqrt{f'_c}$, where W_c = unit weight of concrete = 145 *pcf* (LRFD, Table 3.5.1-1); $E_c = 33,000 \times 0.145^{1.5} \times 3.0^{0.5} = 3.15 \text{ E}+03 \text{ ksi}$.

The construction drawings show top and bottom reinforcement #6@8” for the end and intermediate supports. These supports are provided by steel stringers. The top and bottom reinforcement at mid-spans are #5@12”.

The material properties for other elements were obtained from Table 6A.6.2.1-1, MBE (2011). These are valid for bridges built after 1936. The shear strength was estimated as 0.6 F_u . The Young modulus of steel is 29,000 ksi.

TABLE 3: BRIDGE MATERIAL PROPERTIES.

Material	Yield Strength F_y (ksi)	Tensile Strength F_u (ksi)
Steel	33	49.5

3.1.2. BRIDGE SECTION PROPERTIES AND DIMENSIONS

Bridge section properties and dimensions were taken from construction drawings and AISC Specifications (2005). Figures 10 and 11 show the elements of the truss and floor configuration and the connection location of the bridge with their respective labels. Tables 5 and 6 show dimensions and sections properties of the elements respectively.

Using the parallel-axis theorem, the second moment of the composite area (also known as moment of inertia) is calculated about the horizontal and vertical axes through the centroid (Y_{bc}) as:

$$I_{33} = \sum(I_3 + Ad_3) \text{ and } I_{22} = \sum(I_2 + Ad_2)$$

The radii of gyration are calculated as $\sqrt{I/A}$ using the inertia associated to each local axis.

The following nomenclature was used in the tables mentioned above:

t_3 = outside section depth [*in*]; outside vertical leg [*in*];

t_2 = outside section width [*in*]; outside horizontal leg [*in*];

t_f = flange width [*in*]; horizontal leg thickness [*in*];

t_w = web width [*in*]; vertical leg thickness [*in*];

t_{2b} = bottom flange width [*in*];

t_{fb} = bottom flange thickness [*in*];

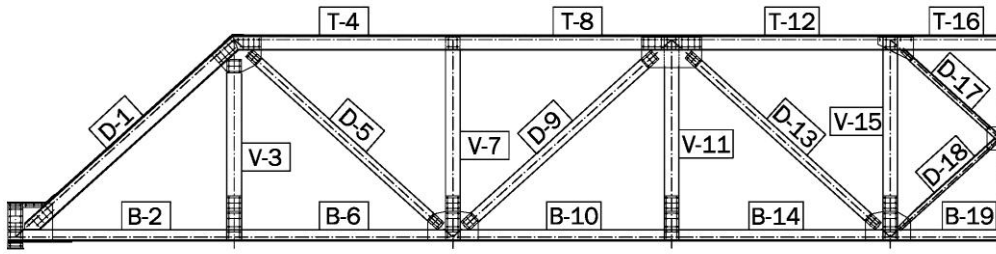
Area = cross-section area;

I_{33} = section moment of inertia about local horizontal axis;

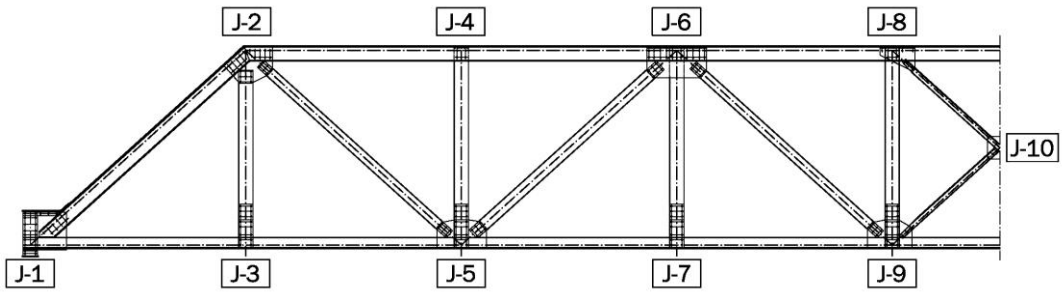
I_{22} = section moment of inertia about local vertical axis;

R_{22} = section radius of gyration about local horizontal axis; and

R_{33} = section radius of gyration about local vertical axis.

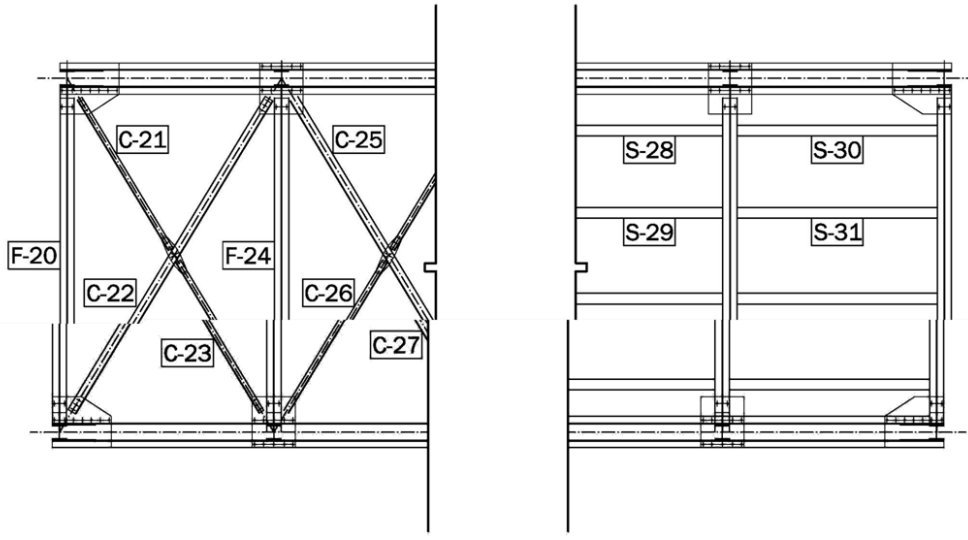


a)

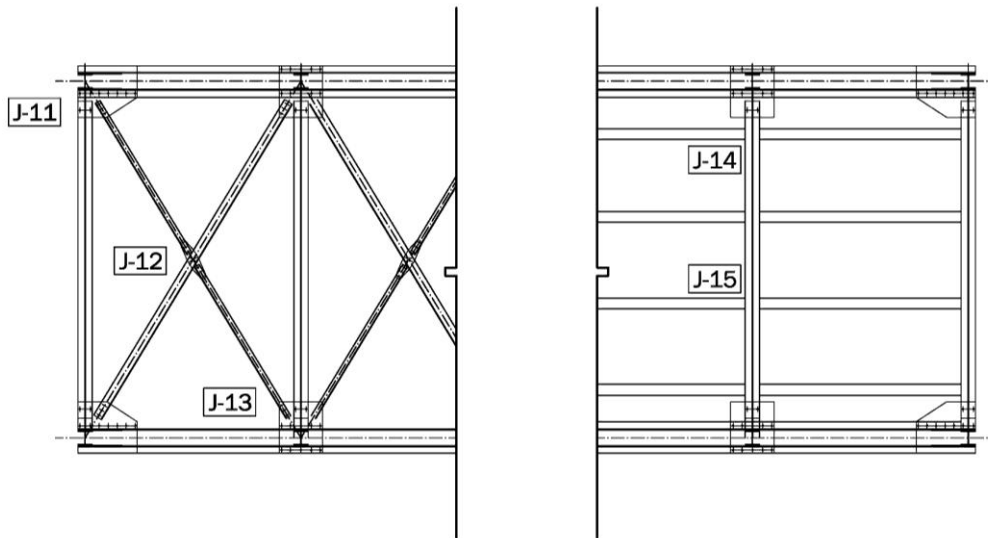


b)

FIGURE 10: COMPONENTS OF TRUSS SECTIONS: A) ELEMENTS, B) JOINTS.



a)



b)

FIGURE 11: FLOOR COMPONENTS: A) ELEMENTS, B) JOINTS.

TABLE 4: ELEMENT DIMENSIONS.

Section	Elements	t3	t2	tf	tw	t2b	Tfb
2C8X13.75	D-1, T-4, T-8, T-12, T-16	8	13.7	0.4	0.3	N/A	N/A
2L6X4X0.5	B-2, B-6	6	16	0.5	0.5	N/A	N/A
2L6X6X0.5	B-10, B-14, B-19	6	20	0.5	0.5	N/A	N/A
W8X17	D-5, D-13	8	5.25	0.3	0.2	5.3	0.3
W8X24	D-9	7.93	6.5	0.4	0.3	6.5	0.4
W8X31	V-3, V-7, V-11, V-15	8	8	0.4	0.3	8	0.4
L2.5X3X1/4	C-21, C-22, C-23, C-25, C-26, C-27	2.5	3	0.3	0.3	N/A	N/A
W10X19	S-29, S-31	10.2	4.02	0.4	0.3	4	0.4
W12X22	S-28, S-30	12.3	4.03	0.4	0.3	4	0.4
W21X62	F-24	21	8.24	0.6	0.4	8.2	0.6

TABLE 5: ELEMENTS SECTIONS PROPERTIES

Section	Area	I33	I22	R33	R22
2C8X13.75	8.1	72.3	215.6	3	5.2
2L6X4X0.5	9.5	34.8	248.8	1.9	5.1
2L6X6X0.5	11.5	39.8	411.5	1.9	6
W8X17	4.93	55.6	7.44	3.4	1.2
W8X24	7.08	82.8	18.3	3.4	1.6
W8X31	9.13	110	37.1	3.5	2
L2.5X3X1/4	1.31	0.74	1.17	0.8	1
W10X19	5.62	96.3	4.29	4.1	0.9
W12X22	6.48	156	4.66	4.9	0.9
W21X62	18.3	1330	57.5	8.5	1.8

3.2. BRIDGE MODEL DESCRIPTION

The target bridge was modeled applying linear-elastic parameters using a 3D FEA software, SAP 2000, version 14. The purpose of this global model analysis is to identify the bridge critical connections. The steel elements comprising the truss, stringers, floor beams and cross bracings were represented by linear beam elements (Figure 12). The concrete slab was represented by four-node shell elements (Figure 12). The corresponding material and section properties were described in Section 3.1.1 and 3.1.2 respectively.

As an initial approach the bridge was modeled for two conditions: a) transferring and b) releasing moments at connections. Due to partial fixity of connections the bridge cannot be represented adequately as transmitting moments among elements. However, some amount of moment transferring occurs, but it is necessary to perform a load testing to calibrate the model. Furthermore, the inclusion of moments for stress calculations exceeded the capacity of some connections even just considering the self-weight. Results of this analysis are shown in Chapter 5.

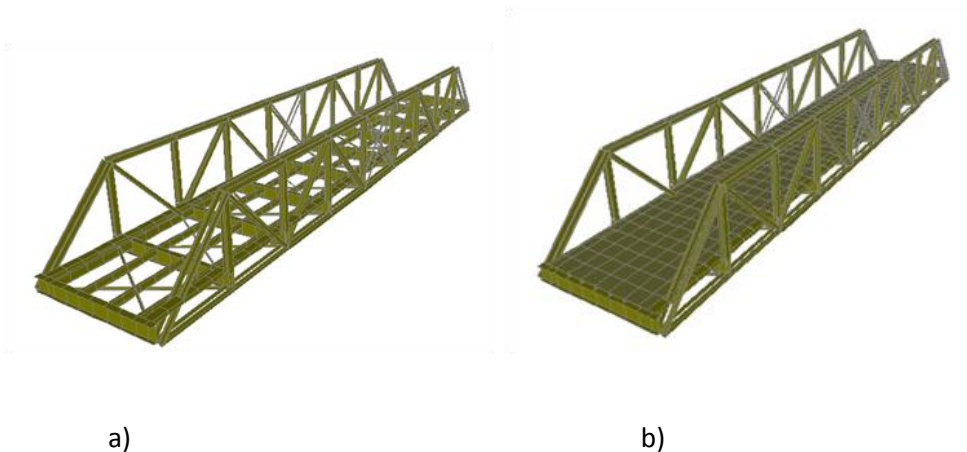


FIGURE 12: GLOBAL MODEL: A) STEEL FLOOR ELEMENTS, B) CONCRETE DECKS.

3.2.1. LOADS CONSIDERED IN THE ANALYSIS

The loads considered in the global model bridge were permanent and transient loads. Permanent loads were based on the existing conditions of the bridge. Wearing surfaces are not present in the bridge, but it has an exposed concrete slab. Thus, dead loads have a DC classification for load factors purposes. The construction drawings and a visual inspection provide the necessary data to calculate the dead load of the bridge. The selection of minimum unit weights of materials shall be in accordance with Table 3.5.1-1 (LRFD, 2007).

The dead loads of the integrated elements of the superstructure (DC_1) considered in the analysis are the weight of the RC slab, all steel elements in the trusses and the floor of the bridge. The weight of elements can be estimated by multiplying the cross-sectional area, its length, and its unit weight (i.e. 490 lb/ft³ for steel and 145 lb/ft³ for concrete). Otherwise, dead loads (DC_2) considered in the analysis as non-structural components resting or attached to the superstructure correspond to the New Jersey barriers (Figure 13) and a steel pipeline. It is commonly acceptable by bridge engineers to represent the weight of barriers as a distributed load in the slab. However, in this study the parapet weight was represented uniformly distributed along the edges of the slab and the pipeline weight was uniformly distributed on the concrete slab. This weight was estimated by $W_{nj} = W_c \cdot \sum_{i=1}^n A_i$, where A_i is the area of each element in the barrier shown in

Figure 14:

$$A_{parapet} = 2.12 \text{ ft}^2$$

$$A_{railing\ post} = 0.02 \text{ ft}^2$$

The uniformly distributed load used for analysis considering the parapet, the railing, and an additional 5% of superimposed dead loads are:

$$W_{parapet} = 0.32 \text{ kip/ft}$$

$$W_{railing} = 0.02 \text{ kip/ft}$$

$$W = (0.32 + 0.02) * 1.05 = 0.355 \text{ kip/ft}$$

Typical superstructure analyses associate the live load to a notional design vehicle defined by AASHTO as the HL-93. This live load is the combination of design truck or tandem, and design lane loads. The longitudinal spacing of axles, the transverse spacing of wheels and the weight for each axle of the design truck are shown in Figure 14. The truck configuration is defined by AASHTO as the HS20-44, where the letters HS indicate three axles consisting of a tractor truck with semi-trailer. The number “44” identifies that the loading was instituted as a design truck with the publication of the Standard Specifications for Highway Bridges, 1944 edition. The tandem (Figure 15) combines two 25 *kip* axles spaced 4 *ft* apart in the longitudinal direction and 6 *ft* apart in the transverse direction. The lane load consists of a 0.64 *k/ft* uniform load distributed over a 10 *ft* width. The design truck and design tandem loads shall be subject to a dynamic load impact factor defined in LRFD, article 3.6.2. A single lane, 12 ft width was selected for the analysis. A moving load analysis was used to represent the trucks along the possible transverse and longitudinal positions inside the lane defined.

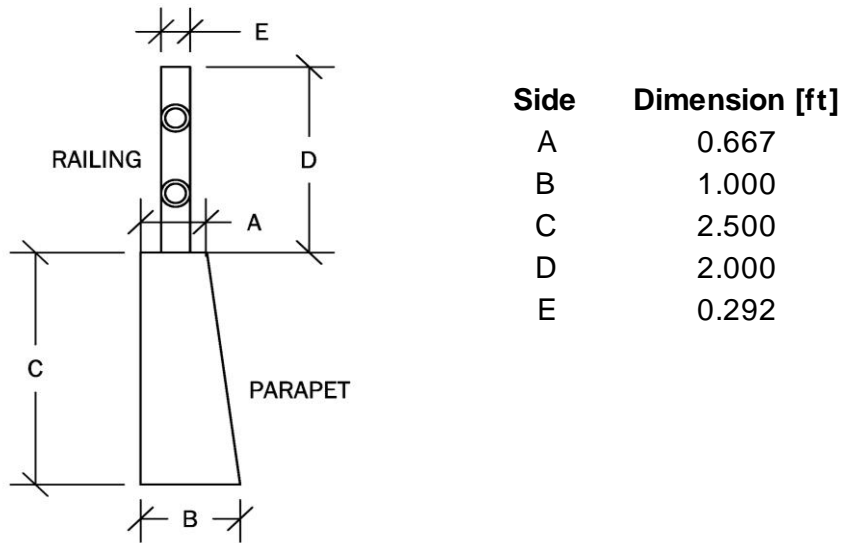


FIGURE 13: DIMENSIONS OF CONCRETE BARRIERS AND RAILING.

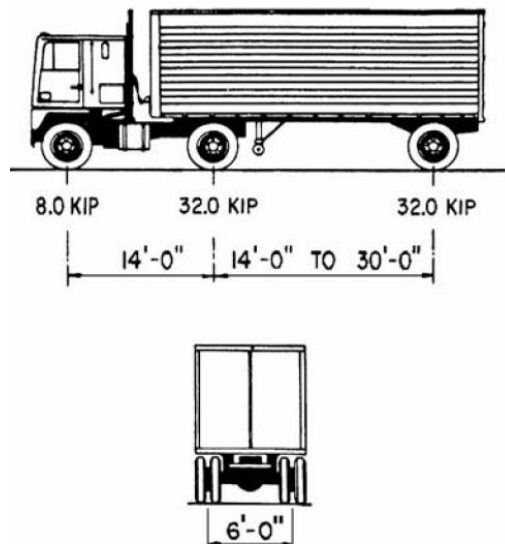


FIGURE 14: DESIGN TRUCK HS-44. OBTAINED FROM LRFD 3.6.1.2.2

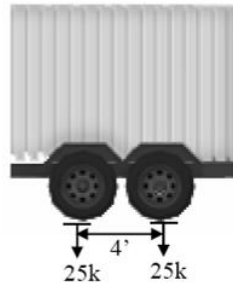


FIGURE 15: LRFD TANDEM LOADING. OBTAINED FROM VARELA (2006)

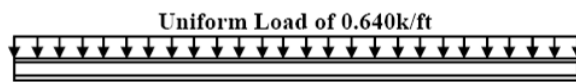


FIGURE 16: LRFD LANE LOADING.

CHAPTER 4

4. LOCALIZED FEA OF CRITICAL CONNECTIONS

4.1. CRITICAL CONNECTIONS SELECTION

The target bridge has 19 connections with similar configurations on each truss side. Based on the results obtained from the global model executed using SAP2000, the critical connections of the bridge are J-2 and J-6. This selection was based on the different load combinations applied to the global model of the bridge described in Section 5.2, Chapter 5. The load rating (LR) results for J-2 and J-6 connections are shown in Appendix A and Table 15 shows a summary of the final LR values. As expected from the global model results, the LR calculations showed that J-2 and J-6 presented the lowest values. In addition, these connections (J-2 and J-6) have geometry and configuration typical of steel trusses bridges. As a result, a detailed FE model of connections J-2 and J-6 is presented in Chapter 5.

4.2. FINITE ELEMENT MODEL DESCRIPTION

Finite element analyses (FEA) of gusset plate connections were modeled in Abaqus CAE 6.11 (Abaqus 2011). The connection geometries were originally developed by CAD drawings obtained from the original bridge construction plans. However, all dimensions shown in the bridge plans were verified during in-site field inspections.

Due to the absence of experimental data, as an initial step this study incorporates the FEA validation procedures recommended by Liao and Okazaki (2009). These procedures are divided in two other independent studies consisting of bolted tension (Hardash and Bjorhovde, 1985) and bolted compression (Yam and Cheng, 1993) connections, respectively. In summary, they recommend to use: i) eight-node linear brick elements, full (C3D8) or reduced integration

(C3D8R); ii) sixteen (16) elements surrounding the bolt holes; iii) two (2) or three (3) elements along the thickness dimension of the gusset plate. Following these recommendations, the computational models within the present study incorporate C3D8R elements selected from Abaqus element library.

Connection J-6 consists of the truss elements sections W8X31, W8X24, W8X17 and C8X13.75, connected through a pair of riveted gusset plates. The gusset plates and the truss elements were modeled as 3-D deformable, solid extrusion parts, while rivets were modeled as cylindrical 3-D deformable and solid extrusion parts interacting with the rivet holes perimeter (Figure 19). A uniform load pressure of 8.2 ksi located 0.3 inches around the rivet head was applied to simulate the pre-tension of the rivets according to the minimum value specified by the Research Council on Structural Connections (RCSC 2004). In addition, the rivets heads were incorporated in the analysis and general contact conditions were applied to provide adequate interaction and load transfer between parts (i.e., rivet and plate). A Coulomb friction model using a coefficient of 0.1 was introduced into the general contact between parts. The entire connection was generated and modeled to adequately represent load and geometry asymmetry conditions.

Accordingly to Berman et al. 2010, a distance of twice the element depth ($2d$) from the gusset plate edge was found to satisfactorily transfer the stresses from the truss member to the gusset plate. The target connection has a transition from solid elements to the beam element representation at a distance $2d$ (Figure 17). The transition from solid elements to beam elements was constrained using kinematic coupling constrains (Figure 18). This feature constrains the motion and transfers the loads of both parts making them to behave like a continuous element. The beam part of the connection was modeled using the Abaqus B31 element, which uses the

Timoshenko beam formulation. The other sub-models presented in this study were developed based on the modeling techniques presented in this chapter.

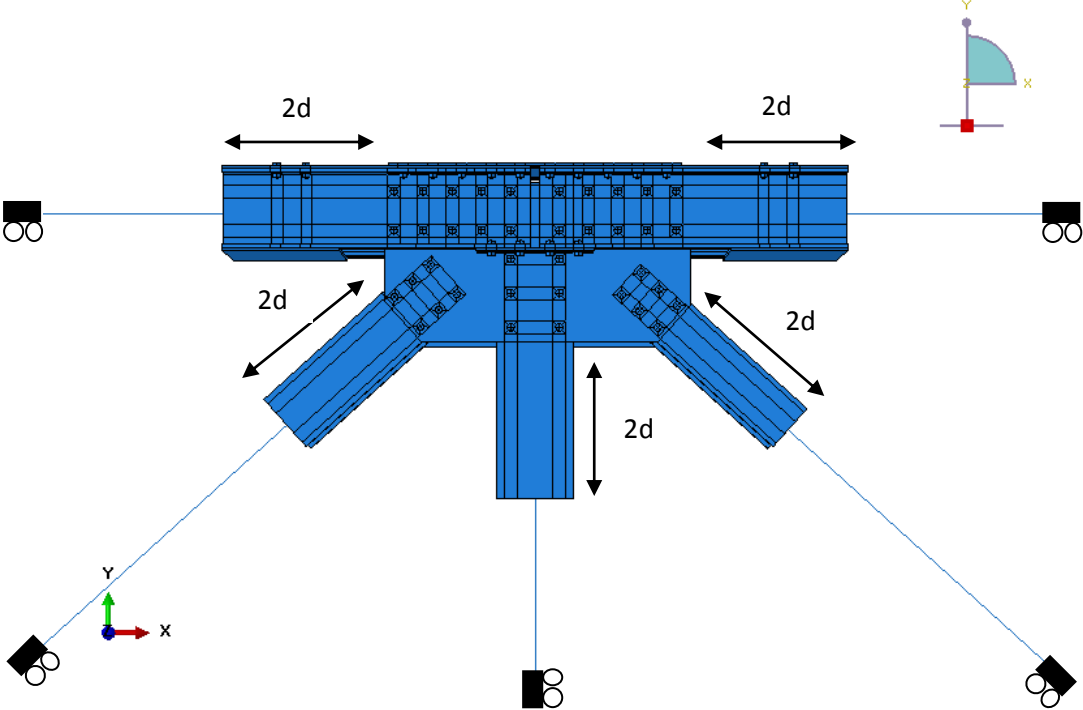


FIGURE 17: GENERAL J-6 CONNECTION MODEL.

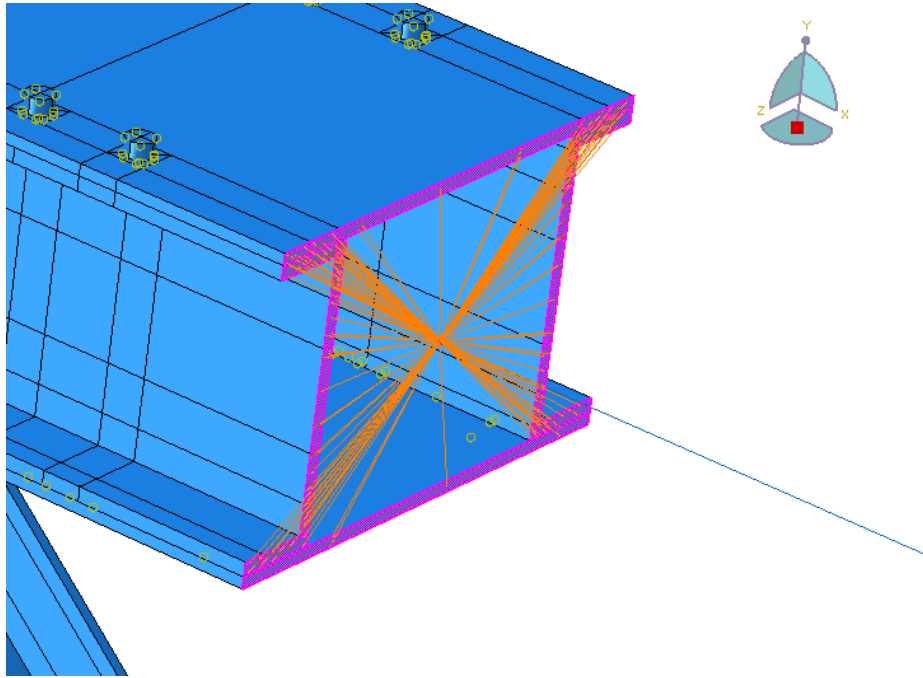


FIGURE 18: KINEMATIC COUPLING CONSTRAIN BETWEEN SOLID AND BEAM ELEMENTS.

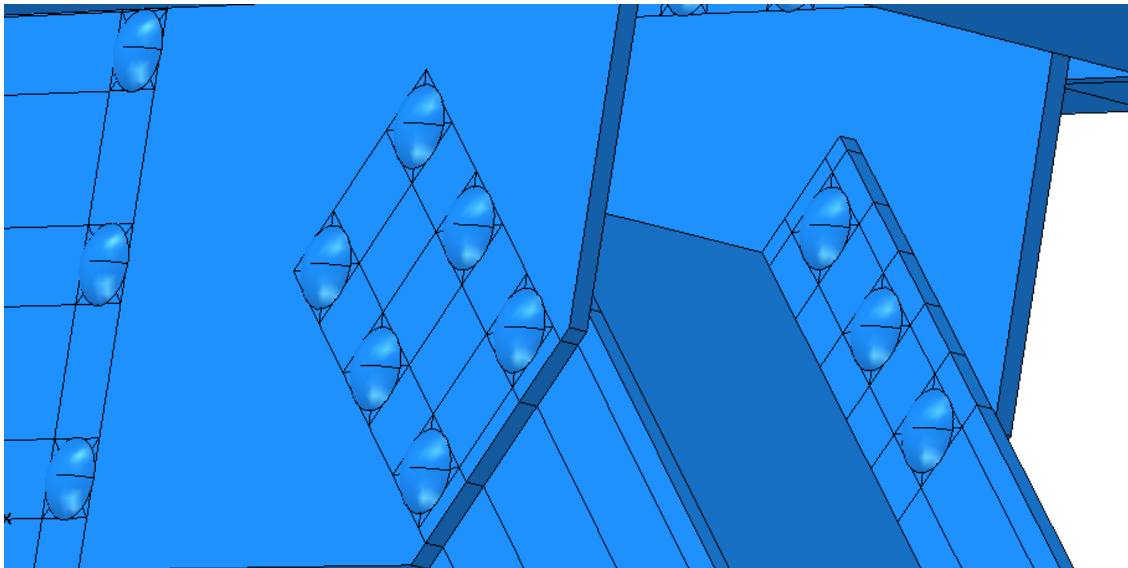


FIGURE 19: RIVETS INTERACTING WITH THE PERIMETER OF RIVET HOLES.

4.3. LOADING, BOUNDARY CONDITIONS, AND MATERIAL PROPERTIES

Internal loading conditions for the FEM representing the connections were obtained from the global model analysis using SAP2000 (Chapter 5, Section 5.2). All translations were restrained except in the longitudinal direction (Figure 17). The type and locations of the boundary conditions provides an adequate representation of the connection when it experiences out-of-plane displacements, avoiding the possibility to develop unrealistic buckling loads results (Berman et al. 2010).

Figure 20 depicts the direction of the internal forces obtained from the global model results, in which three are in compression (D-9, T-8 and T-12) and the other two (V-11 and D-13) are in tension. These internal loads in the global model were axially applied as an external load at the end of each beam element of connection J-6.

Gusset plates, elements and rivets consist of typical isotropic elasto-plastic steel material with yield stress of 33 ksi, modulus of elasticity of 29,000 ksi and a Poisson ratio of 0.3. The stress-strain relationship was transformed into an estimated true stress – true strain constitutive relationship as shown in Figure 21.

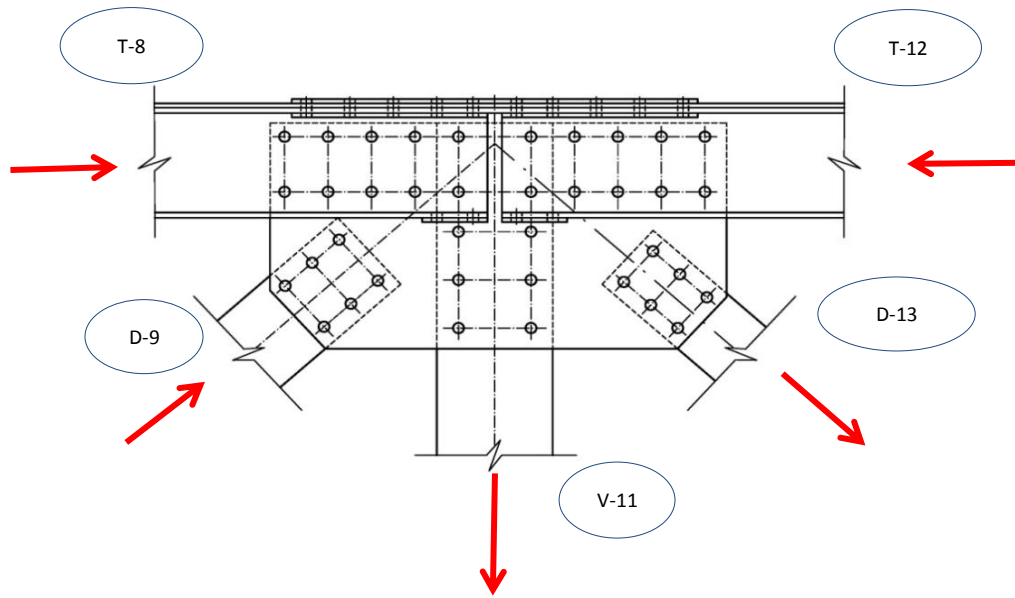


FIGURE 20: FORCES DIRECTION FOR EACH MEMBER.

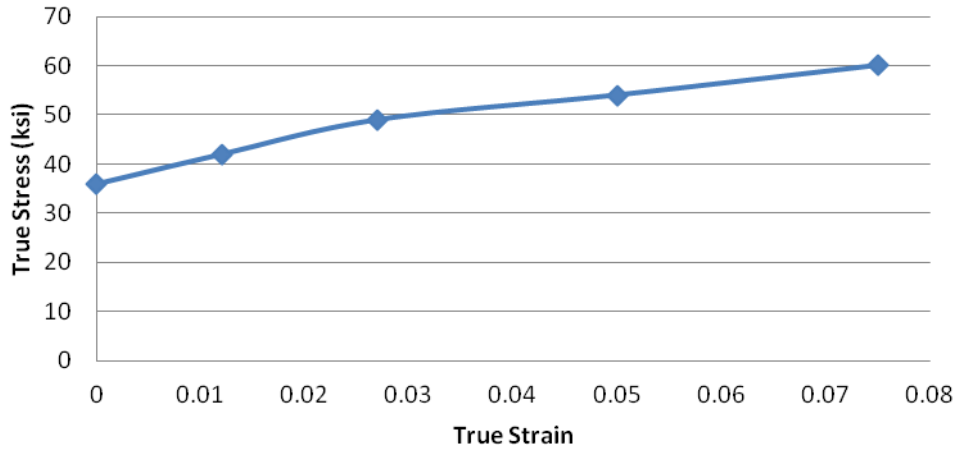


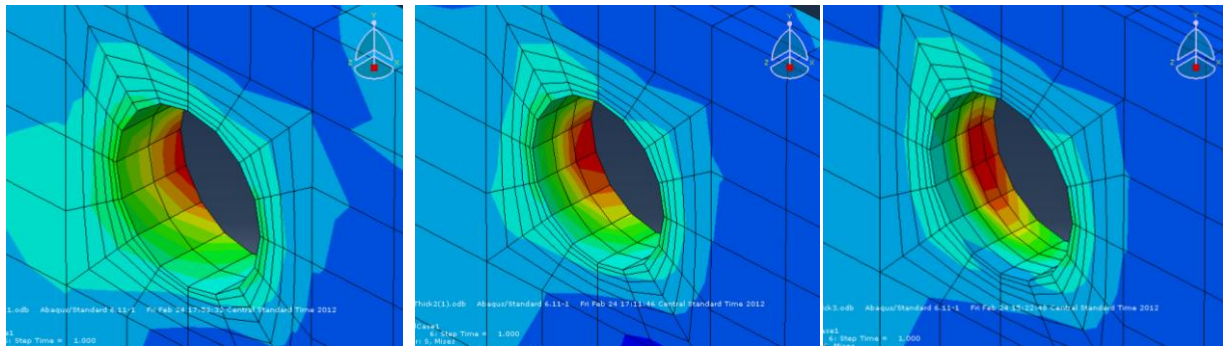
FIGURE 21: STEEL TRUE STRESS-STRAIN CURVE (NON-LINEAR REGIME)

4.4. MESH REFINEMENT

As part of the development of the FE gusset plate connections, a mesh refinement was performed in connection J-6 to obtain a model capable to represent more precise results. The mesh refinement criteria applied was stress convergence, achieved when stress difference between models are 5% or less. Von Mises stress, membrane stress (S_{xx} and S_{yy}) and shear stress (S_{xy}) were calculated. Two directions in the mesh refinements were developed, i.e., across the gusset plate thickness and throughout the X-Y plane.

4.4.1. MESH REFINEMENT ACROSS GUSSET PLATE THICKNESS

Three different models were analyzed to study the effect of element quantity across the gusset plate thickness. These consist of two (case a), three (case b), and five (case c) elements across the gusset plate thickness. Random points within the plate thickness were selected to evaluate the stress convergence. Figure 22 (cases a, b, and c) shows the mesh densities generated across the plate thickness. Table 6 shows an average percentage difference of stresses. Results show that for all stresses between cases b and c (Figure 22) the differences are equal or less than 5%. Therefore, it was determined to use three elements across the thickness to provide reliable results.



a)

b)

c)

FIGURE 22: THREE DIFFERENT THROUGH THE THICKNESS ELEMENTS QUANTITIES: A) TWO ELEMENTS, B) THREE ELEMENTS, AND C) FIVE ELEMENTS.

TABLE 6: PERCENTAGE DIFFERENCES BETWEEN ELEMENTS ACROSS THE THICKNESS.

Stress Percentage of Difference				
Models	Mises(%)	S_{xx} (%)	S_{yy} (%)	S_{xy} (%)
a - b	1.61	4.38	7.26	7.60
b - c	1.53	0.94	3.05	2.19

4.4.2. MESH REFINEMENT THROUGHOUT X-Y PLANE

Four different models were also studied to estimate a reliable mesh density in the X-Y plane. Figure 23 shows the four random points selected for each model in which the following stresses were calculated (Table 8): Von Mises, normal (S_{xx} , S_{yy}) and shear (S_{xy}). A mesh refinement was also studied in the truss members that are connected to the gusset plate, but the variations in results were negligible. Figure 24 shows the four models having 20,847 (case a), 56,601 (case b), 81,480 (case c), and 100,200 (case d) elements, respectively. Table 8 shows the stress percentage difference between the models. Between the cases considered, results showed that case d represents the smallest appropriate mesh density for the final model. Figure 25 shows a general view of connection J-6 with the final selected mesh density.

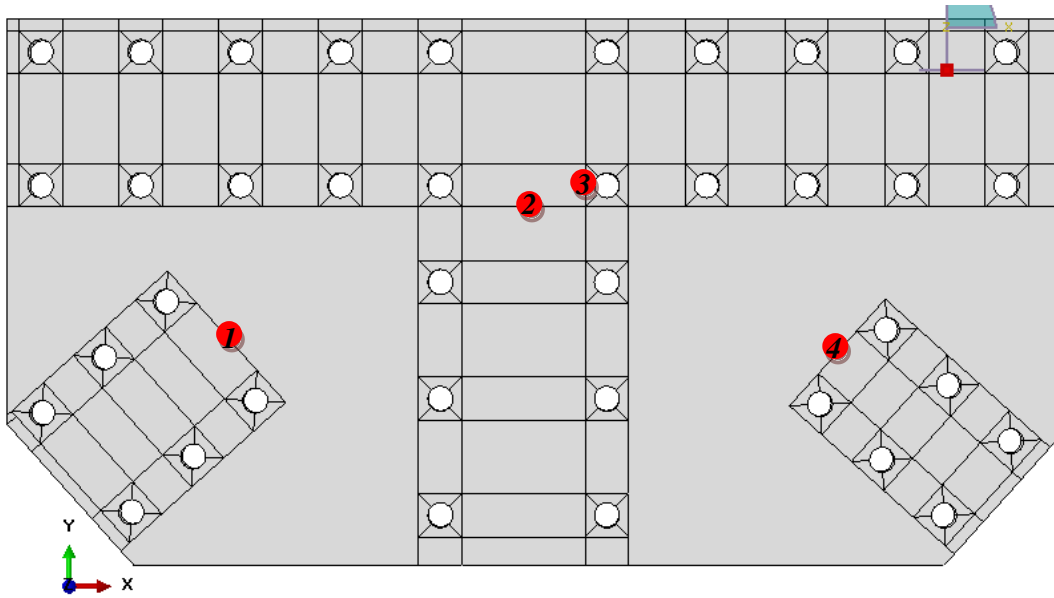


FIGURE 23: POINTS SELECTED IN THE GUSSET PLATE.

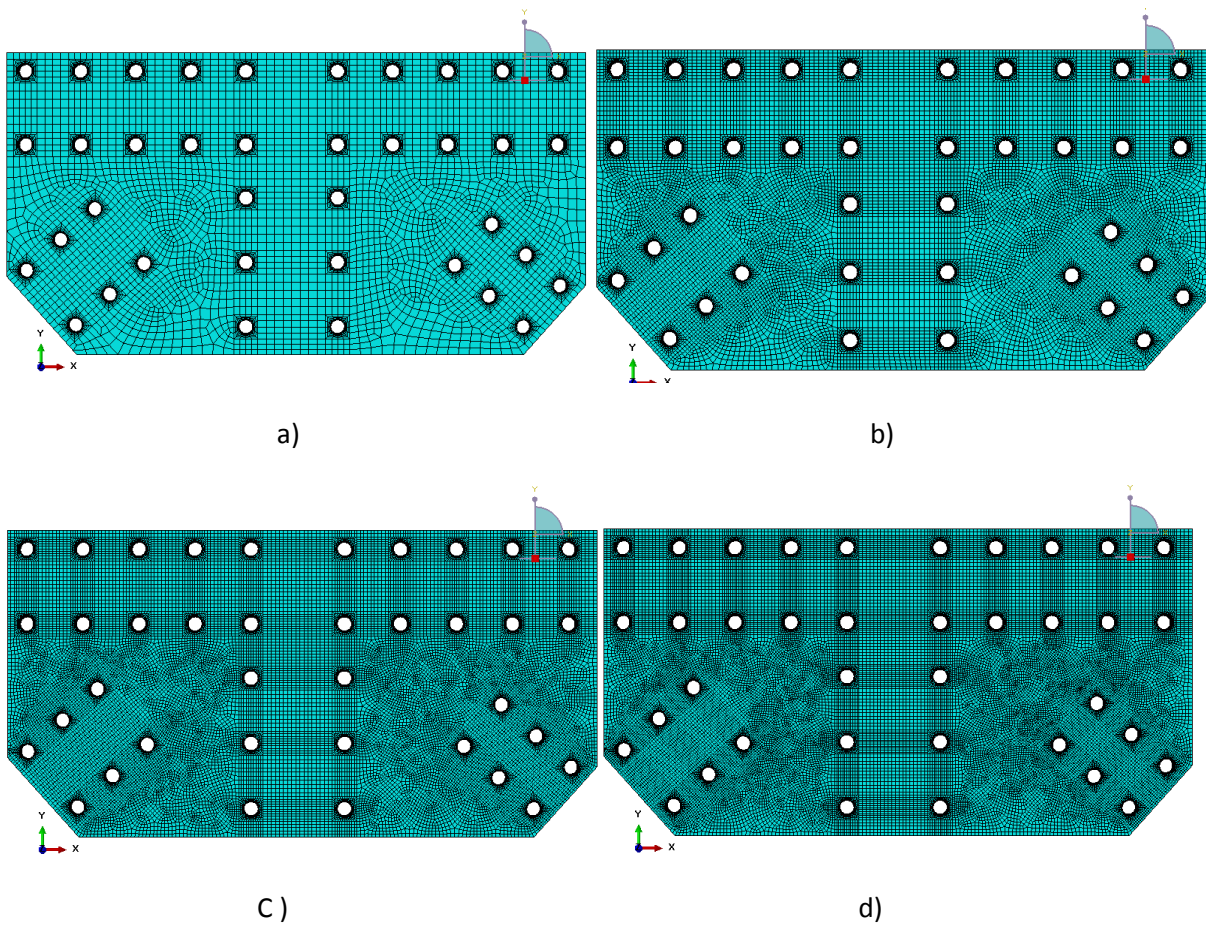


FIGURE 24: THREE DIFFERENT MESH REFINEMENT, A) 20,847 ELEMENTS, B) 56,601 ELEMENTS, C) 81,480 ELEMENTS, D) 100,200 ELEMENTS.

TABLE 7: STRESSES RESULTS FOR THE DIFFERENT MODELS.

Point	Number of Elements	Mises Stress (psi)	S _{xx} (psi)	S _{yy} (psi)	S ₁₂ (psi)
1	20,847	595.74	-411.91	-430.68	235.98
2		964.84	-631.56	-248.81	-456.95
3		7928.16	-91.28	-2440.28	-340.93
4		1206.21	-559.25	-947.08	-519.79
1	56,601	555.74	-417.14	-396.46	215.62
2		936.19	-580.83	-240.14	-455.34
3		7734.03	-105.34	-2787.86	-190.46
4		1149.42	-545.99	-971.04	-457.50
1	81,480	525.13	-367.77	-374.86	212.88
2		929.41	-571.95	-216.03	-450.57
3		7742.98	-81.69	-2806.33	-172.28
4		1102.28	-484.59	-900.26	-438.65
1	100,200	502.65	-358.01	-362.12	203.40
2		968.74	-593.61	-225.40	-458.42
3		7704.72	-79.50	-2820.90	-164.33
4		1059.92	-469.27	-891.03	-422.21

TABLE 8: STRESS PERCENTAGE DIFFERENCES BETWEEN MODELS.

Models	Point	%Diff. Mises	%Diff. S _{xx}	%Diff. S _{yy}	%Diff. S ₁₂
(1-2)	1	7.20	1.25	8.63	9.44
	2	3.06	8.73	3.61	0.35
	3	2.51	13.35	12.47	79.00
	4	4.94	2.43	2.47	13.62
(2-3)	1	5.83	13.42	5.76	1.29
	2	0.73	1.55	11.16	1.06
	3	0.12	28.94	0.66	10.55
	4	4.28	12.67	7.86	4.30
(3-4)	1	4.47	2.73	3.52	4.66
	2	4.06	3.65	4.16	1.71
	3	0.50	2.76	0.52	4.84
	4	4.00	3.26	1.04	3.89

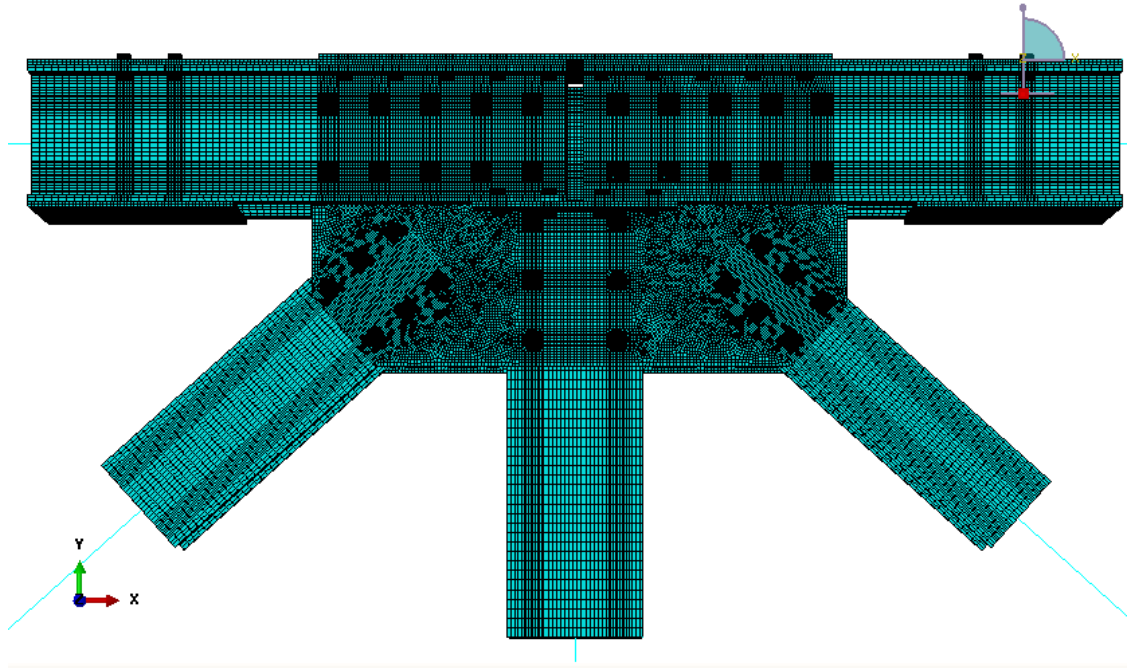


FIGURE 25: FINAL FE MODEL.

CHAPTER 5

5. ANALYSIS AND RESULTS

5.1. INTRODUCTION

The following sections present a computational study of critical connections in the target bridge. Section 5.2 shows the results obtained to evaluate the general condition of the bridge, subjected to the loading conditions specified in the MBE (2011), and the corresponding loads in critical connections. Section 5.3 presents the fatigue analysis of the bridge based on AASHTO 2007. Section 5.4 shows results of two modeling techniques that were selected to study gusset plate connections. For each case, the pros and cons are described in order to select the most reliable method to analyze gusset plate connections with FEM. Section 5.5 presents a FEA of connection J-6. Hand-calculations provided in Appendix A were compared to the FEA results summarized in this section. The computational model applied in this study seems to be the most realistic representation to analyze steel gusset plate connections. It provides techniques to study in detail the structural mechanics of each component (i.e., interaction between rivets, elements, and gusset plates).

Sections 5.6 through 5.8 address possible failures scenarios for the selected critical connections. These are: i) tensile capacity, ii) shear capacity of rivets, and iii) buckling capacity. Section 5.6 is mainly focused in the verification of current equations specified by applicable standards to determine the tensile capacity of gusset plates. Section 5.7 shows the behavior of rivets under variable diameter reductions and due to missing rivets in the connection. Furthermore, the shear capacity equations proposed by different authors to evaluate steel rivets were compared with the computational results of this study. Section 5.8 summarizes results for

the buckling capacity of the critical gusset plate connection (J-6). The study comprises the following parameters: i) thickness reduction in gusset plates and ii) increment in unbraced length.

5.2. COMPUTATIONAL STUDY OF THE TARGET BRIDGE

As an initial task, the target bridge described in Chapter 3 was structurally evaluated based on the Manual for Bridge Evaluation MBE (2011). The entire bridge was modeled using the finite element program SAP2000 (2009). The overall condition of the bridge seems to be satisfactory for the posted loads as reported in previous routine inspections. The bridge description herein is limited to the superstructure since substructure conditions are not considered in the load rating evaluation. A step-by-step approach was used for the different stages leading to the bridge rating results. Inventory and operating ratings were conducted based on the HL-93 loading condition provided by AASHTO. However, these loads exceed the bridge capacity (Load Rating less than 1) and legal load configurations were used in addition to military vehicles to rate the target bridge.

As an illustration, the analysis was made with combinations of live and dead loads on the target bridge. The load factors used were those established by AASHTO for the design vehicle (DL = 1.25, LL = 1.75). The live load factor varies for other conditions and for those cases that are provided legal and permit loads. Details of these factors and their use are provided in Chapters 2 and 3.

The design vehicle used is defined in Figure 16 (Chapter 3), neglecting the tandem and the lane loads. In addition, the bridge posting loads (military and civilian) were considered in the analysis (Figure 26). The axial forces found in the most critical elements and connections are shown in Tables 9 through 13. The controlling live load for the bridge was half the weight of a

Type 3 truck. The axial results obtained from half the weight of a Type 3 truck (Table 11) were used to perform the load rating of connections and these were applied in the computational models of connections J-2 and J-6, as shown in the following sections.

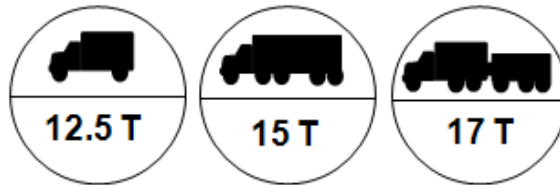


FIGURE 26: BRIDGE POSTING SIGN.

TABLE 9: ENVELOPE FORCES FOR HS20-44 LOADING.

Connection	Element	Service Loads			Factored Loads + Impact	
		S-Dead*	S-Live	S-Live+Imp	F-Dead*	F-Live+Imp [£]
		Kips	Kips	Kips	Kips	Kips
J-2	D-1	-85.1	-50.3	-66.9	-106.4	-117.1
	V-3	19.3	17.5	23.3	24.1	40.7
	T-4	-97.4	-58.1	-77.3	-121.8	-135.2
	D-5	58	38.8	51.6	72.5	90.3
J-6	T-8	-97.4	-58.1	-77.3	-121.8	-135.2
	D-9	-41.6	-34.3	-45.6	-52.0	-79.8
	V-11	15.8	16.4	21.8	19.8	38.2
	T-12	-138.5	-82.1	-109.2	-173.1	-191.1
	D-13	18.9	25.2	33.5	23.6	58.7
J-9	D-13	18.9	25.2	33.5	23.6	58.7
	B-14	108.6	65.5	87.1	135.8	152.5
	V-15	1.8	7.1	9.4	2.3	16.5
	D-18	-3.3	-10.8	-14.4	-4.1	-25.1
	B-19	123.0	72.7	96.7	153.8	169.2

* Includes superimposed dead loads; £ Factored live load and impact

TABLE 10: ENVELOPE FORCES FOR MLC-8 LOADING.

Connection	Element	Service Loads			Factored Loads + Impact	
		S-Dead*	S-Live	S-Live+Imp	F-Dead*	F-Live+Imp [£]
		Kips	Kips	Kips	Kips	Kips
J-2	D-1	-85.1	-5.1	-6.8	-106.4	-11.9
	V-3	19.3	2.5	3.3	24.1	5.8
	T-4	-97.4	-6.0	-8.0	-121.8	-14.0
	D-5	58	4.0	5.3	72.5	9.3
J-6	T-8	-97.4	-6.0	-8.0	-121.8	-14.0
	D-9	-41.6	-3.5	-4.7	-52.0	-8.2
	V-11	15.8	2.4	3.2	19.8	5.6
	T-12	-138.5	-8.5	-11.3	-173.1	-19.8
	D-13	18.9	2.7	3.6	23.6	6.3
J-9	D-13	18.9	2.7	3.6	23.6	6.3
	B-14	108.6	6.8	9.0	135.8	15.8
	V-15	1.8	0.9	1.2	2.3	2.1
	D-18	-3.3	-1.2	-1.6	-4.1	-2.8
	B-19	123.0	7.4	9.9	153.8	17.3

* Includes superimposed dead loads; £ Factored live load and impact

TABLE 11: ENVELOPE FORCES FOR HALF-SCALED TYPE 3 (12.5 TONS) LEGAL NOTIONAL TRUCK.

Connection	Element	Service Loads			Factored Loads + Impact	
		S-Dead*	S-Live	S-Live+Imp	F-Dead*	F-Live+Imp [£]
		Kips	Kips	Kips	Kips	Kips
J-2	D-1	-85.1	-13.6	-18.1	-106.4	-31.7
	V-3	19.3	5.9	7.8	24.1	13.7
	T-4	-97.4	-15.7	-20.9	-121.8	-36.5
	D-5	58	10.6	14.1	72.5	24.7
J-6	T-8	-97.4	-18.9	-25.1	-121.8	-44.0
	D-9	-41.6	-10.5	-13.9	-52.0	-24.4
	V-11	15.8	5.2	6.8	19.8	12.0
	T-12	-138.5	-25.7	-34.1	-173.1	-59.7
	D-13	18.9	7.3	9.7	23.6	17.0
J-9	D-13	18.9	7.3	9.7	23.6	17.0
	B-14	108.6	21.3	28.3	135.8	49.6
	V-15	1.8	2.0	2.7	2.3	4.7
	D-18	-3.3	-2.9	-3.9	-4.1	-6.7
	B-19	123.0	23.9	31.8	153.8	55.6

* Includes superimposed dead loads; £ Factored live load and impact. The LL factor of 1.75 was used for analysis, but it was reduced for load rating

TABLE 12: ENVELOPE FORCES FOR HALF-SCALED TYPE 3S2 (18 TONS) LEGAL NOTIONAL TRUCK.

Connection	Element	Service Loads			Factored Loads + Impact	
		S-Dead* Kips	S-Live Kips	S-Live+Imp Kips	F-Dead* Kips	F-Live+Imp [£] Kips
J-2	D-1	-85.1	-16.8	-22.3	-106.4	-39.1
	V-3	19.3	5.8	7.7	24.1	13.4
	T-4	-97.4	-19.1	-25.4	-121.8	-44.5
	D-5	58	12.6	16.7	72.5	29.2
J-6	T-8	-97.4	-19.1	-25.4	-121.8	-44.5
	D-9	-41.6	-10.6	-14.1	-52.0	-24.6
	V-11	15.8	5.3	7.0	19.8	12.2
	T-12	-138.5	-25.9	-34.4	-173.1	-60.3
	D-13	18.9	7.3	9.7	23.6	17.0
J-9	D-13	18.9	7.3	9.7	23.6	17.0
	B-14	108.6	20.6	27.5	135.8	48.0
	V-15	1.8	2.0	2.6	2.3	4.6
	D-18	-3.3	-2.9	-3.9	-4.1	-6.7
	B-19	123.0	23.2	30.9	153.8	54.0

*Includes superimposed dead loads; £ Factored live load and impact. The LL factor of 1.75 was used for analysis, but it was reduced for load rating.

TABLE 13: ENVELOPE FORCES FOR HALF-SCALED TYPE 3-3 (20 TONS) LEGAL NOTIONAL TRUCK.

Connection	Element	Service Loads			Factored Loads + Impact	
		S-Dead* Kips	S-Live Kips	S-Live+Imp Kips	F-Dead* Kips	F-Live+Imp [£] Kips
J-2	D-1	-85.1	-17.2	-22.9	-106.4	-40.0
	V-3	19.3	5.5	7.3	24.1	12.7
	T-4	-97.4	-19.3	-25.7	-121.8	-44.9
	D-5	58	12.5	16.6	72.5	29.1
J-6	T-8	-97.4	-19.3	-25.7	-121.8	-44.9
	D-9	-41.6	-10.3	-13.7	-52.0	-24.0
	V-11	15.8	4.7	6.3	19.8	11.0
	T-12	-138.5	-26.4	-35.1	-173.1	-61.4
	D-13	18.9	7.0	9.3	23.6	16.2
J-9	D-13	18.9	7.0	9.3	23.6	16.2
	B-14	108.6	20.8	27.6	135.8	48.3
	V-15	1.8	1.6	2.1	2.3	3.7
	D-18	-3.3	-2.7	-3.6	-4.1	-6.2
	B-19	123.0	23.2	30.9	153.8	54.0

*Includes superimposed dead loads; £ Factored live load and impact. The LL factor of 1.75 was used for analysis, but it was reduced for load rating.

5.3. DETERMINISTIC LOAD-INDUCED FATIGUE ANALYSIS

A fatigue analysis was performed to verify that the fracture critical bridge does not present fatigue-induced deterioration. To ensure a safe condition, the connections must provide a nominal fatigue resistance ($\phi\Delta F_n$) greater than or equal to the factored live load stress range due to the fatigue truck ($\gamma\Delta f$). The fatigue limit state factor is $\phi = 1$.

The sample connection #21 is represented in the target bridge (Table 6.6.1.2.3-1, AASHTO LRFD 2007). Therefore, the net section of riveted connections must be checked for a detail category D. The fatigue resistance ΔF_n can be estimated based on a deterministic approach as

$$\Delta F_n = \left(\frac{A}{N}\right)^{1/3} \geq \frac{1}{2}\Delta F_{TH}$$

where, ΔF_{TH} is the fatigue threshold stress (Table 6.6.1.2.5-1, AASHTO LRFD 2007); A is the detail category (Table 6.6.1.2.5-1, AASHTO LRFD 2007); and N is the number of stress range cycles estimated as:

$$N = (365)(n_y)(n)(ADTT) = (365)(53)(11.5) = 222,467.5$$

where, n_y is the number of years since the bridge construction; n is the number of stress-range cycles per truck passage (Table 6.6.1.2.5-2, AASHTO LRFD, 2007); and ADTT is the frequency of the fatigue load, assumed as $115*0.1 = 11.5$. During the visual and physical inspection were observed very low fractions of trucks in traffic. Thus, the fraction of trucks in traffic was estimated as 0.1.

The fatigue resistance results,

$$\Delta F_n = \left(\frac{22 \times 10^8 \text{ ksi}}{222,467.5}\right)^{1/3} = 21.46 \text{ ksi} \geq 1/2(7 \text{ ksi})$$

The single design truck (20 Tons) with rear axles at a spacing of 30 ft was placed within the lane boundaries. Table 14 shows the results obtained in critical connections of the target bridge. The factored live load considers the dynamic load allowance (15%) and the fatigue load factor (0.75). The table also shows the fatigue criteria used, which is based on the net applied tensile stress or cases where the permanent loads produce compression stress levels less than twice the maximum tensile live load stress. From the results in Table 14, the critical truss elements are: V-3, D-5, V-11, D-13, B-14, V-15, D-17, D-18 and B-19. From these, the most critical vertical, diagonal and bottom chord elements were selected and their associated connections, i.e. V-3, D-5, and B-19.

TABLE 14. FATIGUE CHECK CRITERIA TO DETERMINE POSSIBLE FATIGUE CONDITIONS

Element	Service Dead	Tension		Compression		Rate	Net	Fatigue
	SDead*	SLive	FLive+Imp	SLive	FLive+Imp		Tension	Check
	Kips	[Kips]	[Kips]	[Kips]	[Kips]		[Kips]	[Yes/No]
V-3	19.3	12.6	10.9	0	0.0	N/A	12.6	Yes
D-5	58	24.6	21.2	-0.24	-0.2	N/A	24.6	Yes
V-11	15.8	11.3	9.8	-0.11	-0.1	N/A	11.32	Yes
D-13	18.9	14.1	12.2	-5.3	-4.6	N/A	14.14	Yes
V-15	1.8	3.7	3.2	-3.0	-2.6	N/A	3.68	Yes
D-17	-3.2	4.1	3.5	-5.0	-4.3	<2	-7.3	Yes
B-14	108.6	39.9	45.9	0.0	0.0	N/A	39.87	Yes
V-15	1.8	3.7	4.2	-3.0	-2.6	N/A	3.68	Yes
D-18	-3.3	3.5	4.0	-5.6	-4.8	<2	-6.76	Yes
B-19	123.0	44.2	50.8	0.0	0.0	N/A	44.16	Yes

However, the design vehicle is not allowed to transit the bridge due to posting limits previously established. Even though fatigue conditions did not control the target bridge analysis, the following part shows an illustrative example of how to verify if fracture critical details are satisfactory based on the 20 Tons truck (AASHTO LRFD 6.6.1).

Connection J-9, element B-19:

Element W8x17

Fatigue Resistance: 21.46 ksi

Net area: 3.93 in²

γT_{LL} = Factored live load fatigue stress in tension = 5.39 ksi

γC_{LL} = Factored live load fatigue stress in compression = 0.06 ksi

FSR = Fatigue Stress Range = $\gamma T_{LL} + \gamma C_{LL}$ = 5.45 ksi

Fatigue Check: 5.45 < 21.46; OK.

5.4. MODELING TECHNIQUES

For critical connections, two modeling techniques were studied: i) the realistic 3-D deformable contact rivet model and ii) the fastener technique provided by Abaqus. The last technique is the most commonly used in the development of FE computational models of steel connections due to the following: i) simplicity assembling the model, ii) reduction in computational time execution as compared to the 3-D contact model, and iii) small susceptibility to local instabilities problems. Contrarily, the 3-D deformable rivet model is a more realistic technique that takes into account the following: i) rivets strength capacity, ii) interaction between the rivet and holes, iii) connected parts, iv) rivet holes, and v) stress concentration generated around the rivet holes. Two models were developed to compare both techniques, validating the advantages and disadvantages mentioned before and to select which seems the most appropriate to study gusset plate connections.

5.4.1. 3-D DEFORMABLE CONTACT RIVET TECHNIQUE

This technique seems to be the most detailed and realistic load transfer model used for gusset plates connections. As mentioned before, this technique is not commonly used in the study of

gusset plates due to its complexity. It could be suitable when the connection does not have a large number of rivets or bolts. Chu and Ip (2000) and Liao et al. 2010 were ones of the few authors that utilized this technique in their investigations. However, those two studies simplified their models idealizing the rivets as rigid bodies. In this study, the rivets and all the other connection components are modeled as a deformable solid extrusion parts. General contact interaction was used in the model to define contact between parts.

5.4.2. FASTENER TECHNIQUE

The “Fastener” technique has been created in Abaqus to easily develop structural models that contain rivets or bolts. Due to its simplicity, this technique is used frequently to study gusset plates. It generates a point-to-point connection between faces. The fastener technique used in this study is the point based rigid multi-point-constrain (MPC).

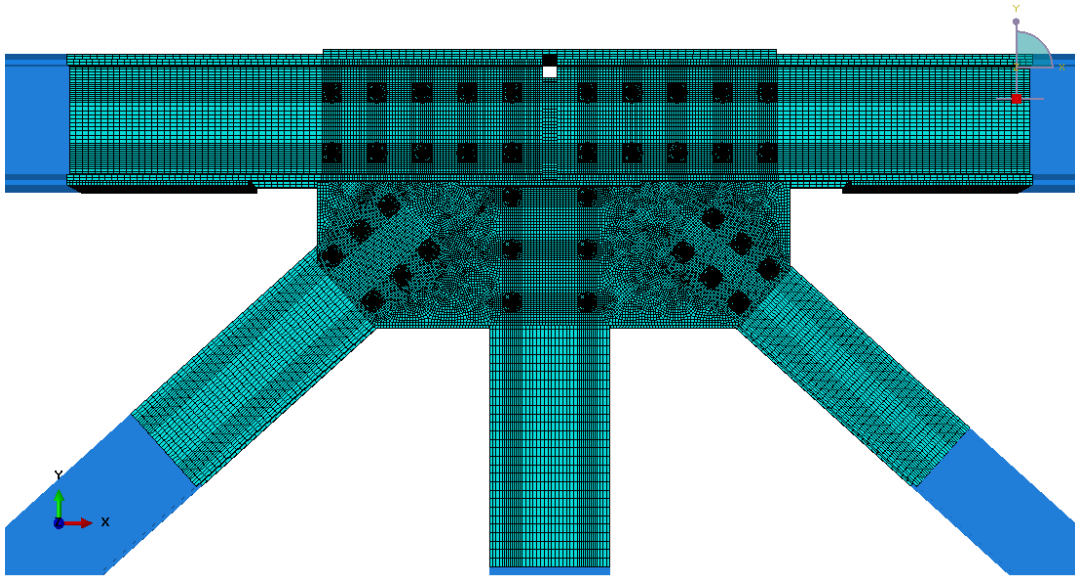
5.4.3. COMPARISON OF MODEL TECHNIQUES

Figure 27 shows the computational models to be compared. Both models have the appropriate mesh density based on the convergence study mentioned in Chapter 4, Section 4.4. They have the same boundary conditions, loads, and material properties. Factorized loads for the Half-Scale Type 3 legal load was applied on each axial element. The results comprise von Mises, shear, and local (axial) stress distribution for connection J-6. The program was executed in the supercomputer located in the Information Technology Laboratory (ITL) of the U.S. Army Research and Development Center (ERDC). The 3-D contact rivet model took 11.28 hours while the fastener model took 8.51 hours to execute the FEA. In terms of computational time, it seems that the fastener technique is 33% more efficient than the 3-D contact rivet technique.

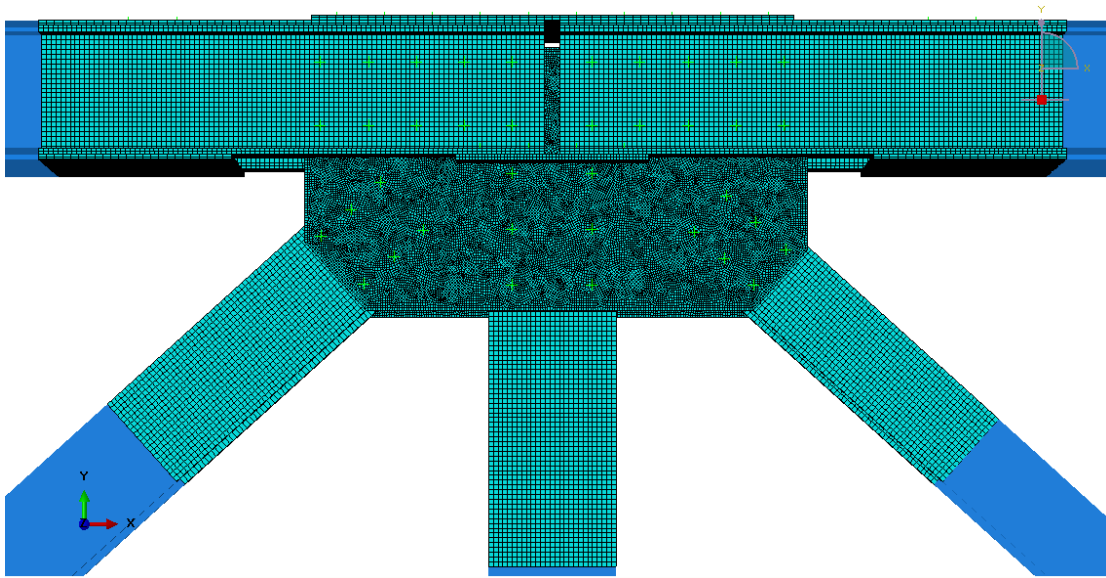
The von Mises stress distributions for the entire connection present very similar stress contours showing the maximum von Mises stress in the same location (Figure 28). A difference

of 1 ksi (3-D = 34 ksi and Fastener = 33 ksi) is obtained in the maximum von Mises stress. The gusset plates present the same results as the entire connection for von Mises and shear stresses distribution (Figure 29 and 30). In contrast to the maximum the von Mises, the maximum shear stress has a difference of approximately 7 ksi located in the first rivet of element T-12 (Figure 31). The local stress (axial direction) in elements D-9 (compression) also showed similar axial stress distribution while the maximum negative stresses values have a difference of approximately 20 ksi for D-9 (Figure 32). These differences in maximum stress could be due to the fact that the fastener technique does not take into account the stress concentration generated in the rivet holes.

Based on these results, the fastener technique seems to be the best method to use due to similarities in stress distribution when compared to the 3-D contact rivets. Furthermore, the simplicity to generate the model, the small potential to involve convergence problems (local instabilities), and the FEA execution (33% faster than the 3-D contact rivet) makes the fastener technique a simple and reliable method for analysis. On the other hand, if the study address stress distributions near the rivet holes and it is desired to quantify the rivet strength in the connection, then the 3-D contact rivets technique is preferable.

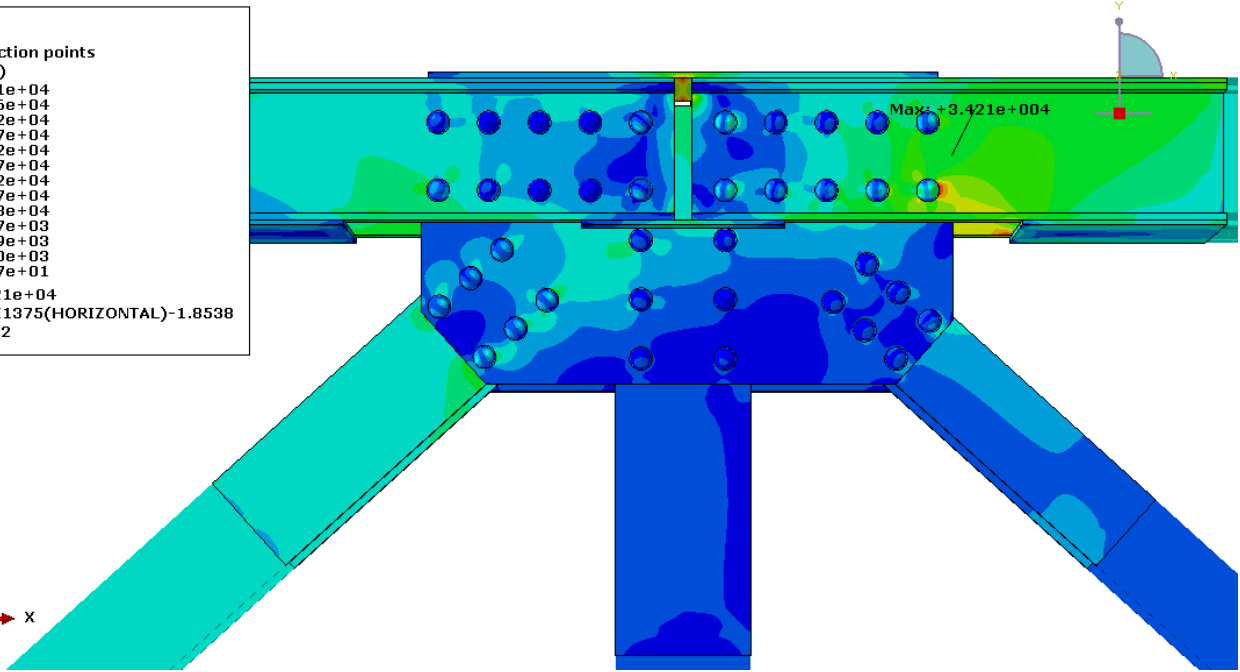
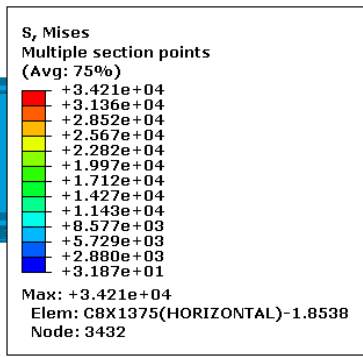


a)

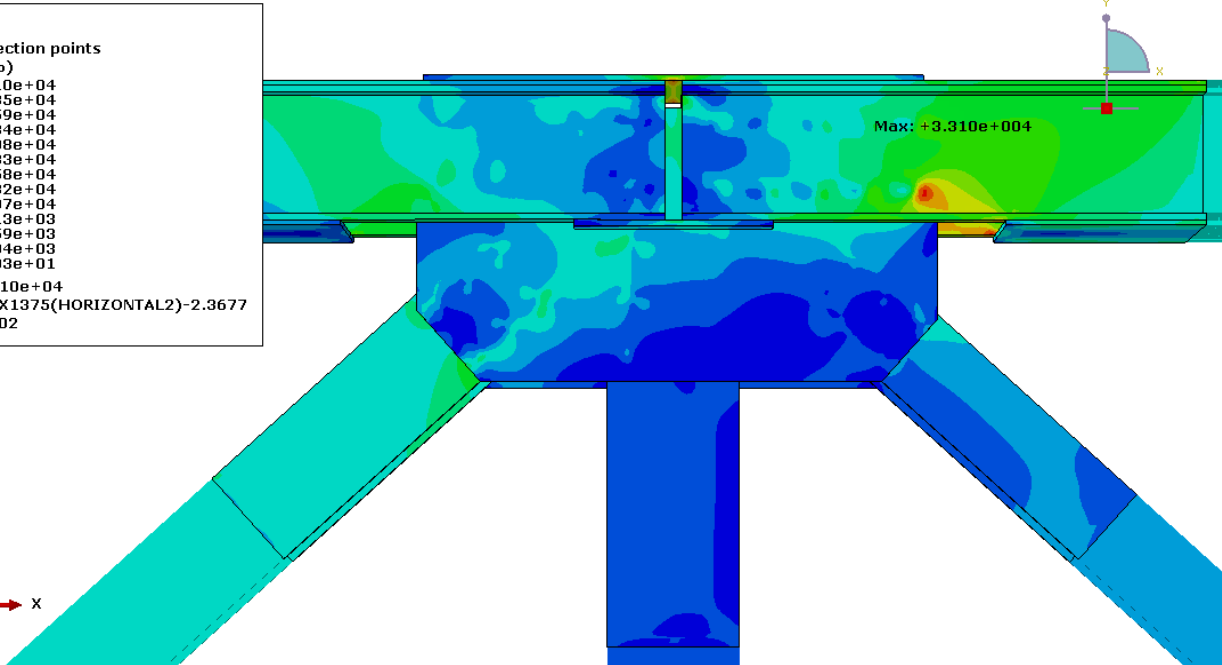
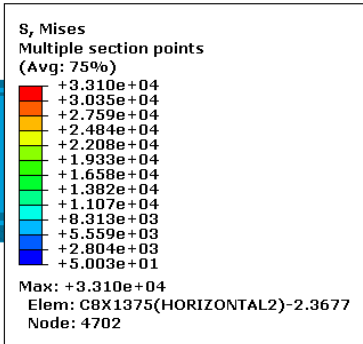


b)

FIGURE 27 : TWO MODELING TECHNIQUES: A) 3-D DEFORMABLE RIVETS AND B) FASTENER RIVETS.

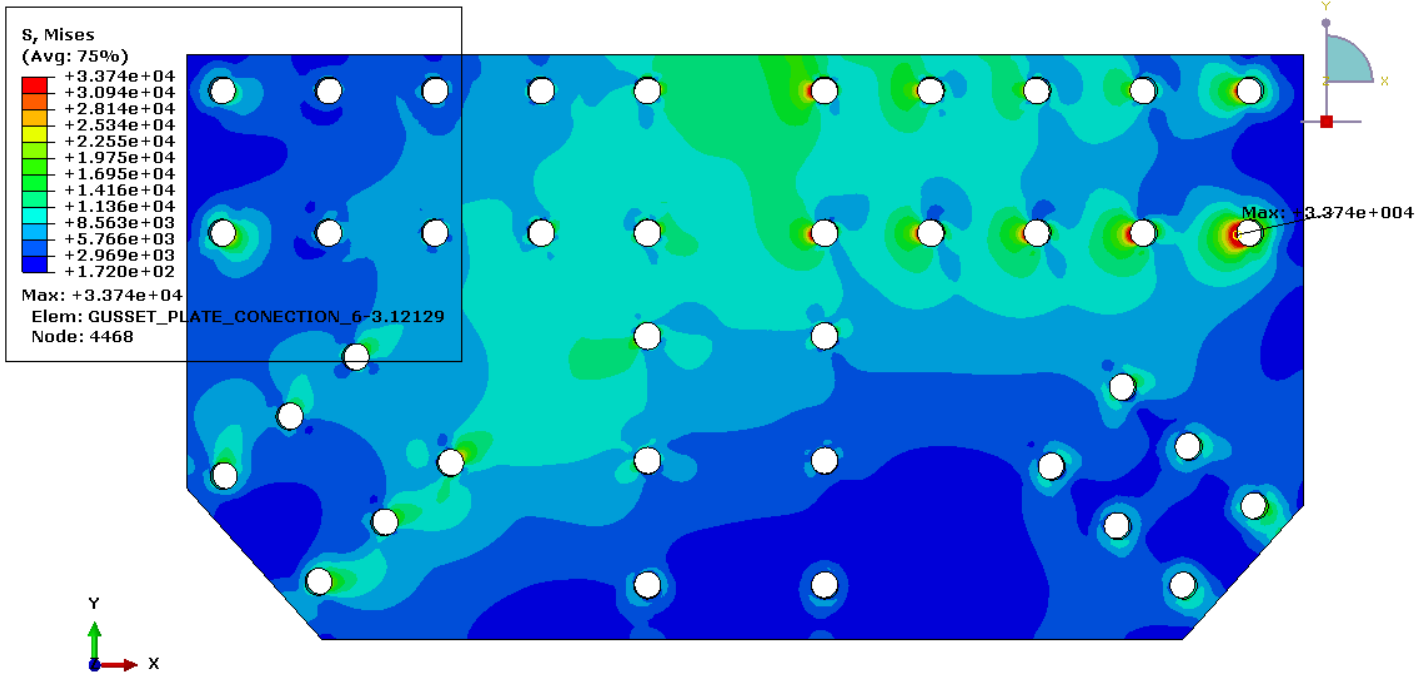


a)

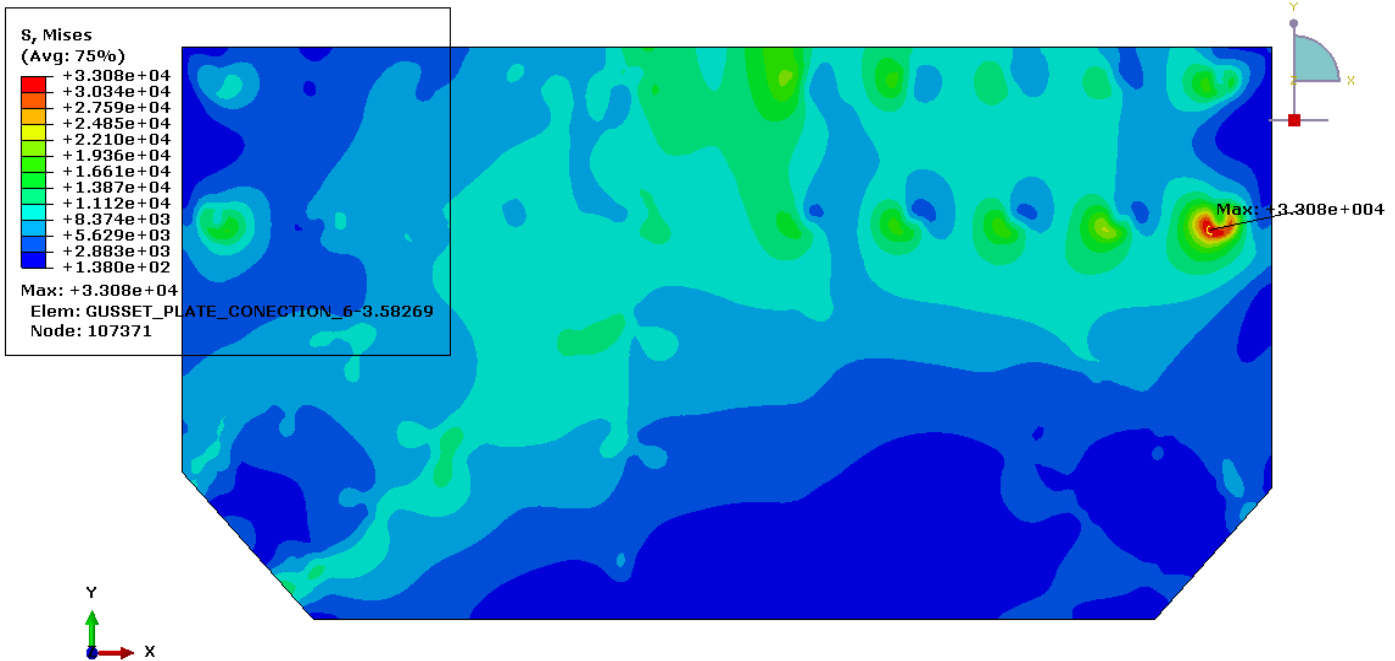


b)

FIGURE 28: VON MISES STRESS DISTRIBUTION OF THE TWO TECHNIQUES (KSI): A) 3-D DEFORMABLE RIVETS AND B) FASTENER RIVETS.

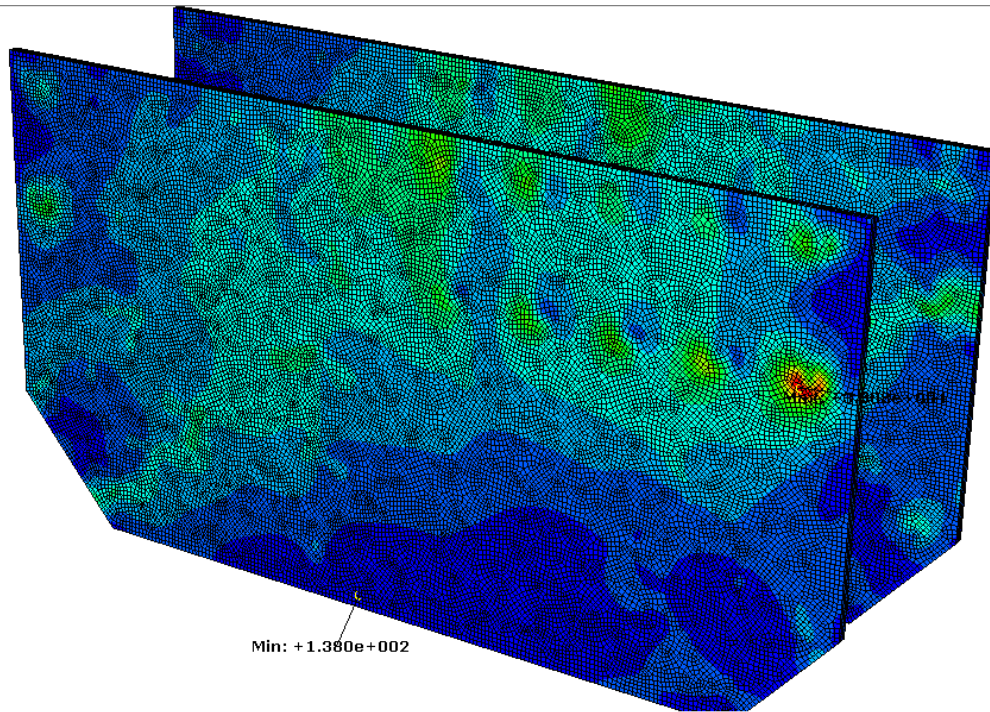


a)

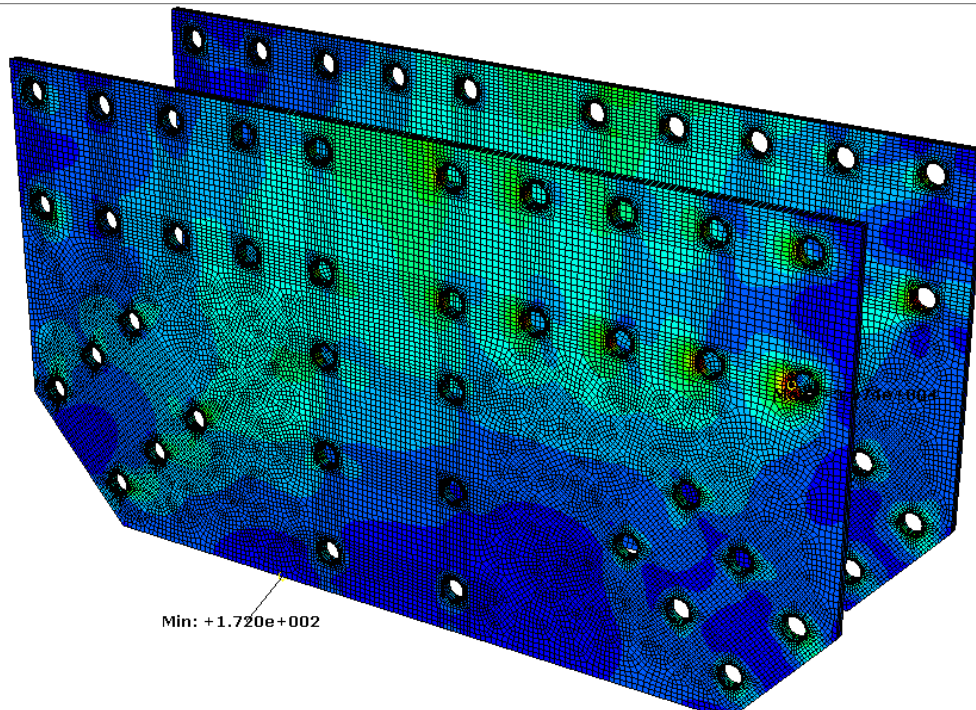


b)

FIGURE 29: VON MISES STRESS DISTRIBUTION FOR THE GUSSET PLATES (KSI): A) 3-D DEFORMABLE RIVETS AND B) FASTENER RIVETS.



a)



B)

FIGURE 30: 3-D VIEW AND MESH ILLUSTRATION OF BOTH TECHNIQUES: A) 3-D FASTENER B) 3-D RIVETS.

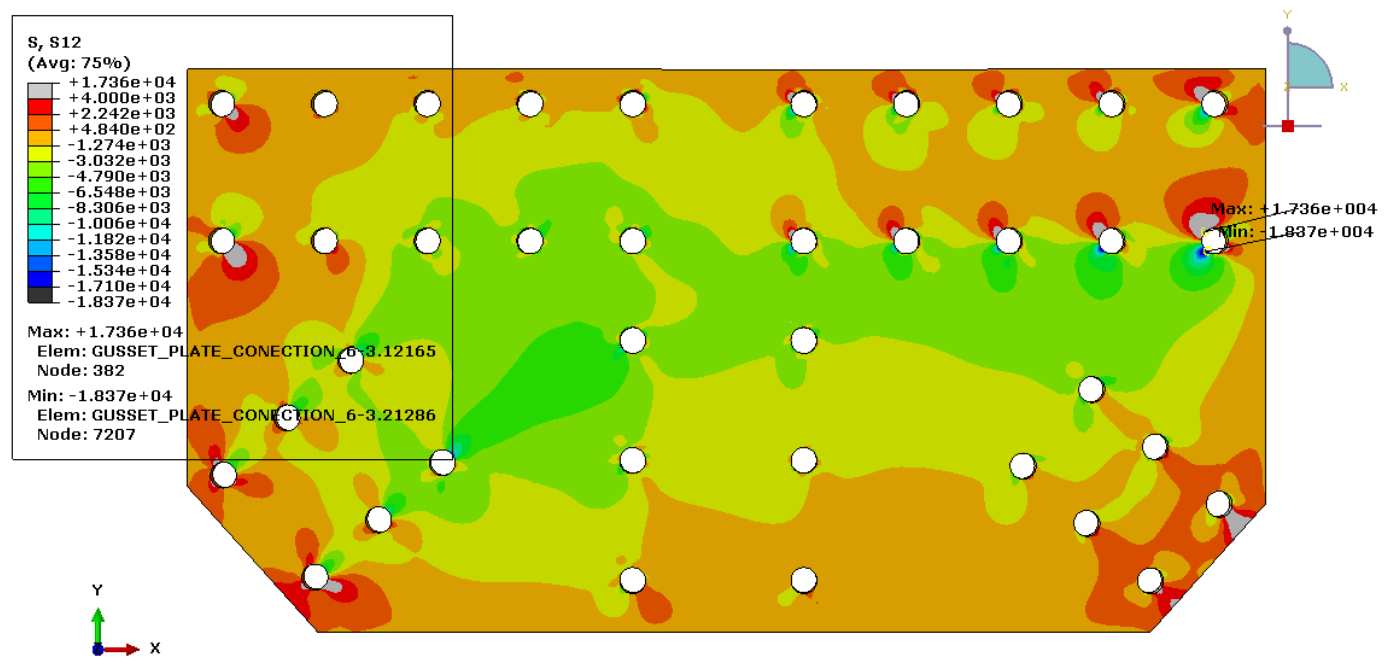
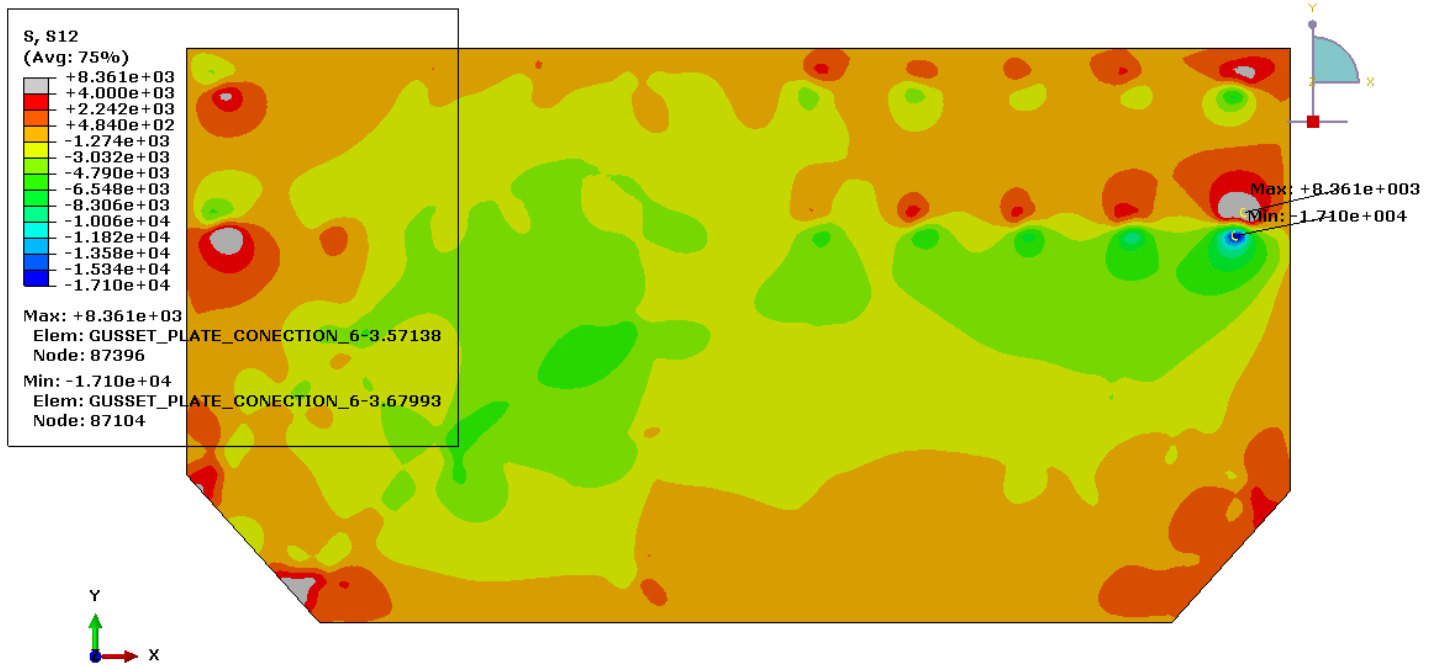
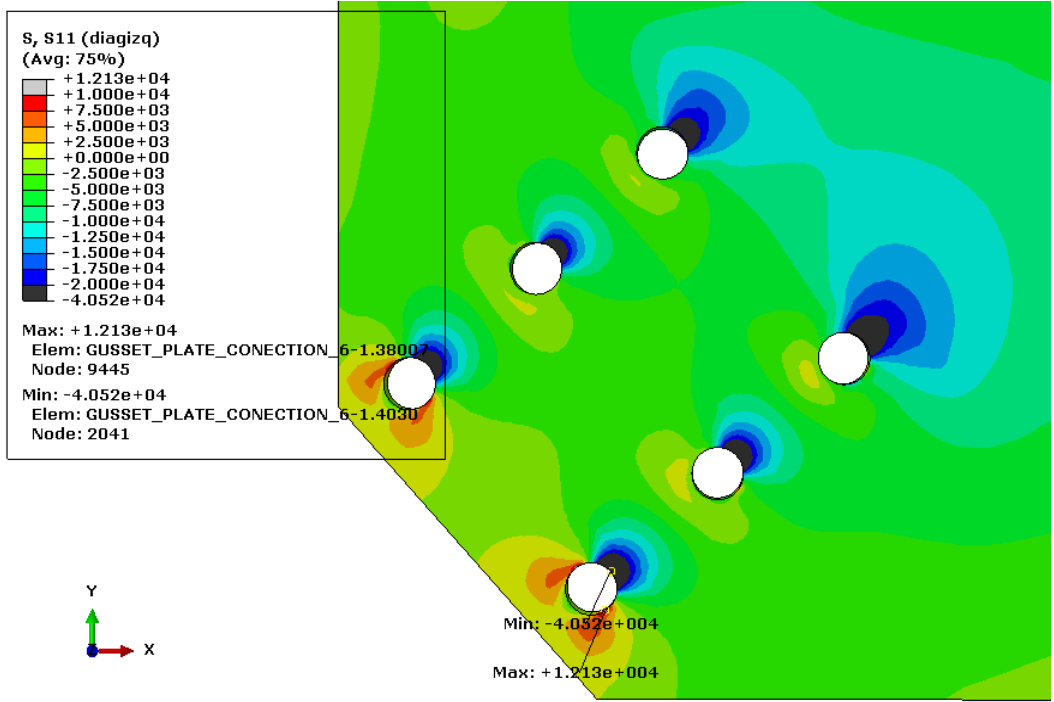
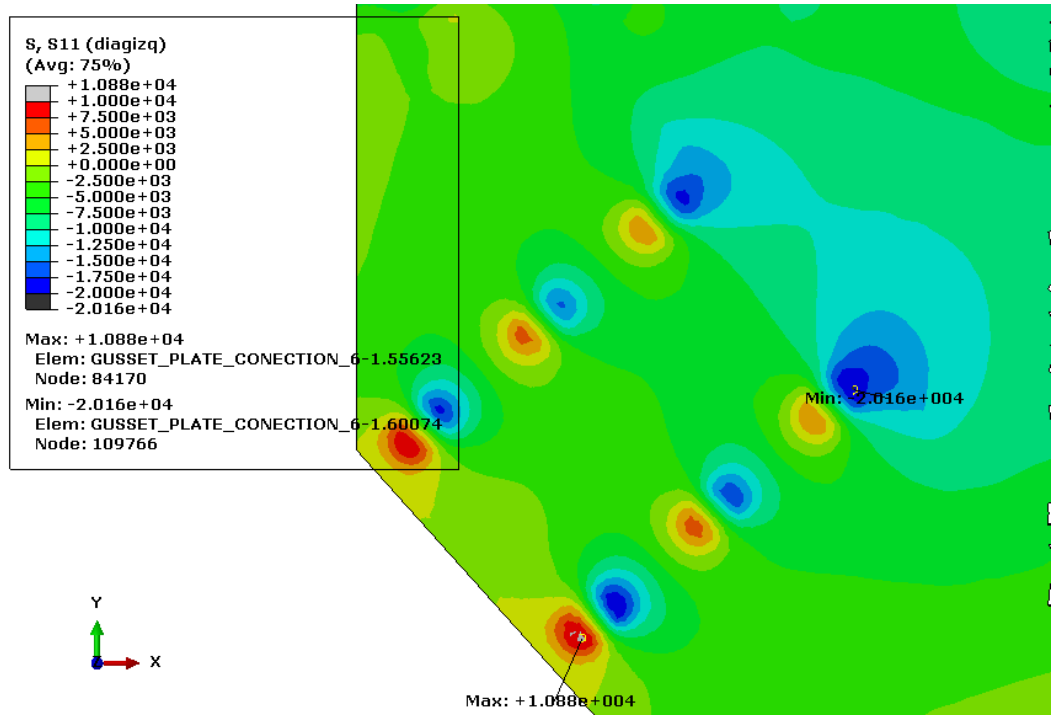


FIGURE 31: SHEAR STRESS DISTRIBUTION COMPARISON (KSI): A) FASTENER AND B) 3-D RIVETS.



a)



b)

FIGURE 32: DIAGONAL D-9 LOCAL STRESS DISTRIBUTION (KSI): A) 3-D RIVET AND B) FASTENERS.

5.5. FEA OF CRITICAL CONNECTION J-6

According to Table 6A.4.2.2-1 (MBE 2011) the corresponding load factors for the target bridge are 1.25 and 1.4 for dead and live loads, respectively. The resulting internal loads obtained from the global analysis (type-3 truck configuration, half the weight) were applied to the elements in connection J-6, as shown in Table 15. The von Mises stress distributions for the whole connection is shown in Figures 33 and 34. According to the von Mises yield criterion, the whole connection does not experience significant yielding zones under the factorized loads. Stress concentration is observed in the rivets, splice plates and surrounding regions of the holes. The areas with the highest stress values are within elements T-12 and D-9, but the peak von Mises stress (34.2 ksi) slightly exceeds yielding in a rivet hole of element T-12 (Figure 34). This rivet holes stress concentration is shown in Figure 35 (a) and it coincides with the equivalent plastic strain (PEEQ) of 0.002683, as shown in Figure 35 (b).

Figure 36 shows the von Mises stress distribution for the gusset plates. The maximum von Mises stress predicted in the gusset plate is 33.7 ksi. It is located at one of the rivet holes connecting element T-12. The average von Mises stress distribution of the gusset plate without taking into consideration the stress concentration of the rivet holes are between 0.2 ksi to 18.2 ksi. Out-of-plane displacements are negligible according to the displacement obtained. As a result, the gusset plate did not display a potential buckling problem under factorized loads. Excluding the shear stress concentration observed in the rivet holes, the gusset plate region between elements D-9, T-8 and V-11 showed the highest shear stress, as shown in Figure 37. The maximum shear stress was 16.7 ksi.

Rivets were the most affected parts found in the FEA. This behavior is in accordance with the FHWA (2009) recommendations for evaluating steel gusset plates. Figure 38 shows the von Mises stress distribution of rivets in one gusset plate. Some rivets experienced yielding zones and

high shear stress, controlling the capacity of the J-6 connection (Figure 38). The maximum von Mises stress is 33 ksi whereas the maximum shear stress is 16 ksi. Figure 39 shows a detail of the von Mises and shear stresses distribution of the critical rivet in the connection.

Table 16 summarizes the LR for connection J-6. The detailed LR based on LRFR calculations is presented Appendix A. Table 16 showed that under these factorized service loads, the LR of the gusset plates exceeds a value of one (1.0), having T-12 and D-9 elements the smallest values for connection J-6 (1.80 and 2.53 respectively). These values mean that under the legal load Half-Scaled Type 3, connection J-6 seems to be adequate. The LR results are in close agreement with the FEA results, as revealed by Von Mises yield criterion and the shear stress values obtained. FEA results show that the connection has initial yielding in regions of stress concentration in the rivet holes, and within rivets, but the magnitude and the area seem negligible.

TABLE 15: FACTORED REDISTRIBUTION LOAD.

Element	DC (Kips)	(LL+IM)* (Kips)	Total (Kips)
D-9	52.04	24.4	76.44
D-13	23.6	17	40.6
V-11	19.7	12	31.7
T-8	121	44	165
T-12	173	59.7	232.7

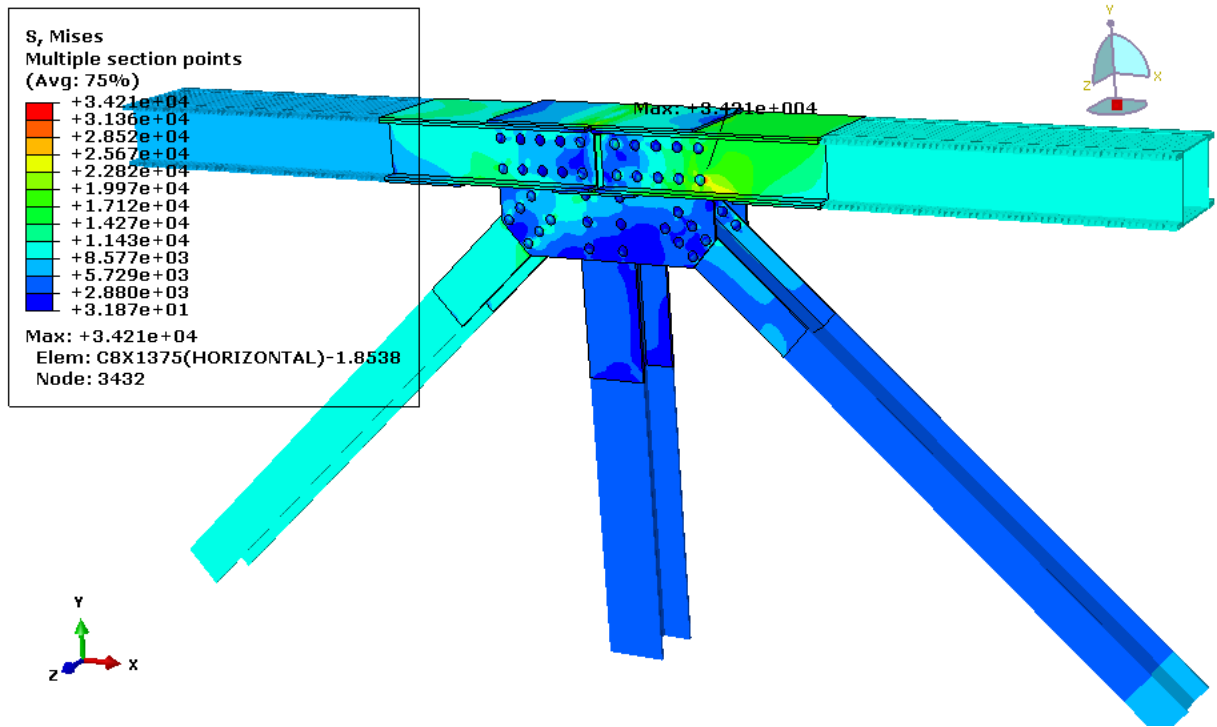


FIGURE 33. GENERAL VON MISES STRESS (KSI) DISTRIBUTION IN CONNECTION J-6

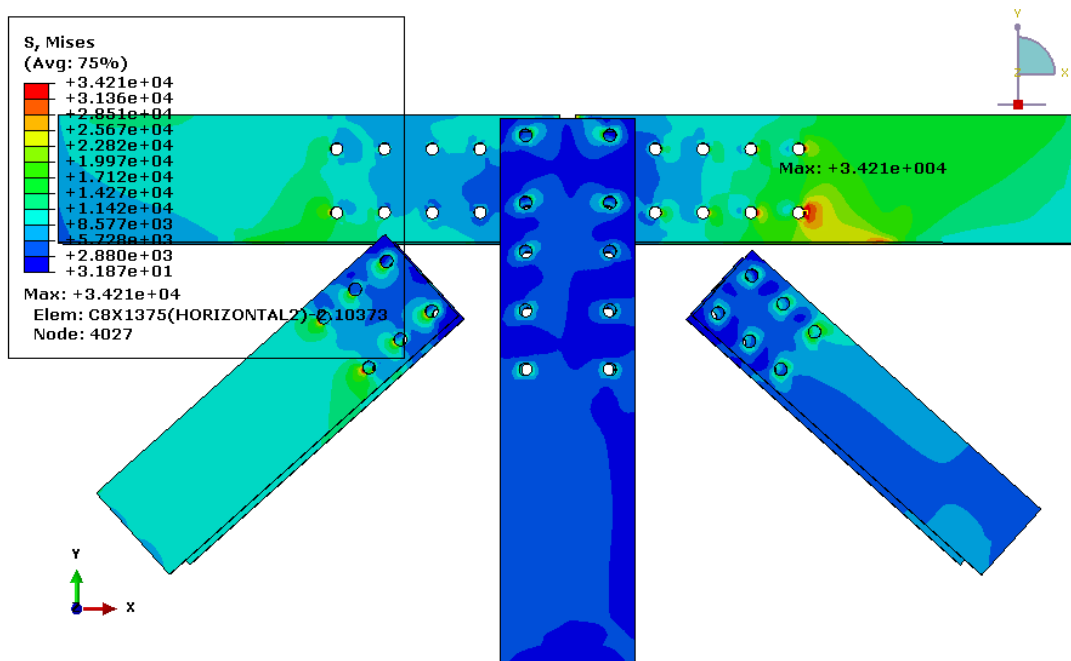
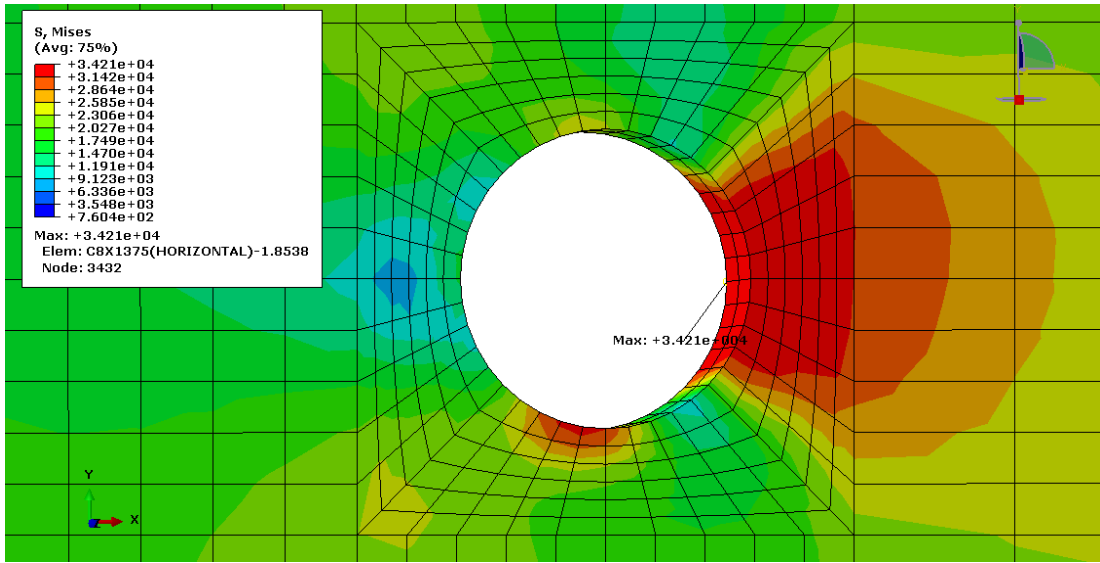
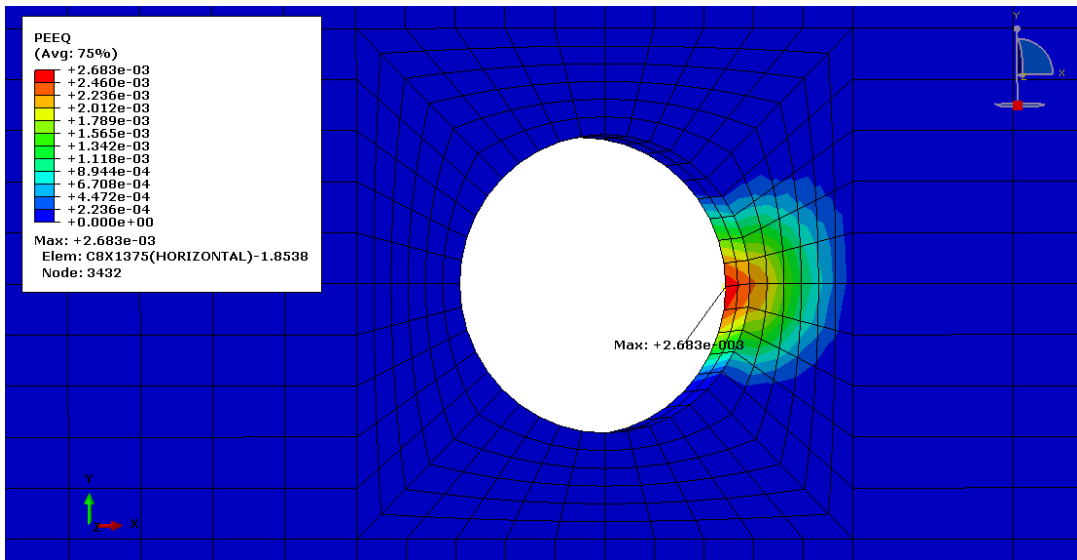


FIGURE 34. VON MISES STRESS (KSI) DISTRIBUTION OF ELEMENTS.



a)



b)

FIGURE 35: VON MISES STRESS AND EQUIVALENT PLASTIC STRAIN (PEEQ) DISTRIBUTION FOR THE RIVET HOLE.

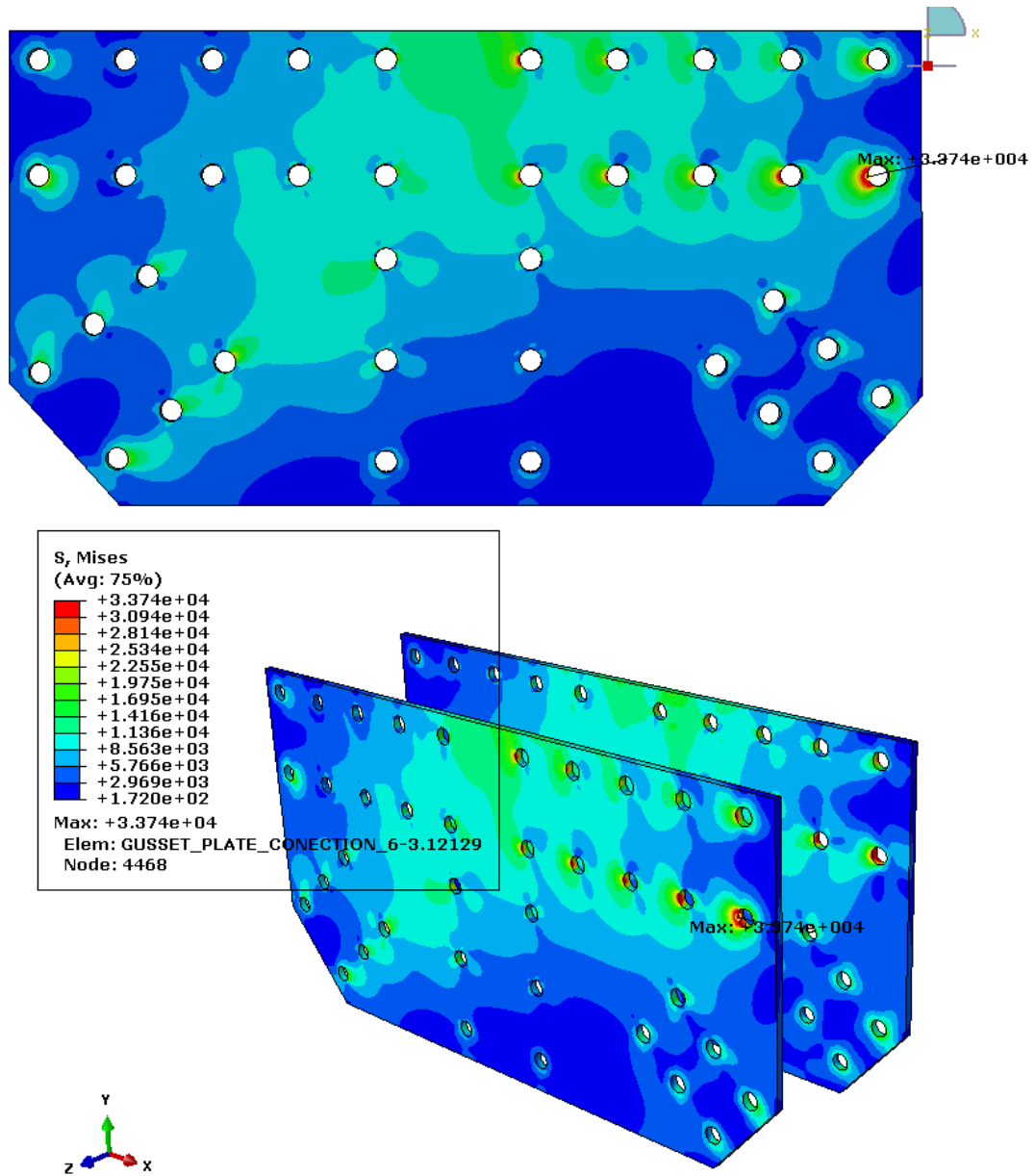


FIGURE 36. VON MISES STRESS (KSI) DISTRIBUTION OF GUSSET PLATES IN CONNECTION J-6

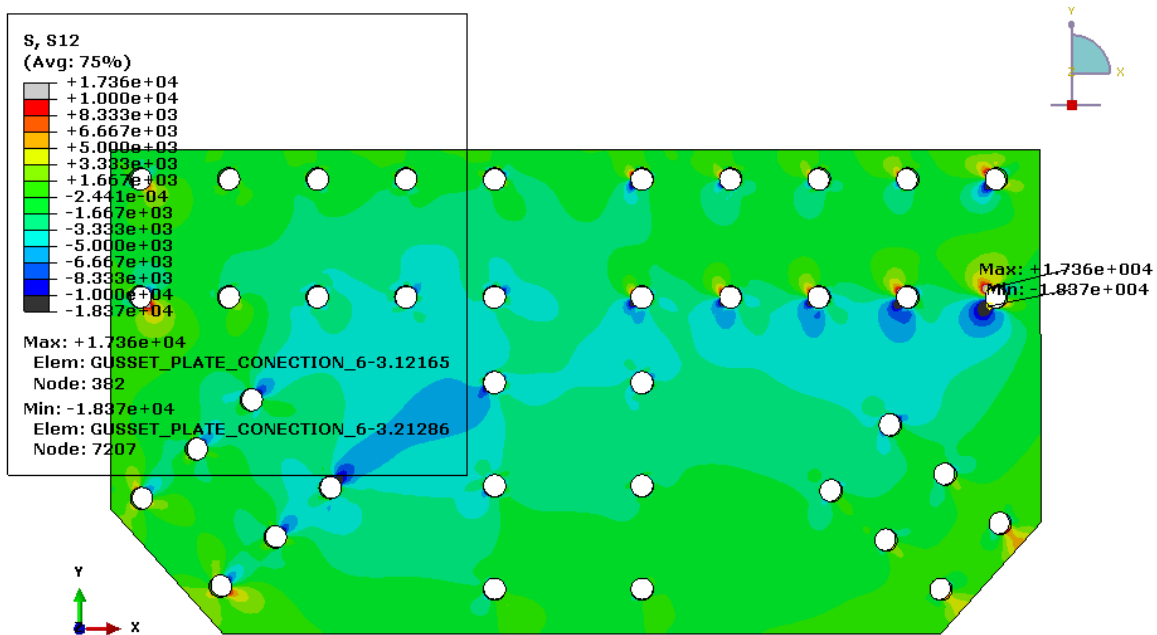


FIGURE 37. SHEAR STRESS (KSI) DISTRIBUTION OF GUSSET PLATES IN CONNECTION J-6

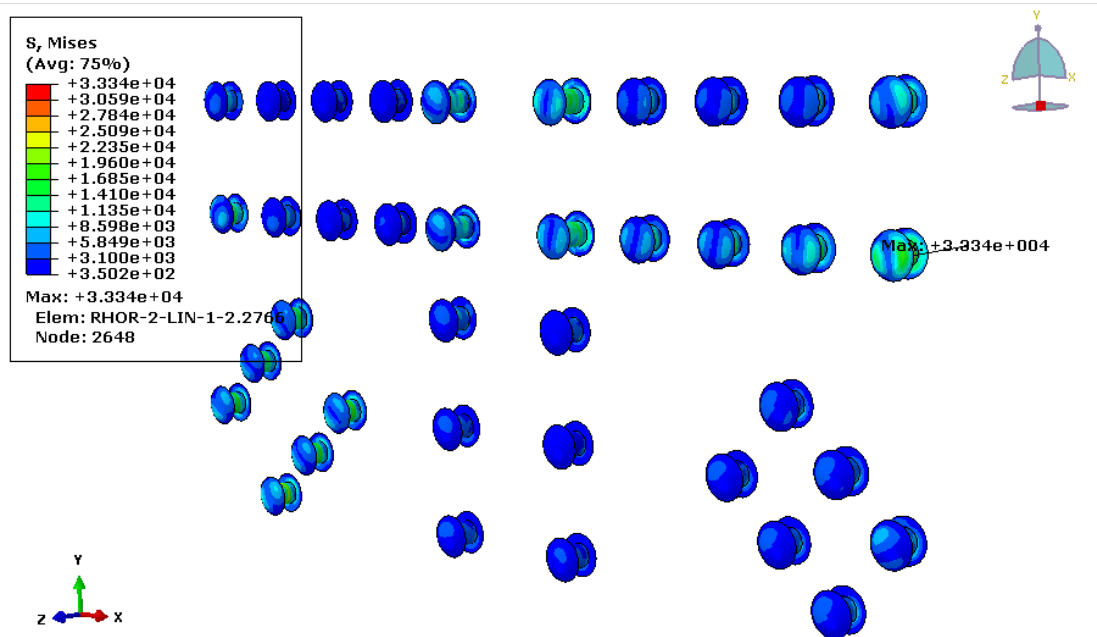


FIGURE 38. VON MISES STRESS (KSI) OF RIVETS IN CONNECTION J-6

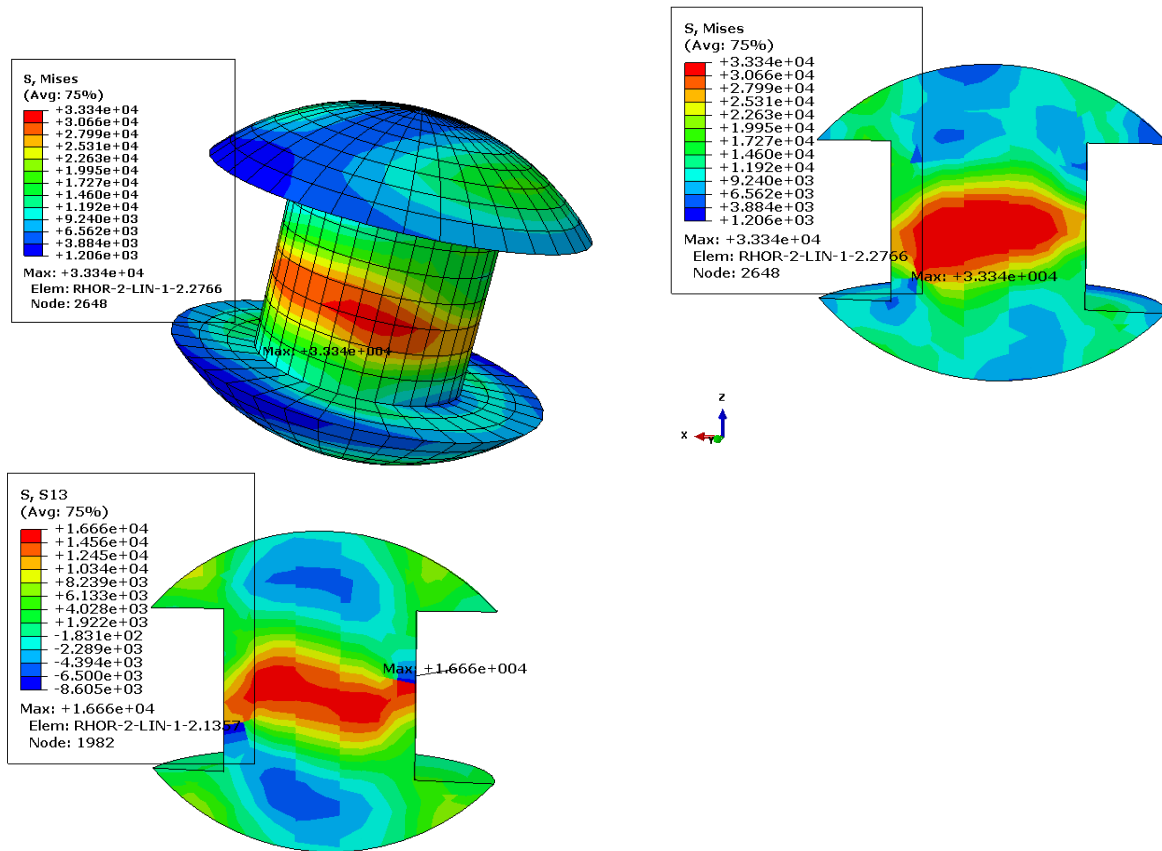


FIGURE 39. VON MISES AND SHEAR STRESS (KSI) DISTRIBUTION IN THE CRITICAL RIVET (CONNECTION J-6)

TABLE 16: LOAD RATING RESULTS FOR CONNECTIONS J-6 AND J-2.

Connection	Element	Controlling Axial Load Resistance	Rating Factor
J-6	D-9	Rivets (shear)	2.53
	D-13	Rivets (shear)	5.76
	V-11	Rivets (shear)	15.82
	T-8	Rivets (shear)	3.93
	T-11	Rivets (shear)	1.80
J-2	D-1	Rivets (shear)	1.77
	D-5	Rivets (shear)	1.44
	V-3	Rivets (shear)	7.12
	T-4	Rivets (shear)	1.75

5.6. NONLINEAR TENSILE ANALYSIS

Tension yielding represents one of the failure causes in gusset plates. The conditions to consider in the tensile evaluation of gusset plates are: i) yield on the gross section, ii) fracture on the net section, and iii) block shear rupture. The smallest value obtained by these conditions will control the capacity. The equations used to evaluate these conditions were presented in Chapter 2 and Appendix A shows a detail calculation for critical connections based on FHWA guidelines (2009). The first two conditions are based in the Whitmore effective width. The Whitmore study concluded that the maximum principal tensile stress occurs in the middle of the last row of rivet holes. Block shear rupture takes into account the parallel and perpendicular planes with respect to the load direction. This combined axial and shear stresses produce a possible failure pattern. This study is mainly focused in the diagonal element D-13 of J-6. The loads applied to the elements in the connection were taken as the factorized load obtained from the half-scale Type 3 legal load.

Figure 41 shows the maximum principal stress contour generated in the gusset plate specified in the D-13 region. The highest value of the maximum principal stress is 12 ksi. It occurs in one of the rivet holes located in the outside region of the GP. This rivet hole has the largest principal stress, however, the last two (inner region) have a larger stress concentration region between rivet holes (red rectangle section shown in Figure 41). This concentration validates Whitmore studies since as mentioned before, the maximum principal stress is located in the same region that Whitmore recommends. It shows close agreement with the Whitmore effective width, commonly applied for yield analysis on the gross section and fracture analysis on the net section. On the other hand, Figure 42 shows the local (axial) stress distribution in the same region. The highest local stress contour follows the axial and perpendicular lines with respect to the axial direction of element D-13 (black line in Figure 42). This highest contour stress is in accordance

with the block shear path. As a result, the equations used to calculate the tensile capacity of gusset plates are validated based on the FEA results.

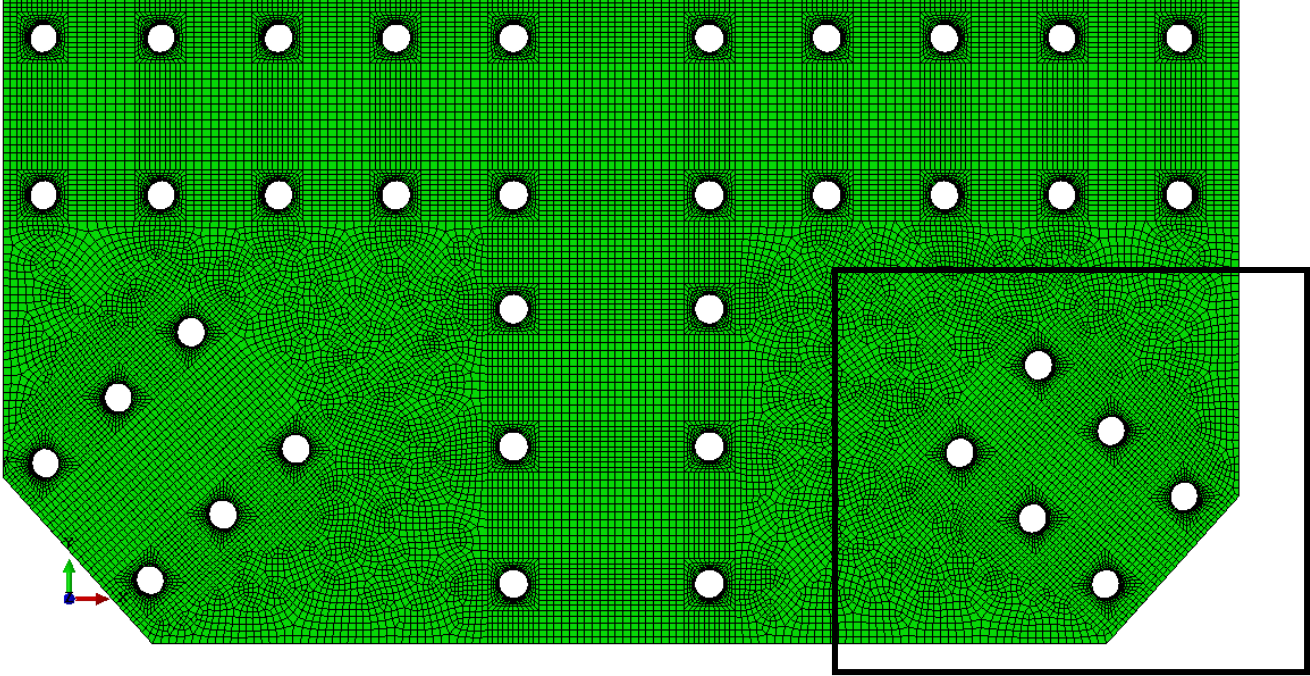


FIGURE 40: GUSSET PLATE OF CONNECTION J-6.

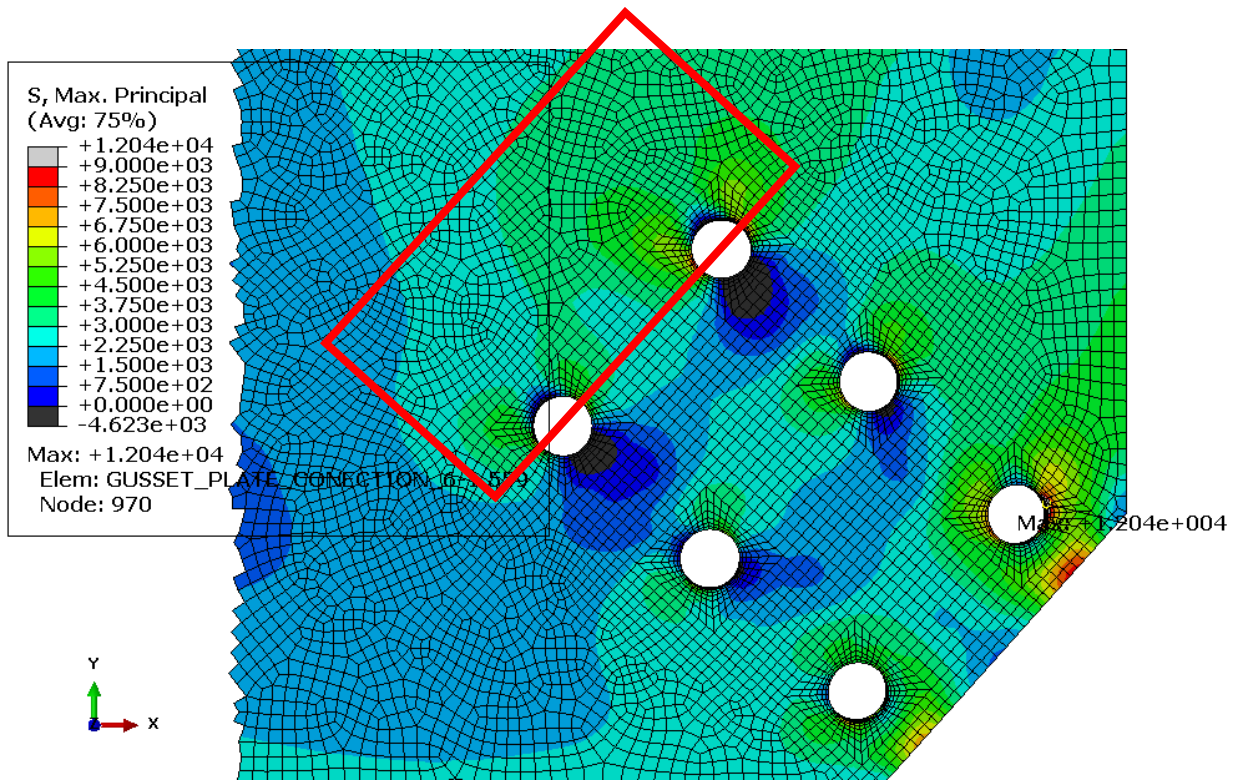


FIGURE 41: MAXIMUM PRINCIPAL STRESS DISTRIBUTION IN THE ELEMENT D-13 REGION.

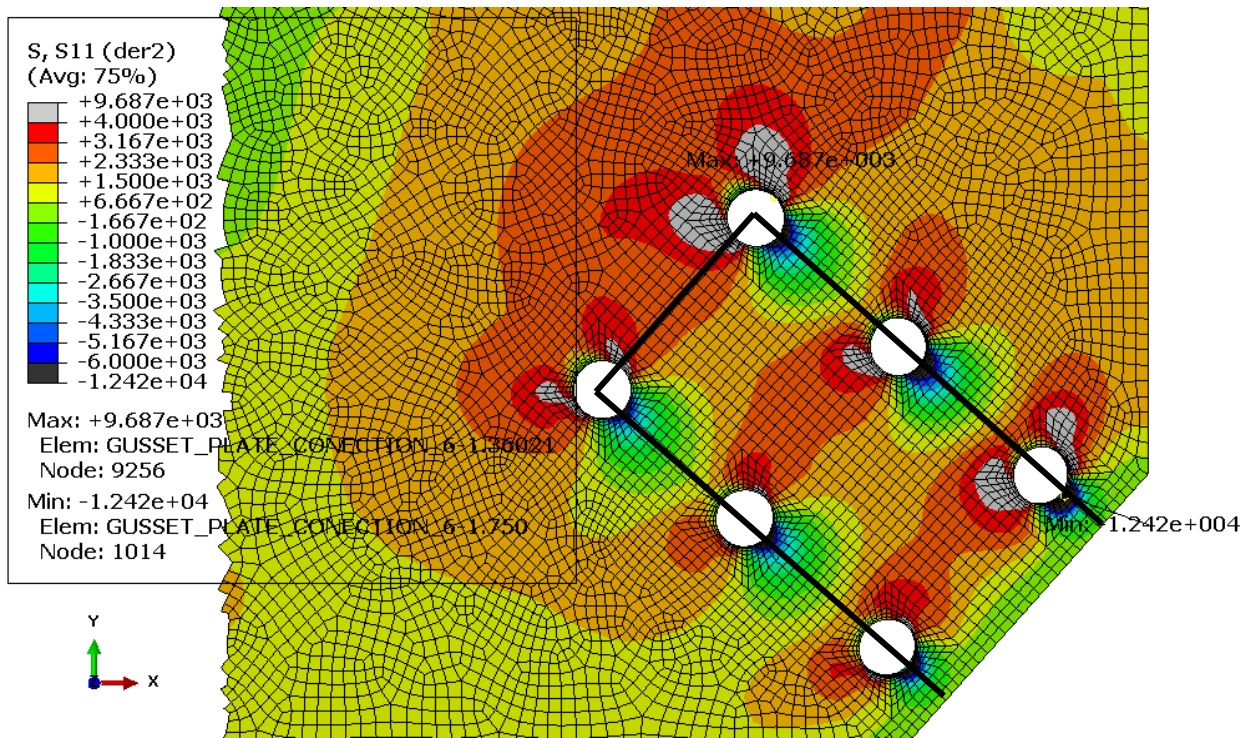


FIGURE 42: LOCAL STRESS DISTRIBUTION IN THE ELEMENT D-13 REGION.

5.7. RIVET ANALYSIS

Rivets and bolts play an important role in the capacity of connections. These could present failures due to rivet shear or plate bearing. The Triagle Evaluation of Gusset Plates in Steel Bridge Connections (TEGP, 2010) conducted a literature survey in which they collected all the experimental data from 1904 to 1941 to compare the specifications presented in the Manual for Load Rating of Gusset Plate (FHWA, 2009) that determine the capacity of rivets. The FHWA manual does not consider the following: i) corrosion effect, ii) strength reduction due to service life, and iii) calibration of the resistance factor ϕ . The study concluded that after comparing the experimental data to the FHWA recommendations, the FHWA manual presented conservative values to represent the rivets capacity.

According to the load rating results (Appendix A), the rivets controlled the capacity of connections for all elements. Element D-5 (Figure 48) presented the most critical condition in the LR results for connection J-2. Thus, it was decided to study the shear stress distribution in the rivets analyzing material and geometrical nonlinearity. Furthermore, the corrosion effects were represented in the analysis reducing the diameters by 1%, 3%, and 6%. Finally, the effects due to loss of rivets, as observed in the visual inspections of the target bridge, were also studied.

5.7.1. RIVETS DIAMETER LOSS DUE TO CORROSION EFFECT

From the FEA and the LR results it seems that the target bridge capacity is controlled by shear strength of rivets. The rivets located in element D-5 for connection J-2 present the most critical case. During the on-site visual inspections, several areas of corrosion in the target bridge were found in the bridge components (gusset plates, elements, etc.), but the regions of major

concern were the rivets and the gusset plate holes. FHWA 2009 guidance for LR gusset plate connections estimates the rivet shear resistance capacity as (Chapter 2, Sec. 2.5):

$$\phi R = \phi F m A_r$$

where:

ϕR = Factorized load capacity;

ϕF = Factored shear strength of one rivet (Table 1, FHWA, 2009);

m = number of shear planes; and

A_r = cross-sectional area of the rivet.

The rivets in the target bridge have a factored shear strength value (ϕF) of 21 ksi in accordance to FHWA guidance (Table 1 FHWA, 2009). Kulak et al. 2001 established that for design purposes, the shear strength capacity for a rivet is $0.76\sigma_v$. During the rivet evaluation, it seems that minor reductions in the rivet diameter produce drastic reductions in shear strength. Therefore, it was decided to analyze a sub-model to calculate shear stress due to reductions in diameter. This diameter reduction was assumed constant along the rivet perimeter. The corresponding material properties for the gusset plate and the rivet previously discussed were applied in the sub-model shown in Figure 43. A mesh refinement was performed in the areas of detail study (rivet and rivet hole) based on the convergence criteria mentioned in Chapter 4, Section 4.4. The final mesh is 0.02 inches in the circumferential and axial direction of the rivet (Figure 43). A pre-tension stress of 8.2 ksi was applied on the rivet head based on the Liao and

Okazaki (2009) recommendations. Four different diameters were studied: i) 0.76 in (0%), ii) 0.7524 (1%), iii) 0.7372 (3%), and iv) 0.7144 (6%).

According to the FHWA guidance, the capacity of a rivet with a diameter of 0.75 in. is about 9.5 kips. Assuming that the loads for each element are equally distributed in the rivets, the largest load value that rivets could sustain for the critical connection is 6.4 kips. A conservative value of 9 kips, less than the rivet capacity and higher than the maximum load that rivets could sustain in the bridge critical connection was applied to one of the plates while the other plate was fixed, as shown in Figure 43. During the analysis, both plates were simulated as rigid bodies with a friction coefficient of 0.1.

Nonlinear analyses were performed to investigate how the shear stresses increase while the rivet experienced a reduction in diameter, representing effects due to corrosion. Figures 44 and 45 show the stresses distribution for no reduction and a 6% diameter reduction, respectively. The stress contour for both stresses (von Mises and shear) presented an increase in maximum stress region at the center region of the rivet cross section. Figure 46 compares the shear stress, von Mises stress and load percentage differences obtained from the FEM and equations given in the FHWA manual. From the nonlinear results, it seems that shear strength is not very sensitive to a rivet diameter reduction as suggested by FWHA equations.

Finally, the FHWA shear capacity equation results were used to compare the shear stress results obtained from the FEA. The sub-model previously described was applied for the analysis of this part. The maximum load obtained from the FWHA shear capacity equation was applied in each computational FEA case. Loads and FEA results are presented in Table 18. Figure 47 shows the computational FEA results for different rivet diameter reductions and the results

obtained by FHWA and Kulak et al. 2001. As noted in Figure 47, the maximum shear stress obtained from the FEA are below and very close to the factorized shear strength ($\phi F=21 \text{ ksi}$). From the FEA results, it seems that FHWA rivet capacity equation overestimate the shear stress developed in the rivet.

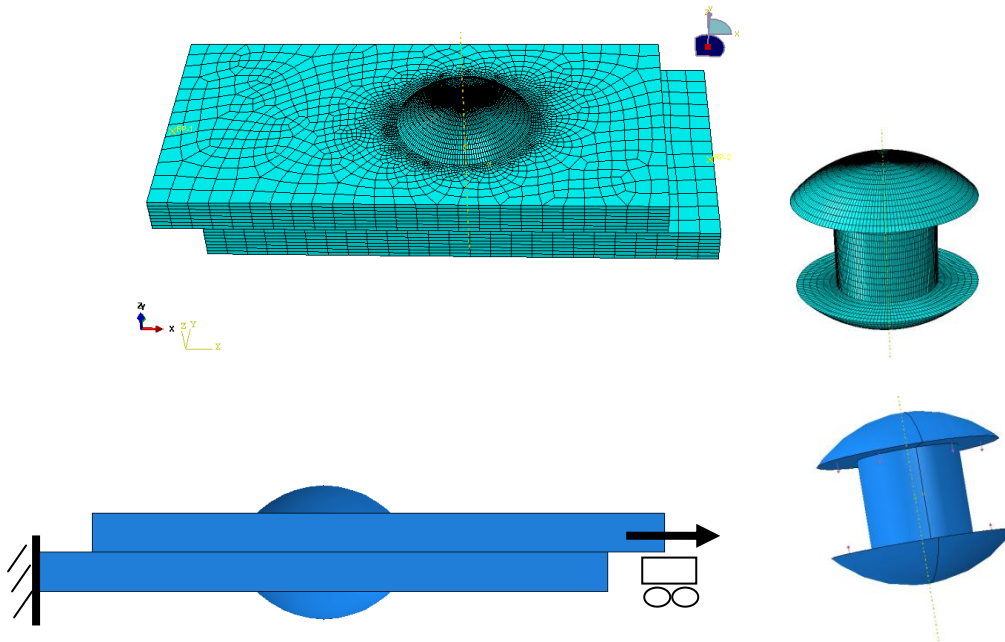
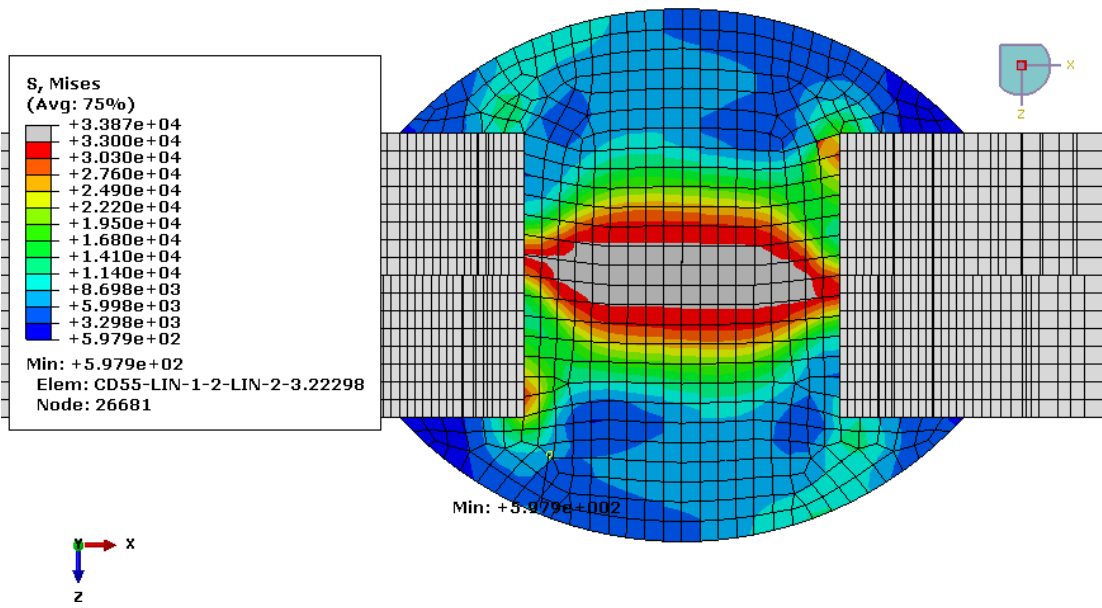
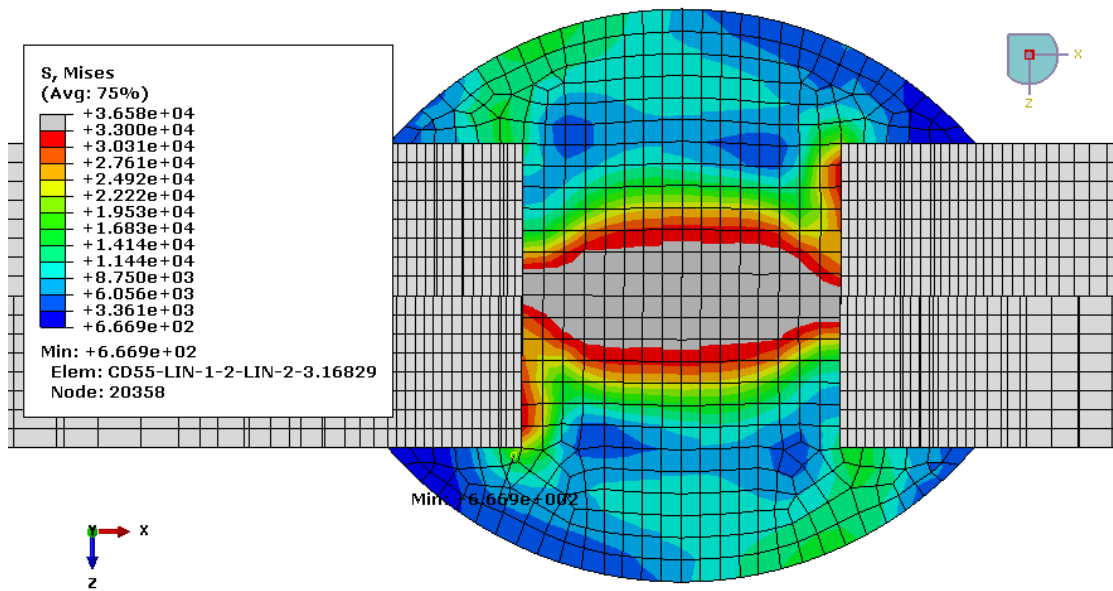


FIGURE 43: GENERAL FE MODEL FOR CONNECTION J-2

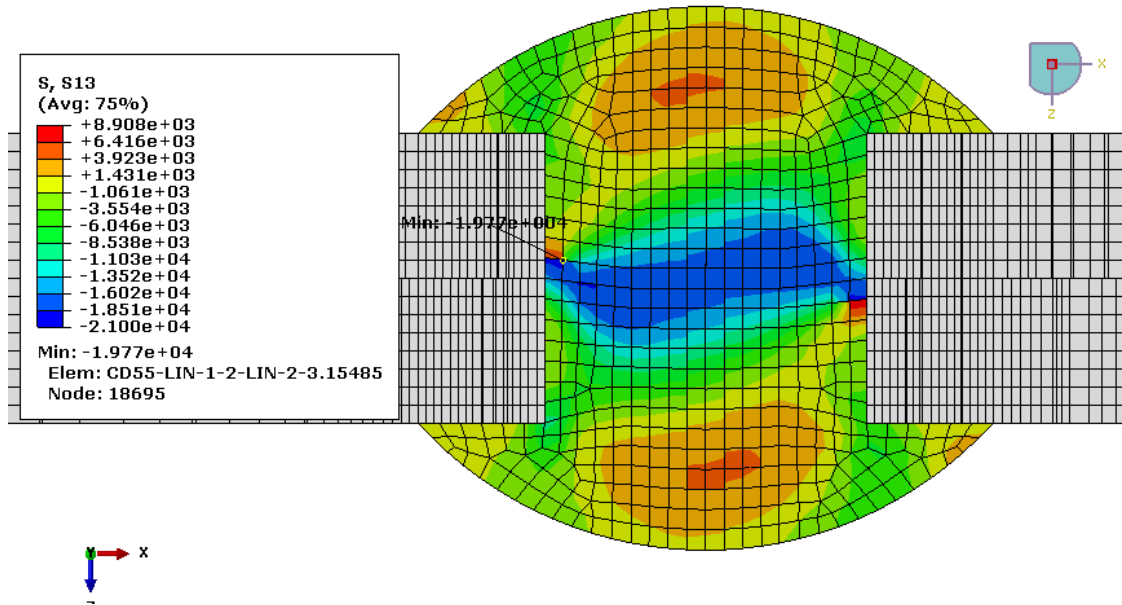


a)

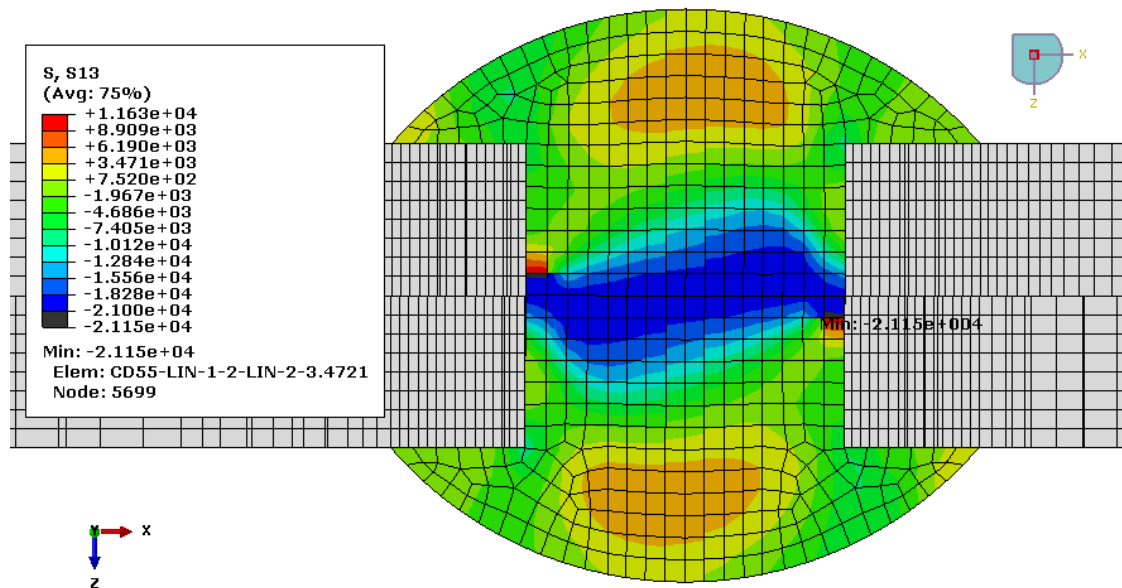


b)

FIGURE 44: VON MISES STRESS DISTRIBUTION (KSI) FOR: A) NO REDUCTION IN DIAMETER AND B) 6% REDUCTION IN DIAMETER.



a)



b)

FIGURE 45: SHEAR STRESS DISTRIBUTION (KSI) FOR: A) NO REDUCTION IN DIAMETER AND B) 6% REDUCTION IN DIAMETER.

TABLE 17: SHEAR STRESS REDUCTION.

Rivet Diameter Loss (%)	Max. Shear Stress (ksi)	Shear Stress % Difference	FHWA Max. Load % Diference
0	19.77	-	-
1	19.88	0.56	1.99
3	20.21	2.23	5.98
6	21.15	6.98	11.65

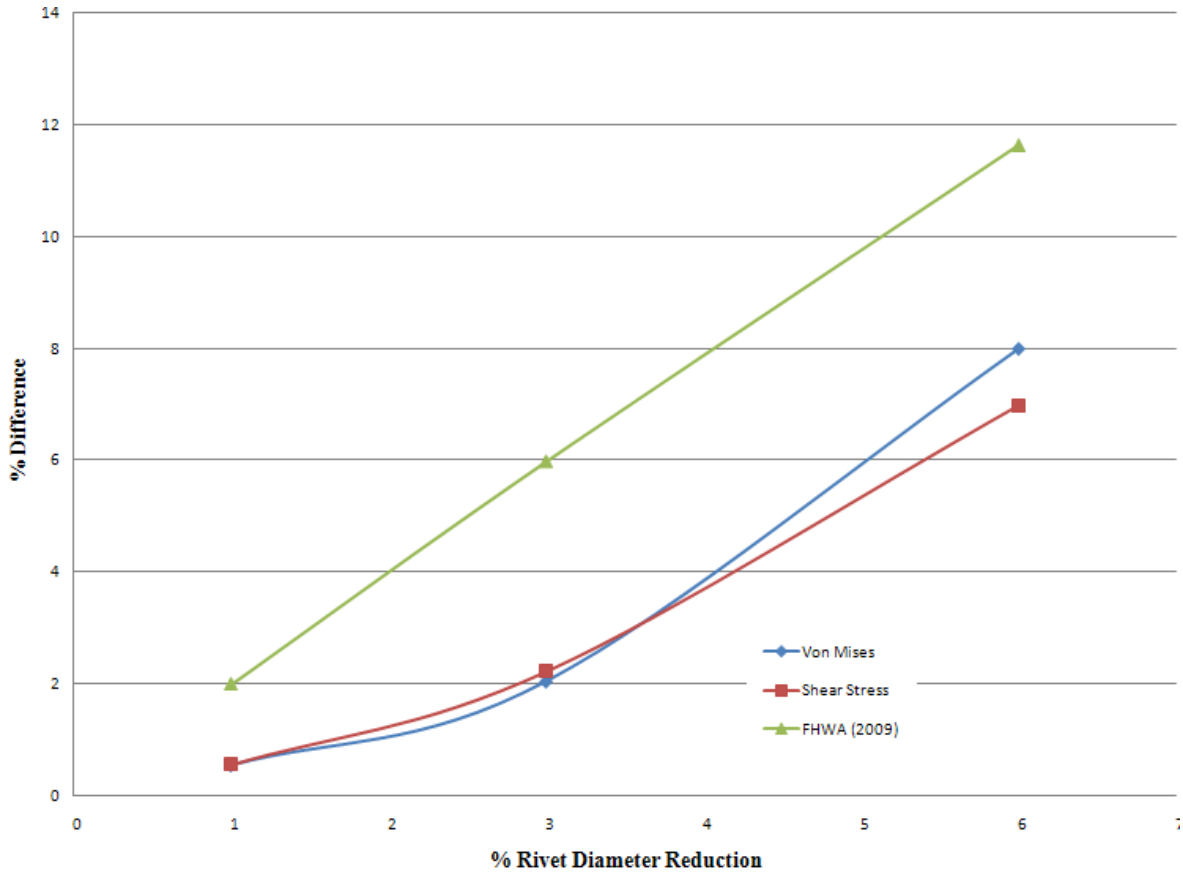


FIGURE 46. SHEAR STRESS, VON MISES STRESS AND FHWA SHEAR RIVET EQUATION PERCENTAGE DIFFERENCE RESULTS DUE TO A RIVET DIAMETER REDUCTION.

TABLE 18: SHEAR LOAD CAPACITY, MAX. VON MISES AND MAX. SHEAR STRESS RESULTS.

Rivet Diameter Loss (%)	Shear Load Capacity (FHWA) (kips)	Max. Von Mises Stress (FEA) (ksi)	Max. Shear Stress (FEA) (ksi)
0	9.53	34.69	20.24
1	9.34	34.70	20.19
3	8.96	34.49	20.16
6	8.42	34.43	20.10

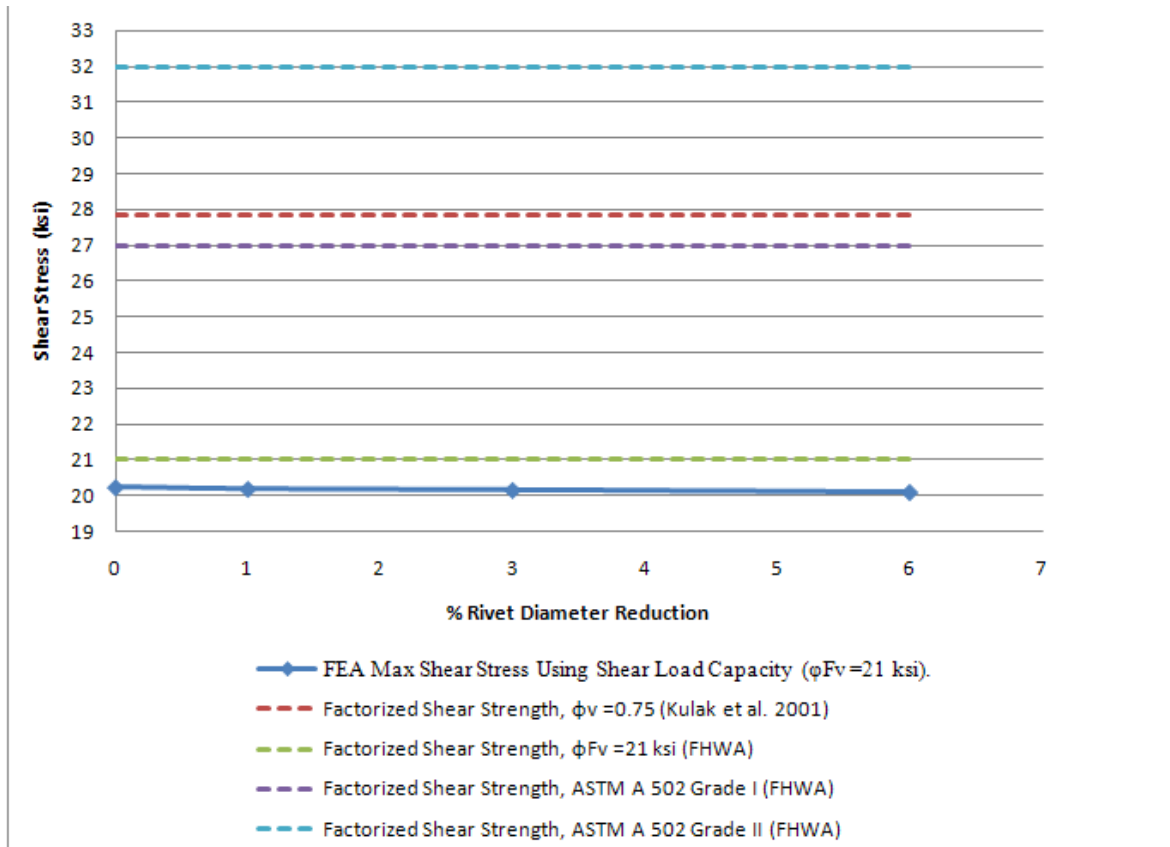


FIGURE 47: SHEAR STRESS VS. % RIVET DIAMETER REDUCTION.

5.7.2. LOSS OF RIVETS

A field visit was performed to inspect the target bridge condition and corroborate unclear dimensions in the construction plans. Some of the irregularities found were associated to corrosion, rivets that are not adequately fixed and lack of rivets in some connections. The last condition (lack of rivets) could present a significant reduction in rivet capacity. In order to study how this lack of rivets affect the structural capacity of bridge connections, a FEA was performed removing one and two rivets for each gusset plate face in element D-5 of connection J-2. The reason for choosing this element is that it represents the most critical condition in the LR analysis. A detailed sub-model (Figure 49) was developed to reduce the computational time of execution. In this case, all displacements in the diagonal element were restrained except in the axial direction and the gusset plate was fixed in two sides. An axial tension load of 72.3 kips was applied to element D-5. This load represents the maximum internal load due to service loads in element D-5 at connection J-2. Rivets were numerically labeled as shown in Figure 49. The von Mises stress and the shear stress were compared with the unaltered connection. Five cases were studied: i) unaltered connection; ii) loss of rivets #1 and #2, located in the upper row perpendicular to the diagonal truss element axial direction (cases 2a and 3a), respectively and iii) loss of rivets #5 and #6 in the lower row perpendicular to the diagonal truss element axial direction (cases 2 b and 3b), respectively. Figures 50 and 51 show the differences in the maximum shear stress presented in the rivets for cases 1a and 2a and cases 1b and 2b, respectively. From these results, it seems that loss of rivets in the critical connection J-2 could be hazardous due to an increase in shear stress in the order of 18%. This result can also apply to other bridge connections with the same geometry and configurations.

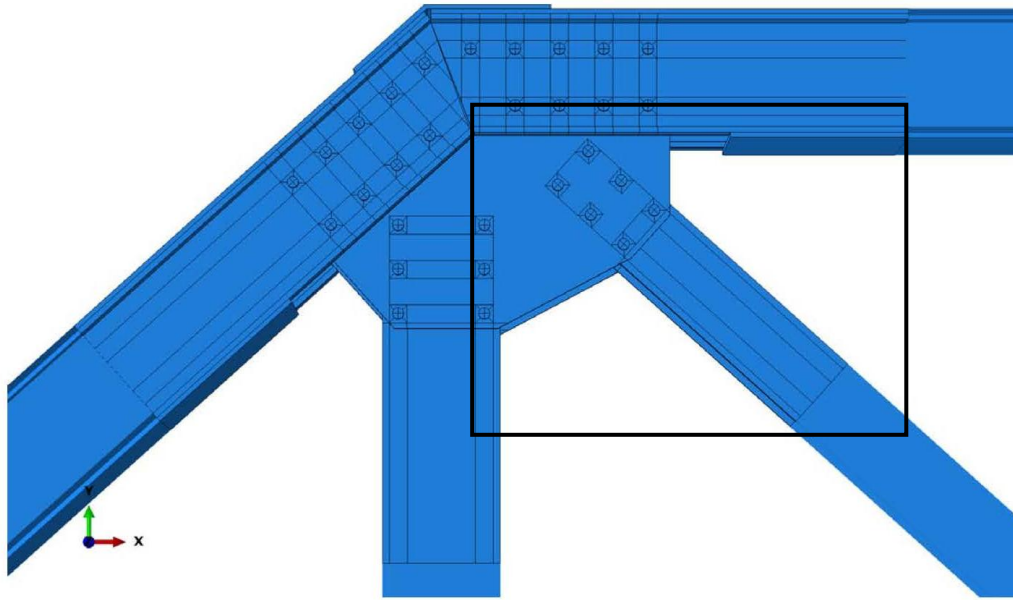


FIGURE 48: CONNECTION J-2.

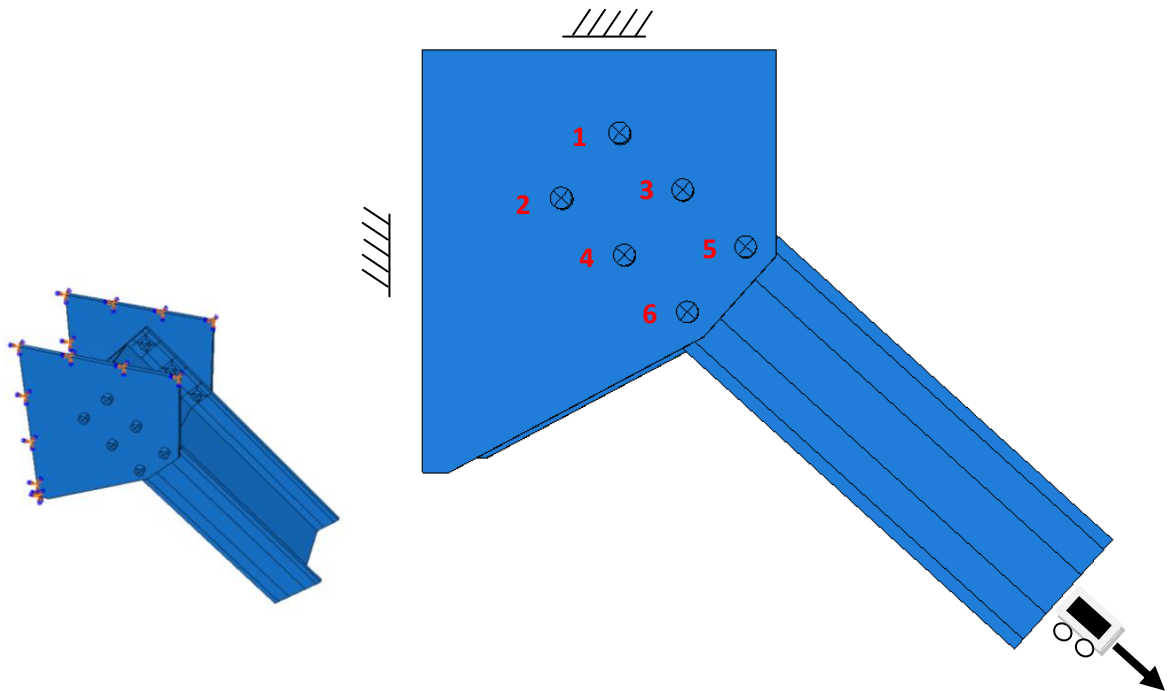


FIGURE 49: SUB-MODEL OF CONNECTION J-2.

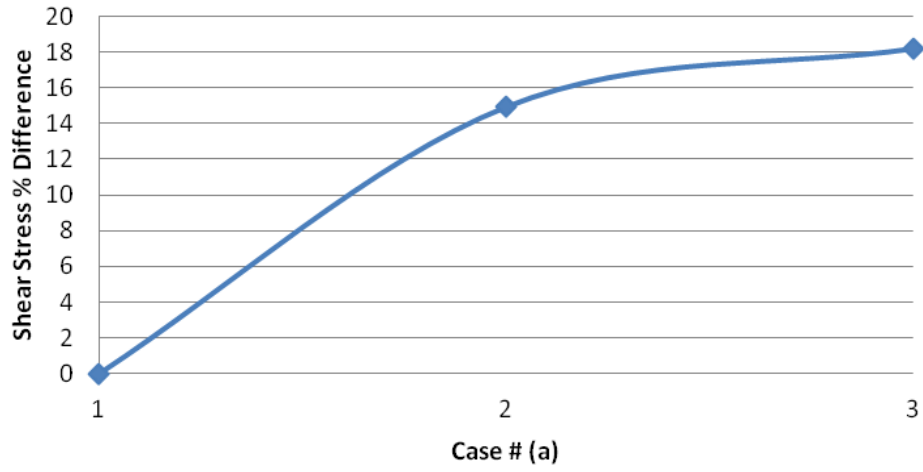


FIGURE 50: SHEAR STRESS VARIATION FOR CASE A.

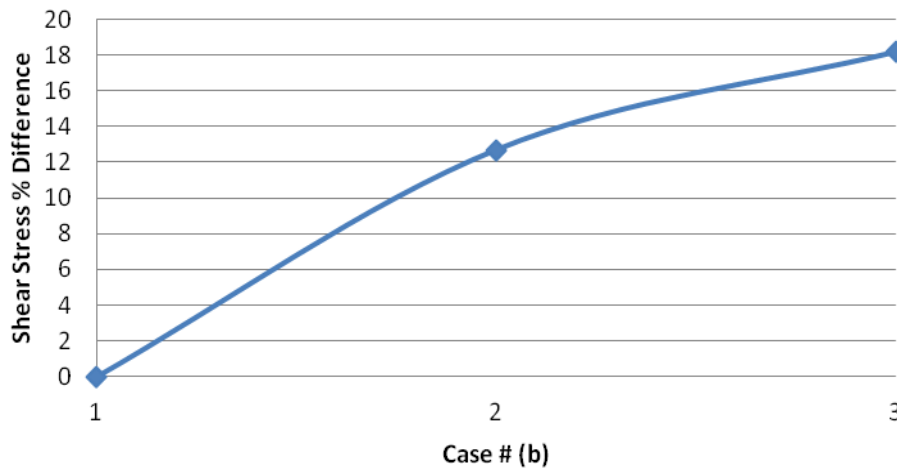


FIGURE 51: SHEAR STRESS VARIATION FOR CASE B.

5.8. NONLINEAR BUCKLING ANALYSIS

Buckling is one of the principal failures of gusset plate connections. Numerous analytical and experimental investigations have been carried out to quantify and compare the current methods used to design and verify gusset plate connections (see Chapter 2). Studies conducted to determine the causes of the I-35 Minneapolis Bridge collapse, revealed that a buckling failure generated in one of the gusset plate connections was the origin of this tragedy. After this collapse event, subject matter experts have debated the buckling equations commonly adopted.

A nonlinear analysis based on the modified Riks algorithm was performed to study the critical buckling loads in the target connection. As mentioned in Chapter 2, the modified Riks algorithm is an accepted method to study large geometric changes in structures prior to buckling. This method estimates the static equilibrium of elements by an iterative process dependent of an incremental load. Material and geometric nonlinear parameters were considered in the analysis. In order to reduce computational time, a sub-model was created in the compressive diagonal member of connection J-6 (element D-9), as shown in Figure 53. This element does not represent a critical condition of the target bridge as revealed by the small stress values produced by the maximum truck loading. However, this connection is typical of steel truss-type bridges and for other cases and loading conditions could be critical. Boundary conditions and load direction are presented in Figure 53. Translation in the x, y, and z directions were restrained in the first rows of fasteners closest to adjacent members. The element can only move in the axial direction and it was characterized as a rigid body. Rivets were modeled by fasteners techniques presented in Abaqus. A mesh refinement was performed based on the stress convergence as presented in Chapter 4. The final model has 83,692 elements (see Figure 54).

Thickness and unbraced length sensitivity analysis were developed based on maximum axial compression loads and out-of-plane displacements. Currently, there are three methods to calculate the critical buckling load in gusset plates: i) Thornton Method, ii) Modified Thornton Method, and iii) Yoo Method (see Chapter 2 and Figure 2 for more information). The FHWA manual for gusset plate evaluation uses the Thornton Method. These three methods will be compared with the FEA results to determine which method best represents the buckling capacity of the connection. In addition, a structural sensitivity study in the gusset plate taking into account thickness and unbraced length variations will be presented.

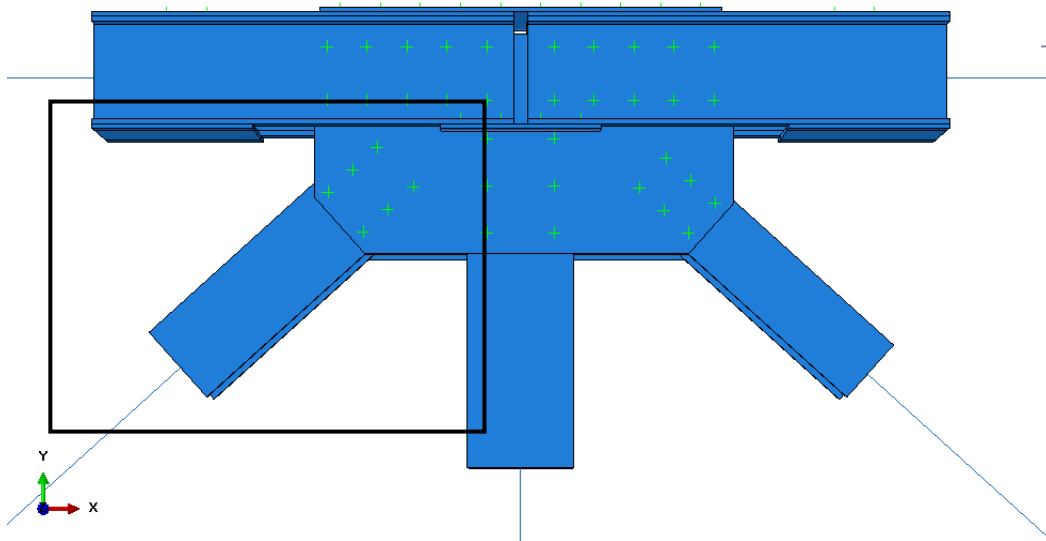


FIGURE 52: GENERAL FEM OF CONNECTION J-6.

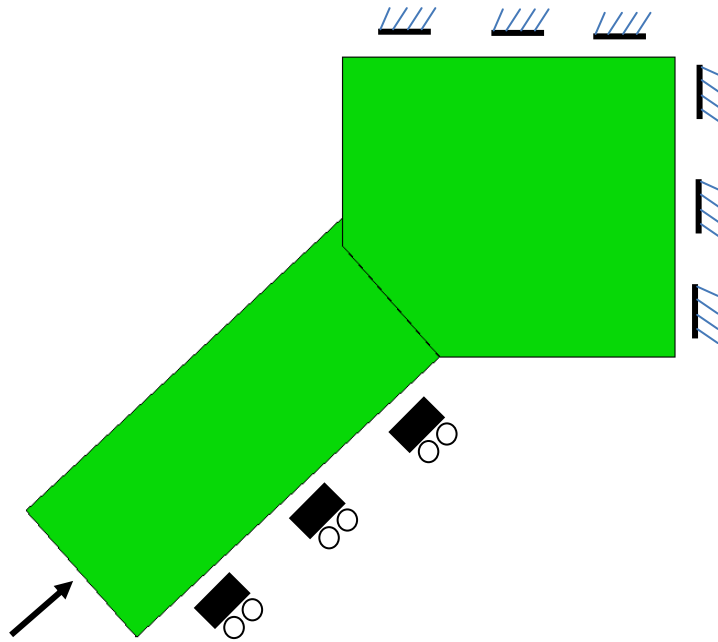


FIGURE 53: SUB-MODEL OF CONNECTION J-6

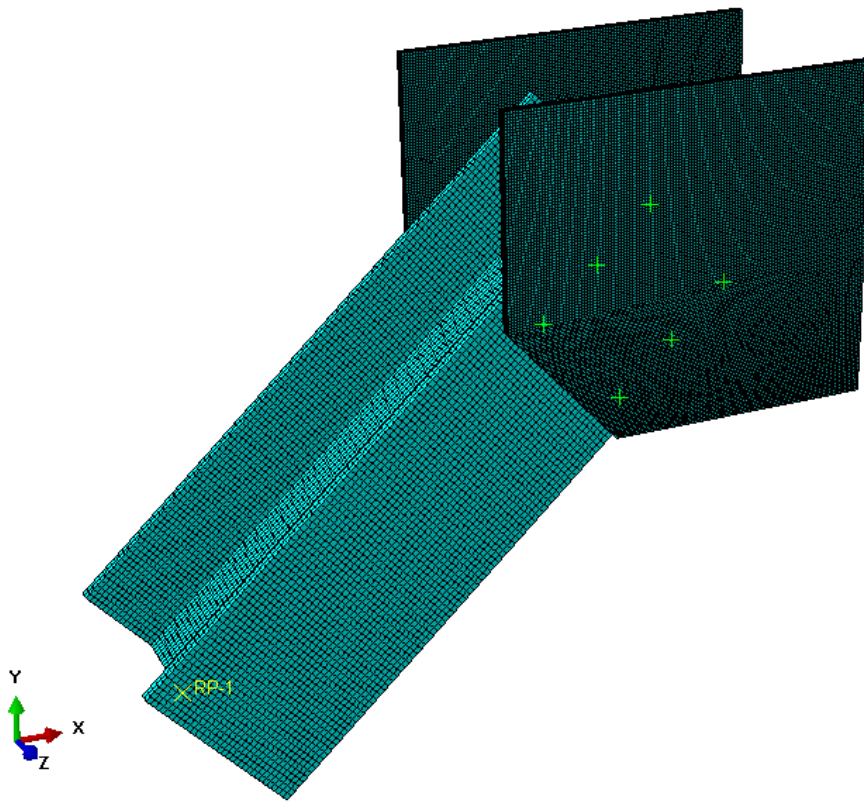


FIGURE 54: MESH REPRESENTATION FOR J-6 FE SUB-MODEL.

5.8.1. THICKNESS VARIATION

Corrosion is one of the major problems in steel structures. Millions of dollars are invested every year in maintenance of bridges with corrosion damage. The loss of thickness affecting the structural connection capacity in gusset plate connections is mainly due to corrosion problems. It is known that the gusset plate thickness plays an important role in buckling, shear, and yielding capacity of structural elements. Previous investigations have been performed to study the effect of thickness in gusset plates due to compression loads (Chapter 2). All studies concluded that the thickness reduction is directly proportional to a decrease in buckling load capacity. In this study, four different thicknesses were modeled to investigate the loss of structural capacity of the connection due to corrosion. The maximum compressive loads (critical loads) are compared with current buckling methods (Thornton, Modified Thornton, and Yoo Method). The thicknesses to be evaluated are 0.341 in. (100%), 0.32395 in. (95%), and 0.3069 in. (90%), and 0.28985 (85%). Maximum compressive load and out-of-plane displacement were the two criteria used in the study.

Figures 55 through 62 show the buckling modes with the out-of-plane displacement contours and their respective load-displacement curves for the corresponding cases. The buckling modes have an incremental deformation scale factor of 5%. All cases present inelastic buckling instabilities. Figure 63 present the comparison of load-displacement curves for all cases. The curves show similar behavior with a maximum load reduction tendency as the thickness decrease. These results are in agreement with previous investigations.

Table 19 presents the structural capacity reduction percentages for the different cases based on maximum compressive loads. FEA and hand calculations (methods) results are presented in the table. The FEA results show a maximum buckling capacity loss of approximately 20% (Case 1 = 379 kips and Case 4 = 302 kips). The Modified Thornton method and the FEA display very

similar percentage reductions with a difference between them of approximately 1.5 %. The other two methods show a difference in the order of 3% as compared to the FEA results. As a result, the hand-calculations show good percentage buckling capacity reduction in accordance to the FEA results. Figure 64 shows that the reduction curves for all methods and the FEA.

As mentioned before, the FEA results are compared to the classical hand calculations methods used to determine the buckling capacity in gusset plates (Table 20). Appendix B shows examples of the calculations of buckling capacity using these methods. A difference of approximately 76% was found when the FHWA (Thornton) method was compared with the FEA results. This means that the critical load obtained from FEA is 1.76 times the FHWA (Thornton) load. The Yoo Method has a difference of approximately 23 % when compared to the FEA (FEA load is 1.23 times the Yoo load). According to the FEA results, the FHWA buckling capacity methods (i.e., the Thornton method) seems to be very conservative while the Yoo method shows reasonable conservative results. As a result, the Yoo Method is recommended to obtain the buckling capacity for inelastic buckling in gusset plate connections.

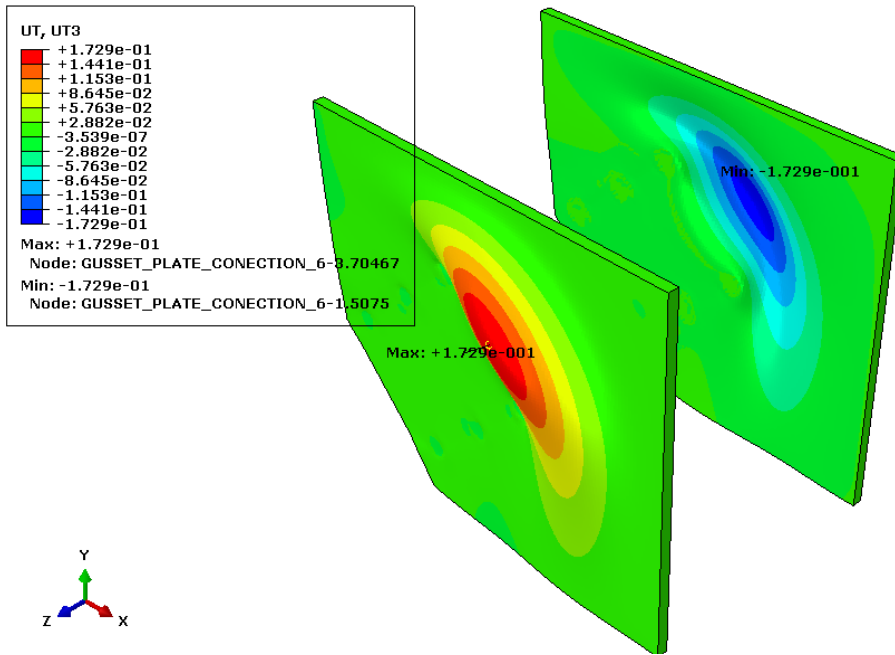


FIGURE 55: BUCKLING MODE FOR THICKNESS CASE1.

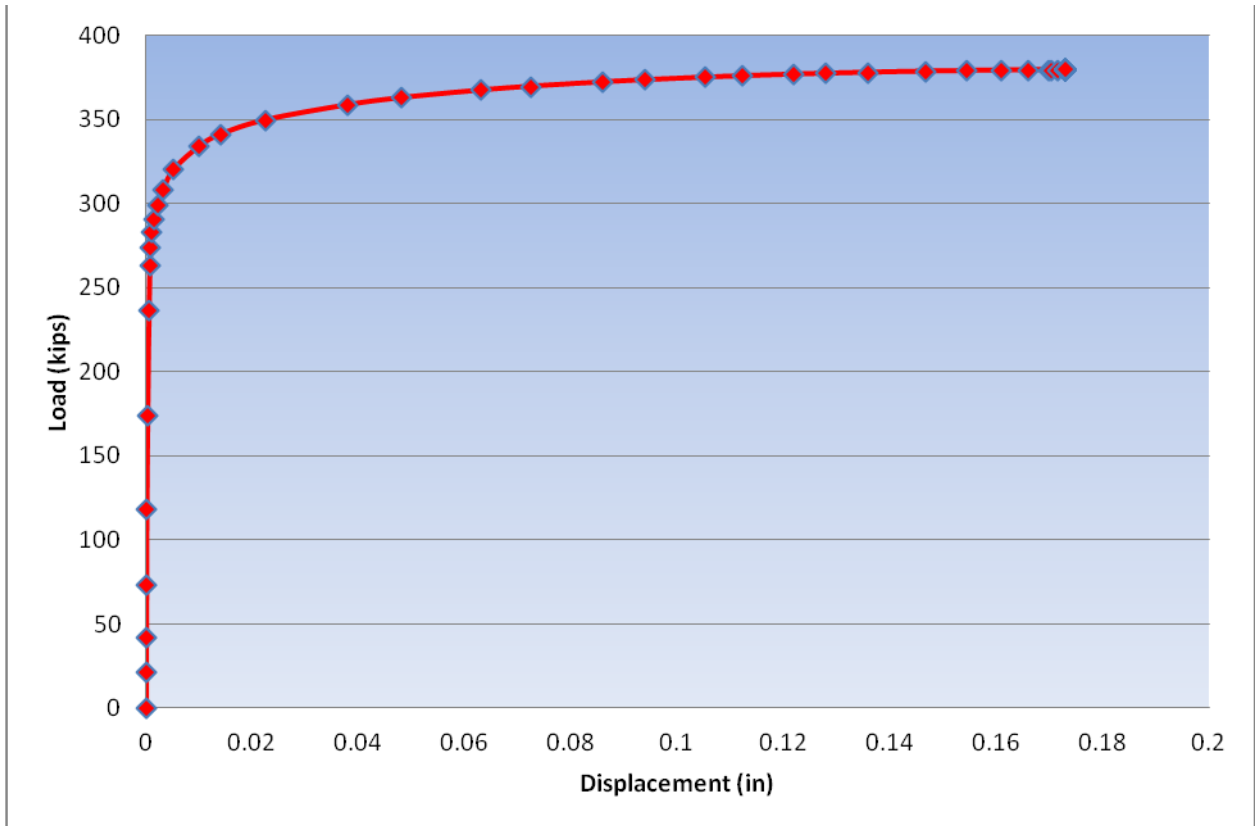


FIGURE 56: LOAD-DISPLACEMENT CURVE FOR THICKNESS CASE 1.

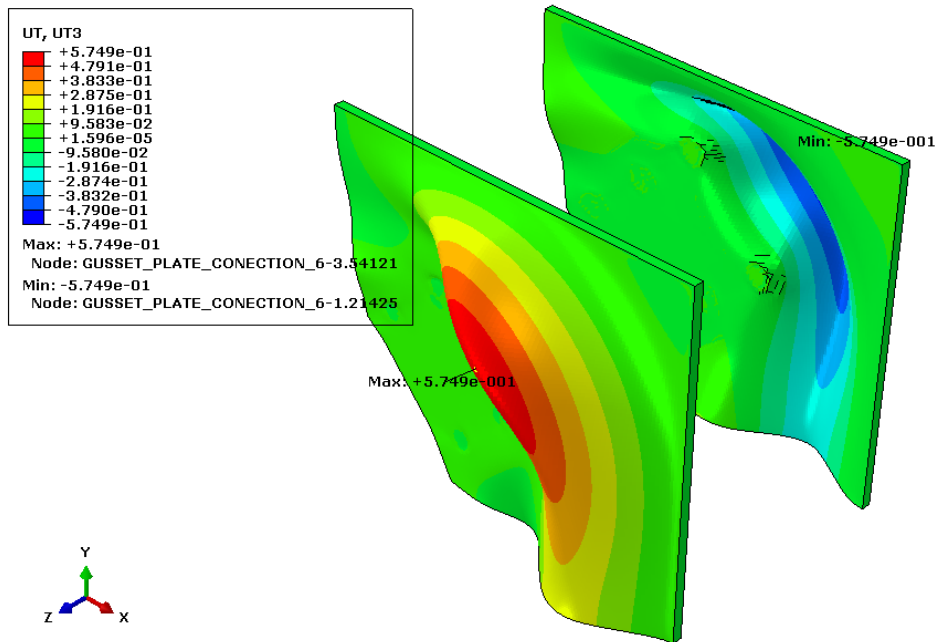


FIGURE 57: BUCKLING MODE FOR THICKNESS CASE2.

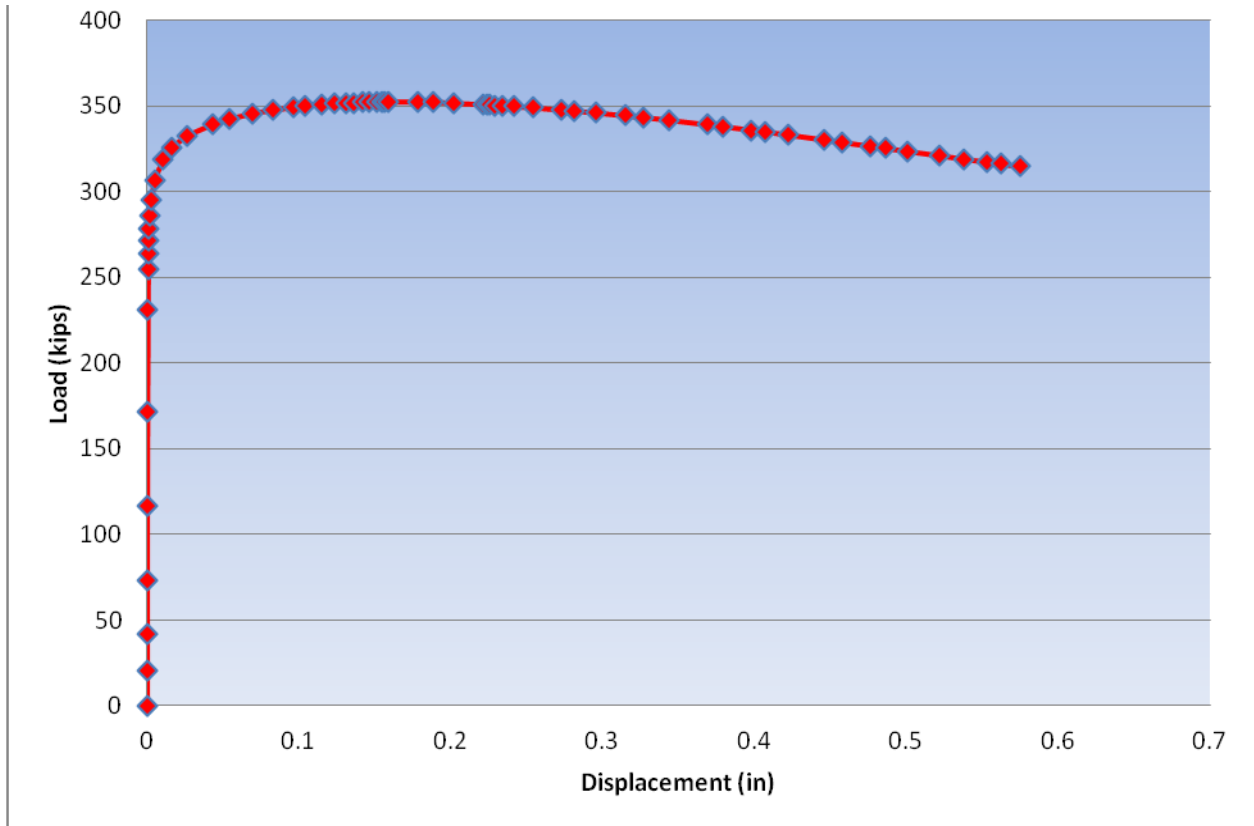


FIGURE 58: LOAD-DISPLACEMENT CURVE FOR THICKNESS CASE 2.

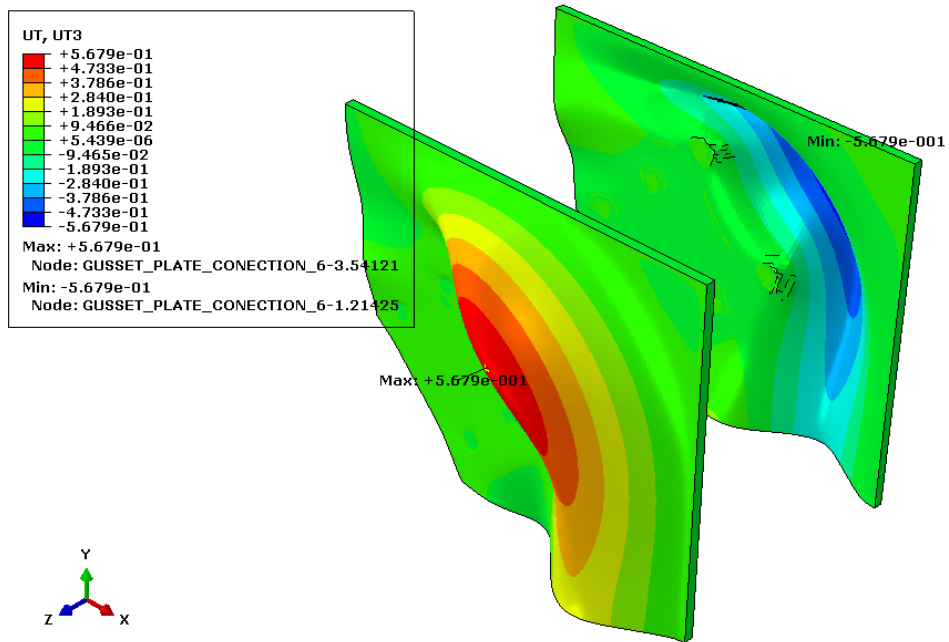


FIGURE 59: BUCKLING MODE FOR THICKNESS CASE3.

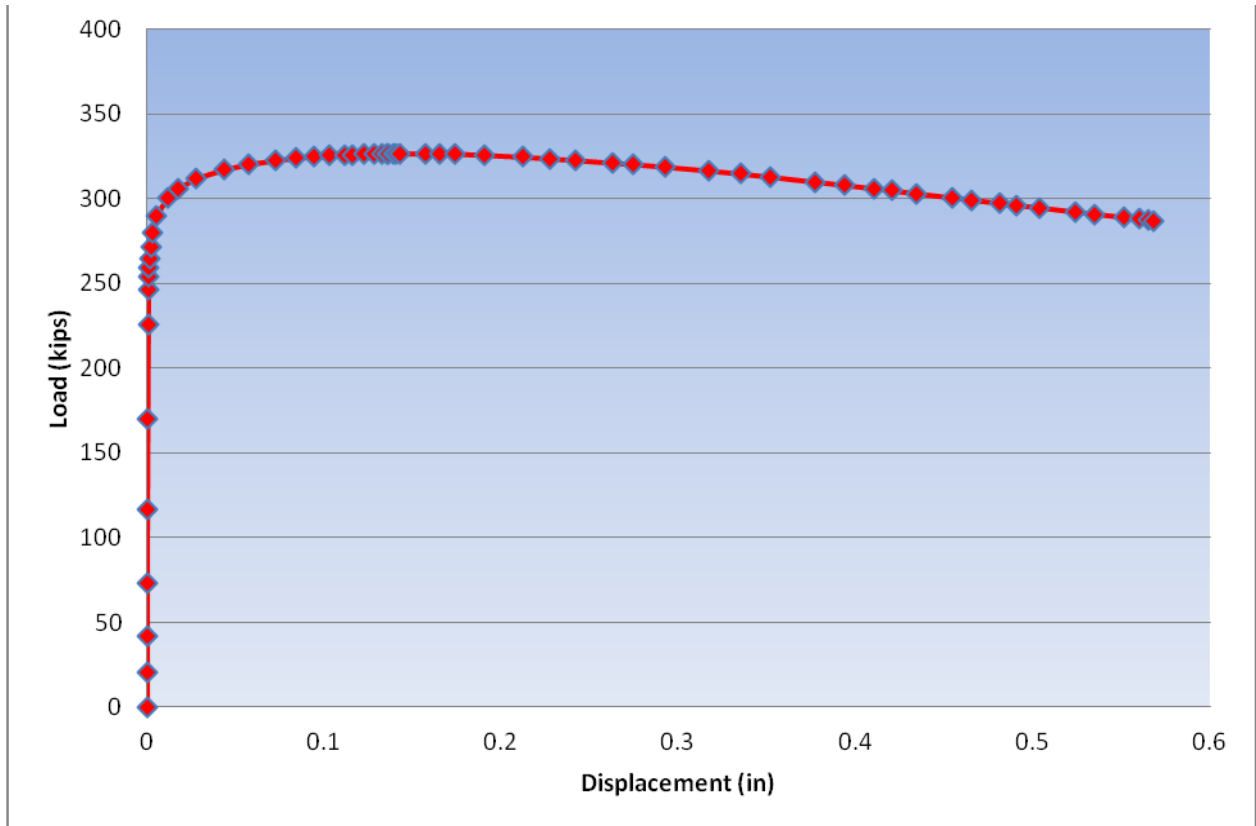


FIGURE 60: LOAD-DISPLACEMENT CURVE FOR THICKNESS CASE 3.

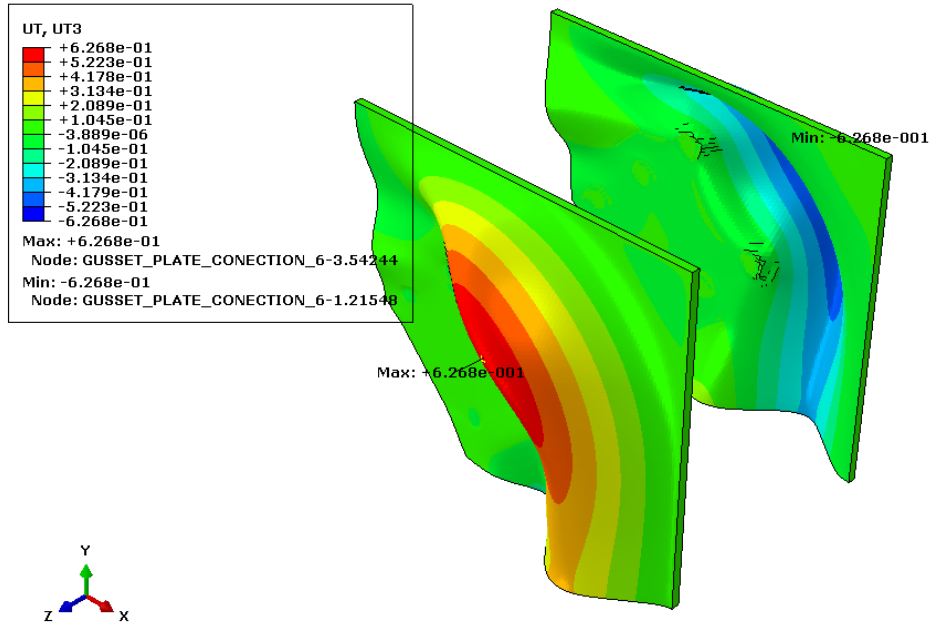


FIGURE 61: BUCKLING MODE FOR THICKNESS CASE 4.

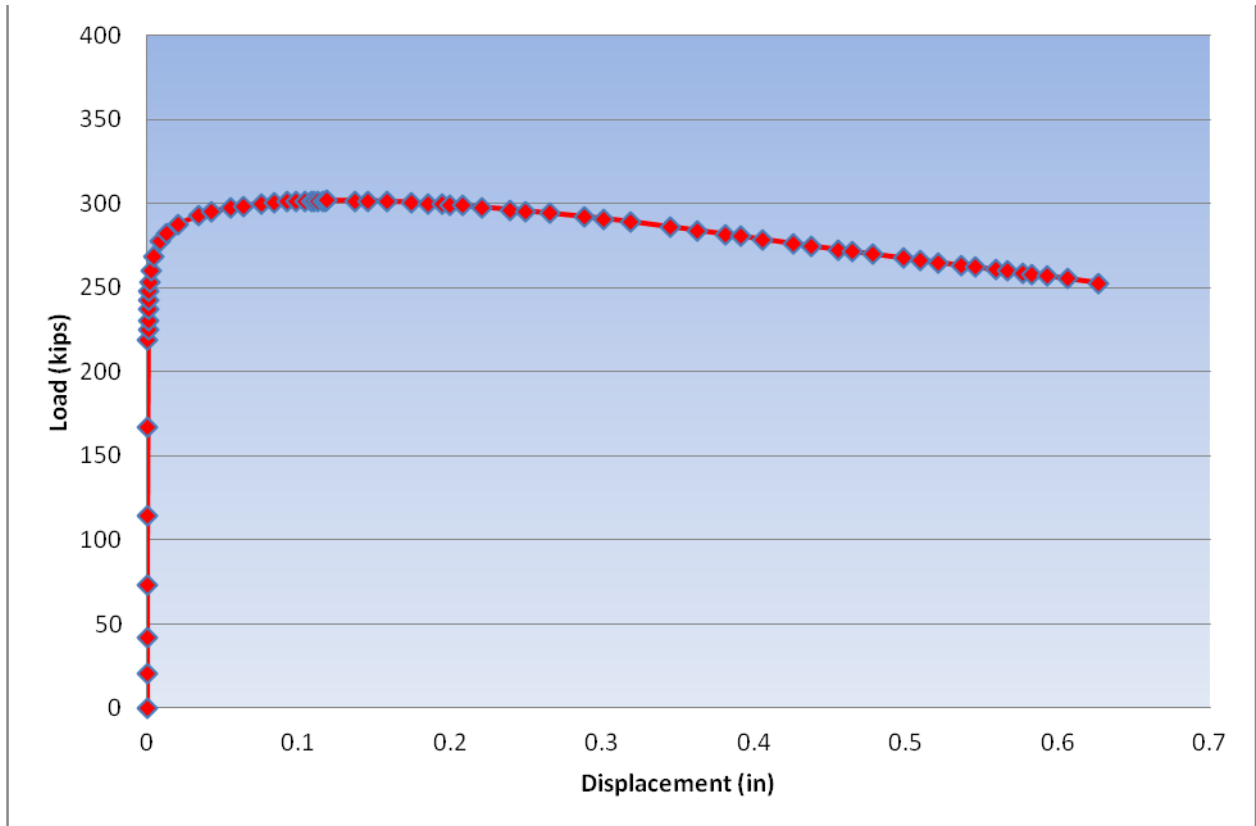


FIGURE 62: LOAD-DISPLACEMENT CURVE FOR THICKNESS CASE 4.

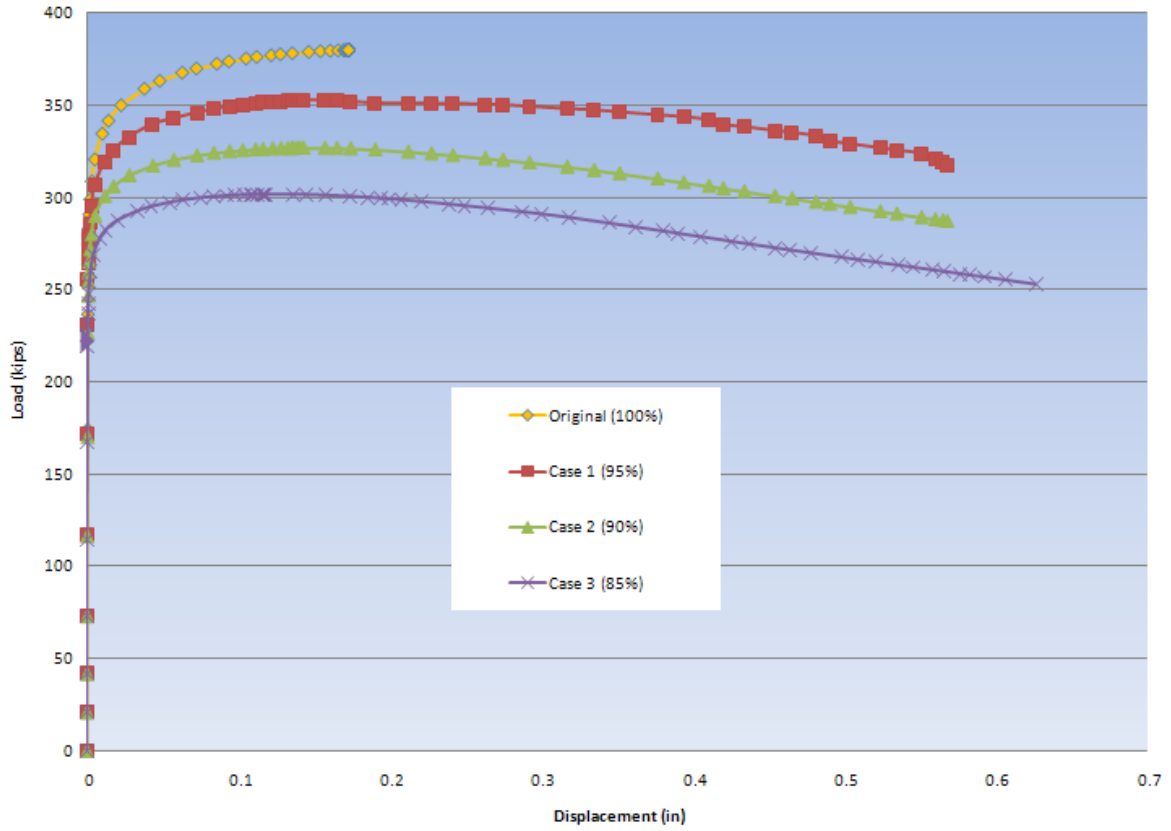


FIGURE 63: LOAD-DISPLACEMENT FOR THE FOUR THICKNESS CASES.

TABLE 19: PERCENTAGE DIFFERENCE OF CRITICAL LOAD BETWEEN HAND CALCULATIONS AND FEM (THICKNESS VARIATION).

Cases	% Difference (FHWA)	% Difference (M Thorn.)	% Difference (Yoo)	% Difference (FEA)
Cases 1-2	5.49	6.17	5.49	7.11
Cases 1-3	11.01	12.39	11.01	13.93
Cases 1-4	16.56	18.67	16.56	20.51

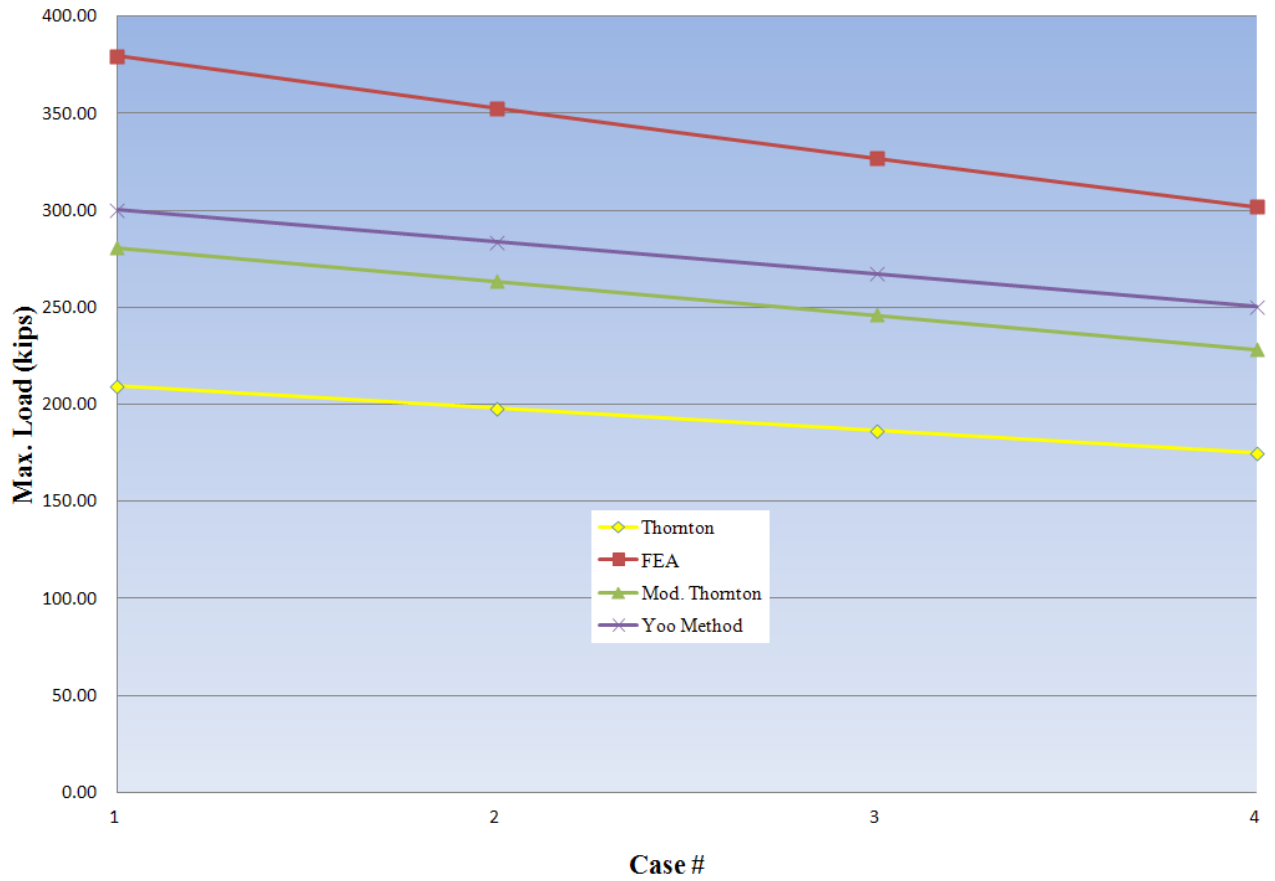


FIGURE 64: MAXIMUM LOAD FOR EACH CASE NUMBER.

TABLE 20: MAXIMUM CRITICAL LOADS AND THEIR RATIO WITH RESPECT TO THE FEA RESULTS FOR THICKNESS VARIATION.

Cases	Critical Load (FHWA) (kips)	Critical Load (Modified Thornton) (kips)	Critical Load (Yoo Method) (kips)	Critical Load (FEA) (kips)	P_{FEA}/P_{FHWA}	P_{FEA}/P_{MThorn}	P_{FEA}/P_{Yoo}
Case 1 (Original)	209.60	280.85	300.2	379.55	1.81	1.35	1.26
Case 2 (95%)	198.08	263.52	297.82	352.57	1.78	1.34	1.18
Case 3 (90%)	186.51	246.04	267.15	326.67	1.75	1.33	1.22
Case 4 (85%)	174.88	228.41	250.49	301.70	1.73	1.32	1.20

5.8.2. UNBRACED LENGTH VARIATION

In addition to the thickness variation, another important parameter to consider in buckling analysis of gusset plates is the unbraced length. This length represents the distance between the Whitmore effective width and the closest fastener rivet rows in the closest adjacent member (see Figure 65). This study is presented in the same manner as the thickness variation.

Figure 65 and Table 21 present the changes in unbraced lengths considered for the different cases. Four cases were studied with change in ΔL of 0.5 in. except the last case (Case 4) in which $\Delta L = 1.5$ in. Figure 66 through 73 show the buckling mode with the out-of-plane displacement contour and their respective load-displacement curve for the four cases. The buckling modes have an incremental deformation scale factor of 5%. Figure 74 present the comparison of load-displacement curves for the four cases. The comparison shows a slightly decrease in maximum load except case 4 as a result of a higher ΔL increment.

The percentage in structural capacity reduction presents similar results except for case 4. The buckling capacity for case 4 predicts a reduction in critical load of 6% in the FEA results while the hand calculations methods show a reduction of approximately 13% (Table 22). It seems that for large unbraced length changes, the hand-calculations may overestimate the reduction in buckling capacity, when compared to the computational results. Figure 75 shows a buckling capacity reduction with an increase in the unbraced length.

The unbraced length results are in accordance with the thickness variation, showing conservative results with respect to the Thornton method (FHWA). The Yoo method has the closest results when compared to the FEA. Again, based on the modifications of unbraced lengths, the Yoo method is recommended to verify the inelastic buckling capacity for non-slender gusset plate connections.

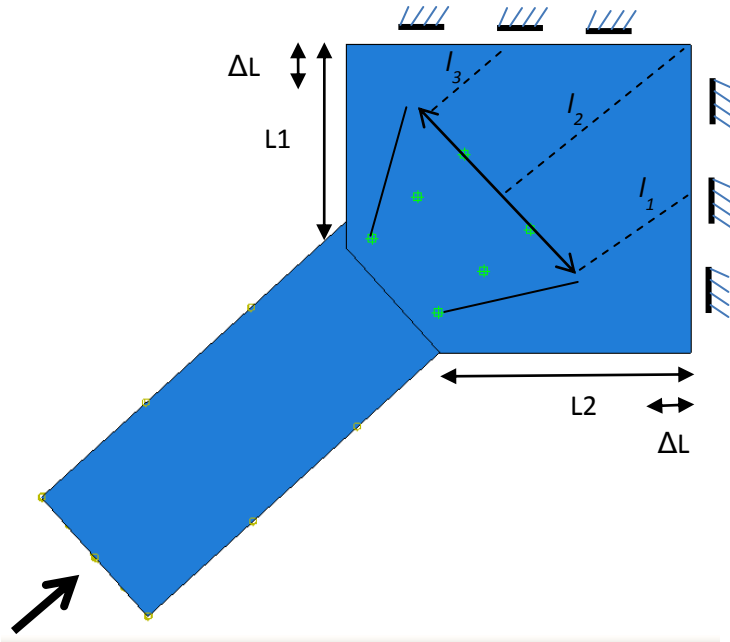


FIGURE 65: UNBRACED LENGTH AND LENGTH INCREMENT LOCATION FOR THE J-6 SUB-MODEL.

TABLE 21: LENGTH VALUES FOR THE DIFFERENT CASES.

Cases	L1 (in.)	L2 (in.)	ΔL (in.)	l_1 (in.)	l_2 (in.)	l_3 (in.)
1	7.17	9.19	0	5.07	7.42	1.94
2	7.67	9.69	0.5	5.74	8.21	2.69
3	8.17	10.19	1	6.41	8.97	3.44
4	10.17	12.19	3	9.1	11.97	6.43

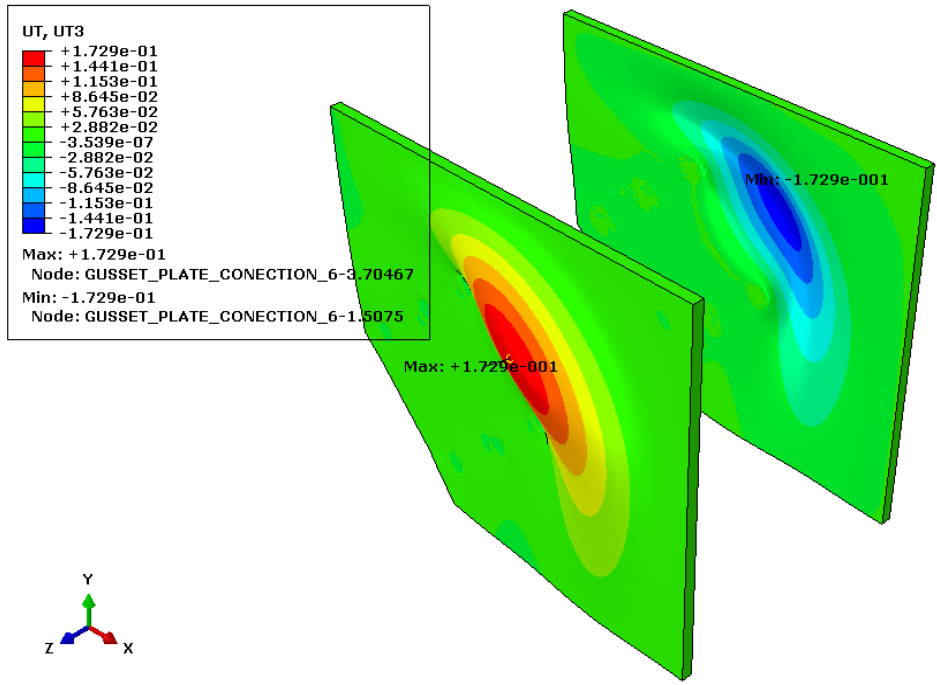


FIGURE 66: BUCKLING MODE FOR UNBRACED CASE 1.

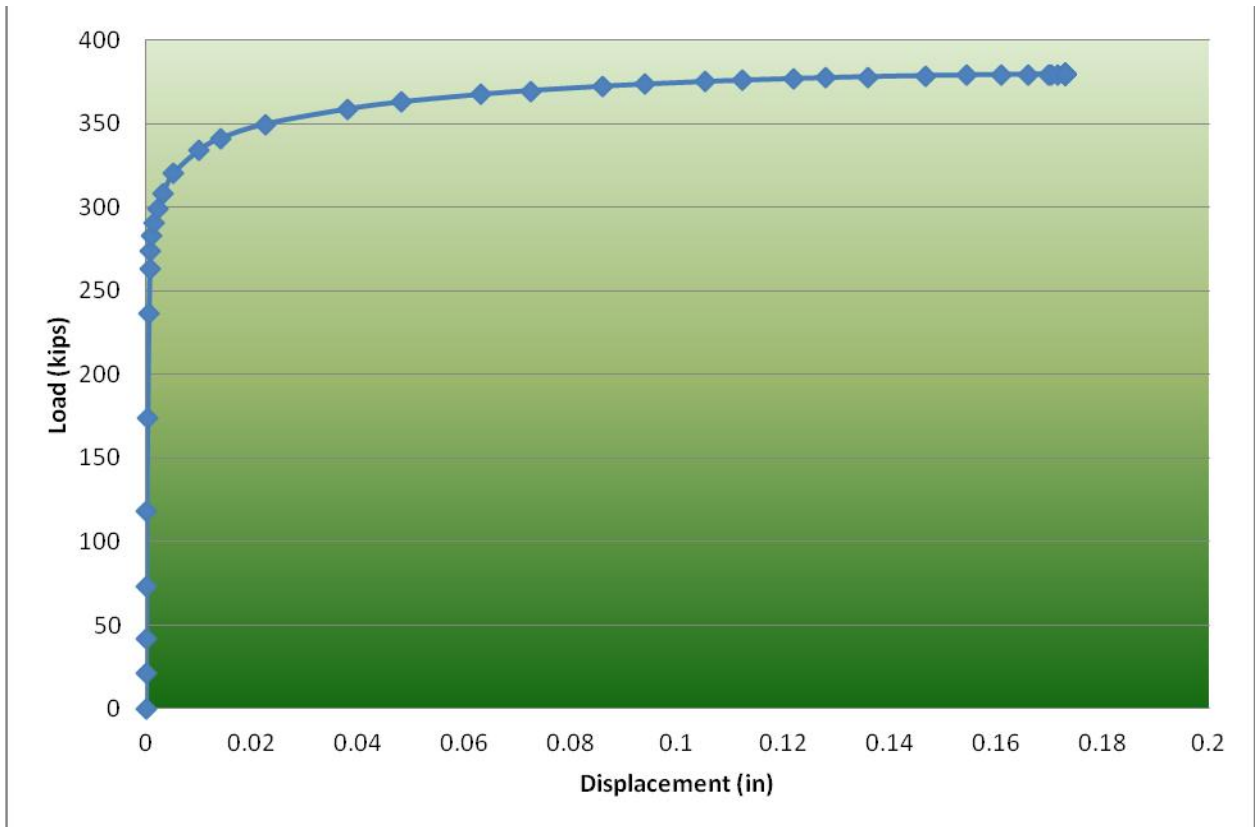


FIGURE 67: LOAD-DISPLACEMENT CURVE FOR UNBRACED CASE 1.

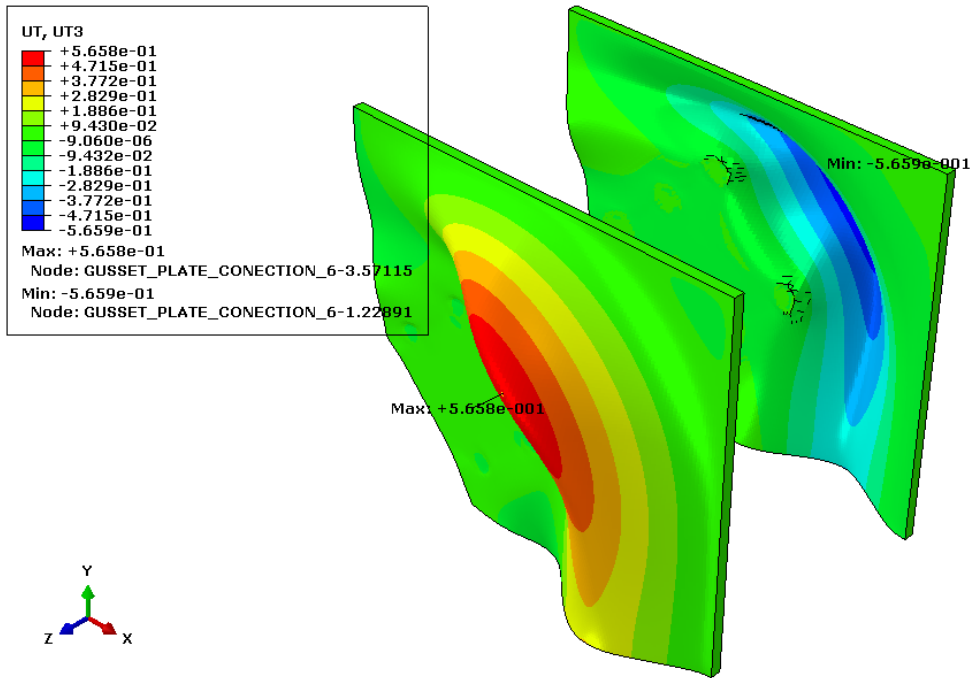


FIGURE 68: BUCKLING MODE FOR UNBRACED CASE 2.

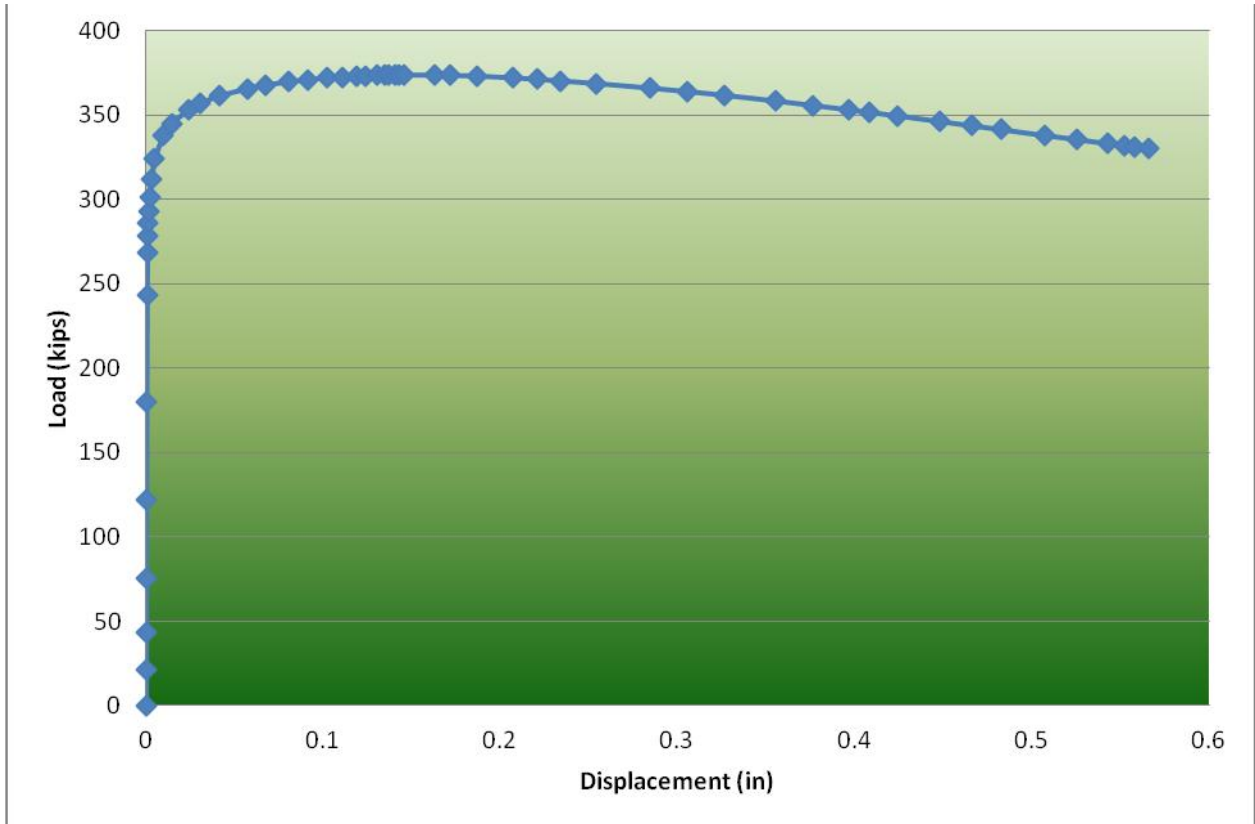


FIGURE 69: LOAD-DISPLACEMENT CURVE FOR UNBRACED CASE 2.

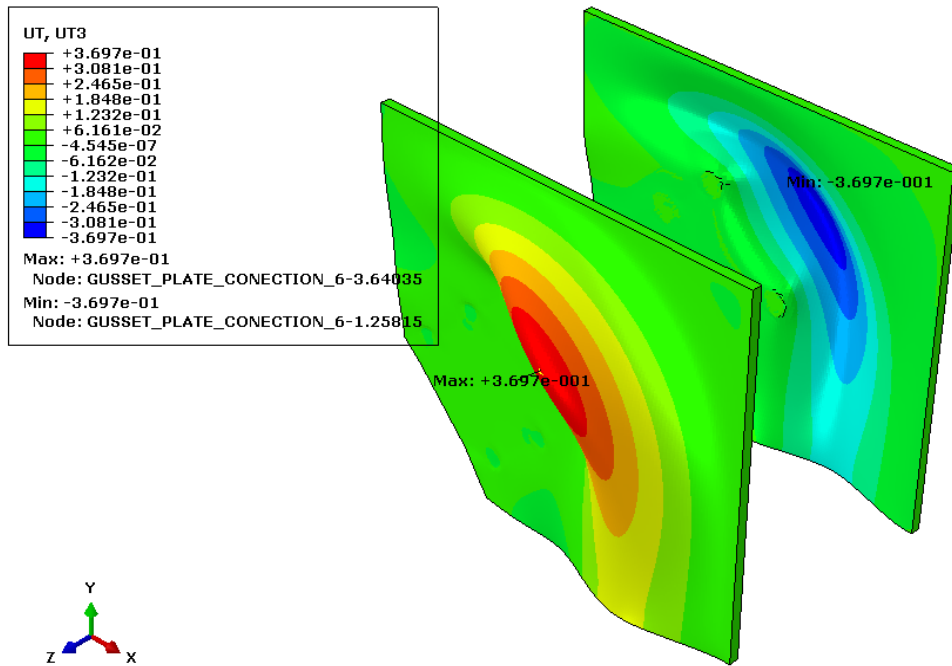


FIGURE 70: BUCKLING MODE FOR UNBRACED CASE 3.

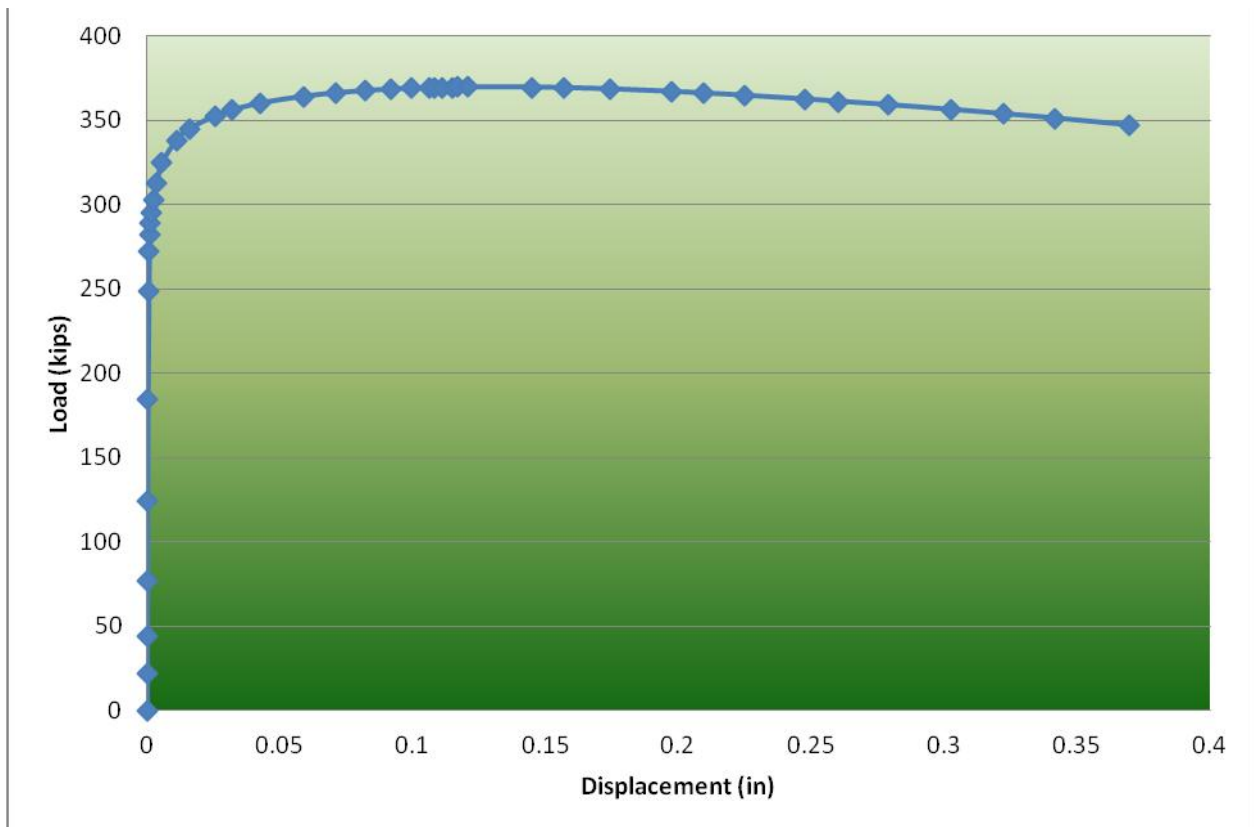


FIGURE 71: LOAD-DISPLACEMENT CURVE FOR UNBRACED CASE 3.

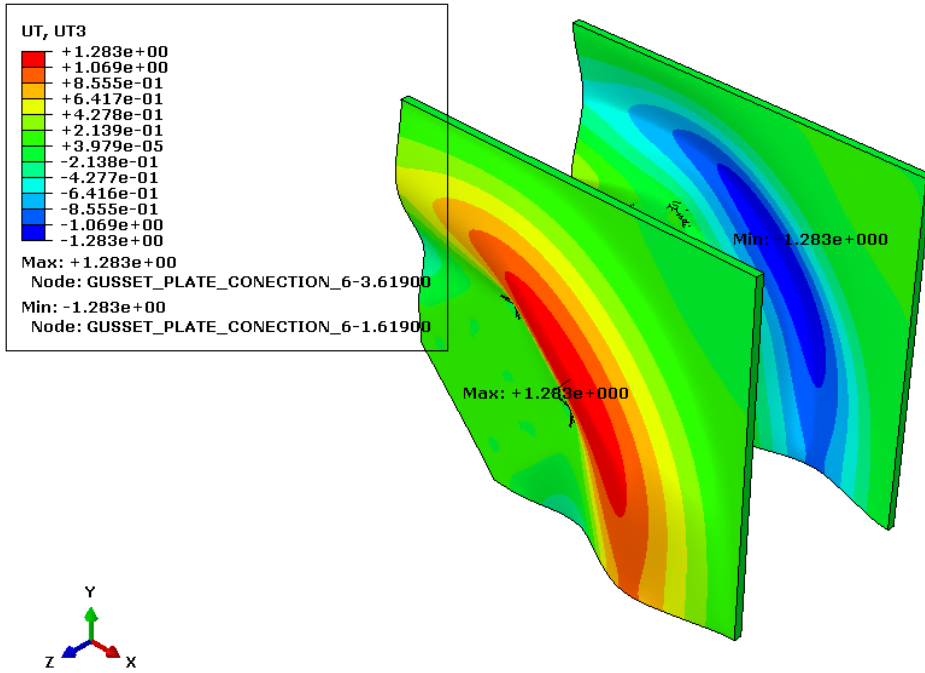


FIGURE 72: BUCKLING MODE FOR THICKNESS CASE 4.

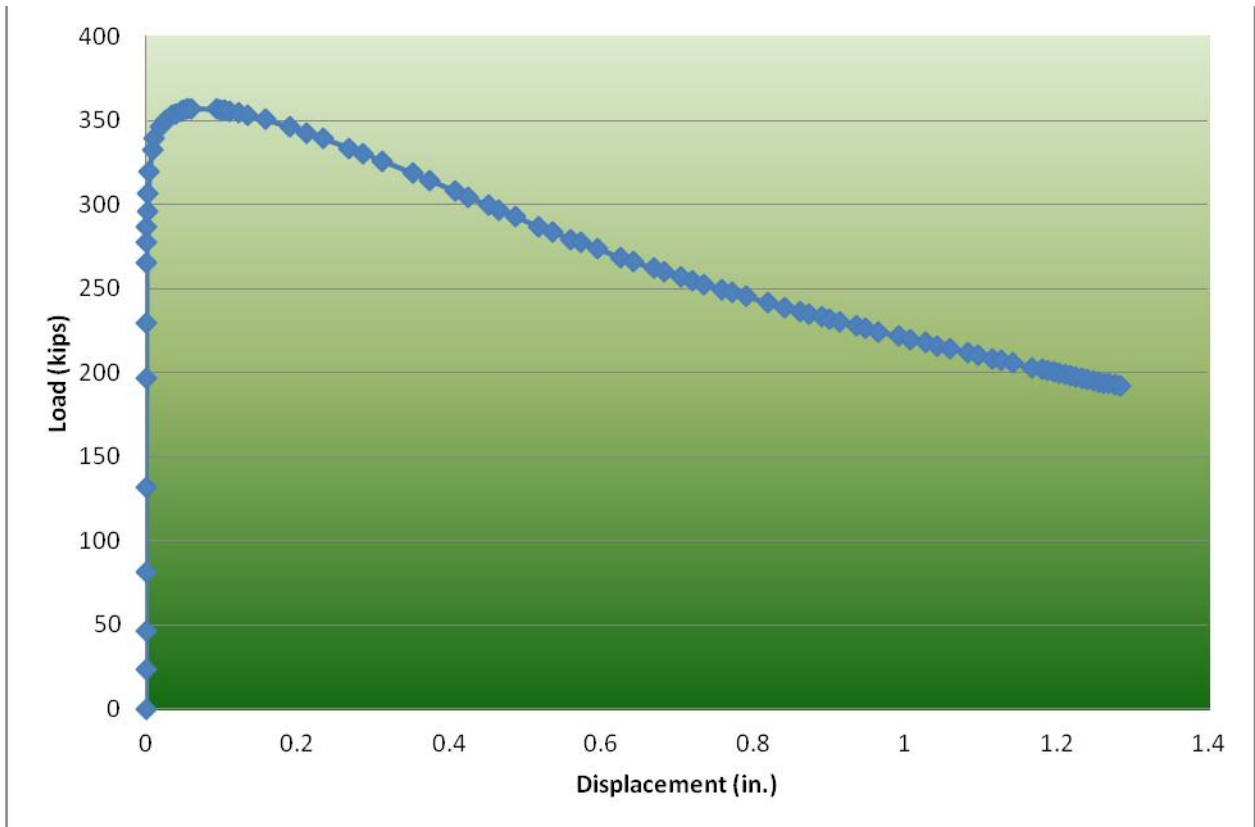


FIGURE 73: LOAD-DISPLACEMENT CURVE FOR UNBRACED CASE 4.

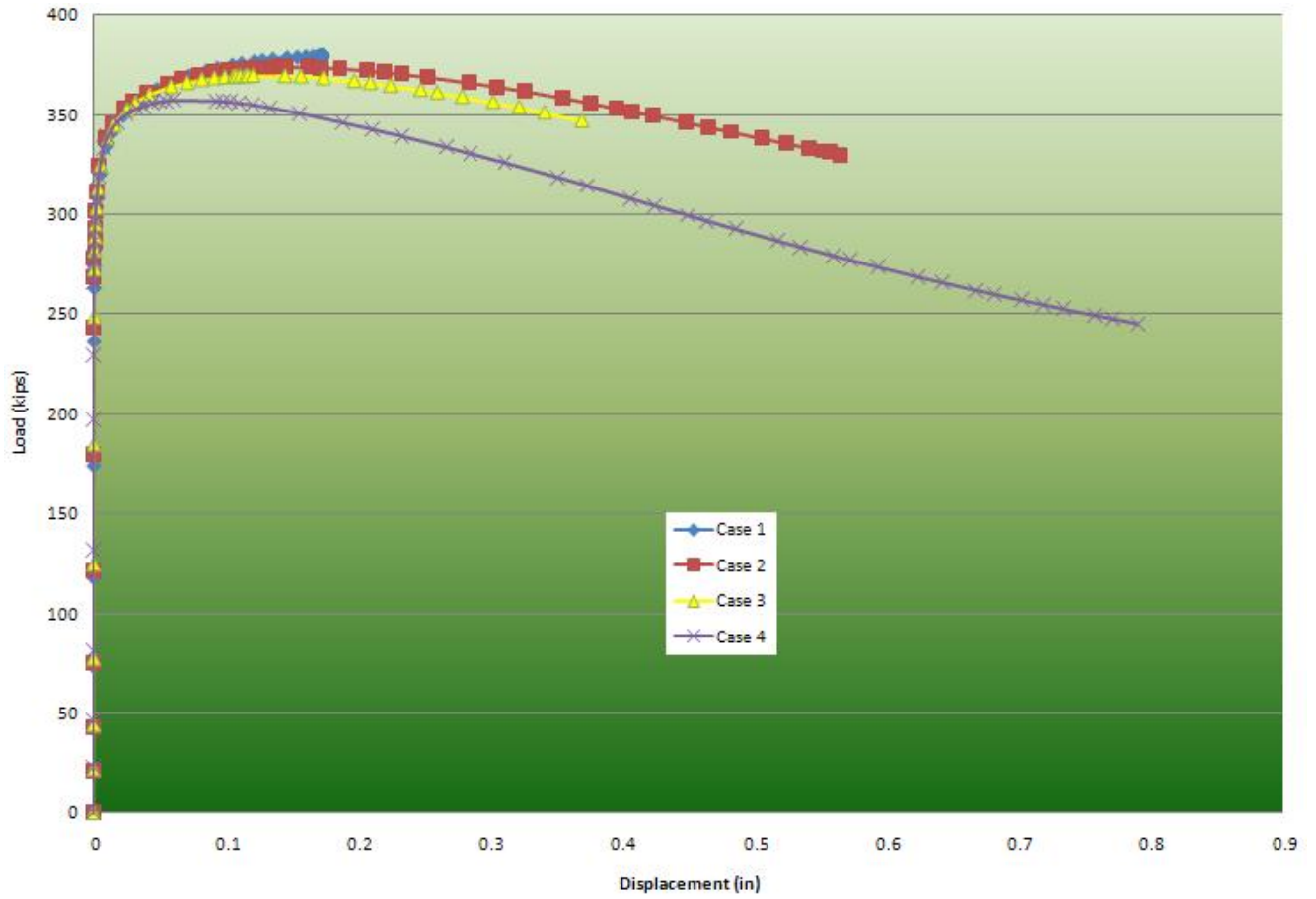


FIGURE 74: LOAD-DISPLACEMENT FOR THE FOUR UNBRACED CASES.

TABLE 22: PERCENTAGE DIFFERENCE IN CRITICAL LOAD BETWEEN HAND CALCULATIONS AND FEM (UNBRACED LENGTH VARIATION).

Cases	% Difference (FHWA)	% Difference (M Thorn.)	% Difference (Yoo)	% Difference (FEA)
Cases 1-2	1.58	2.55	1.58	1.51
Cases 1-3	3.33	5.17	3.32	2.59
Cases 1-4	11.94	16.83	11.94	5.90

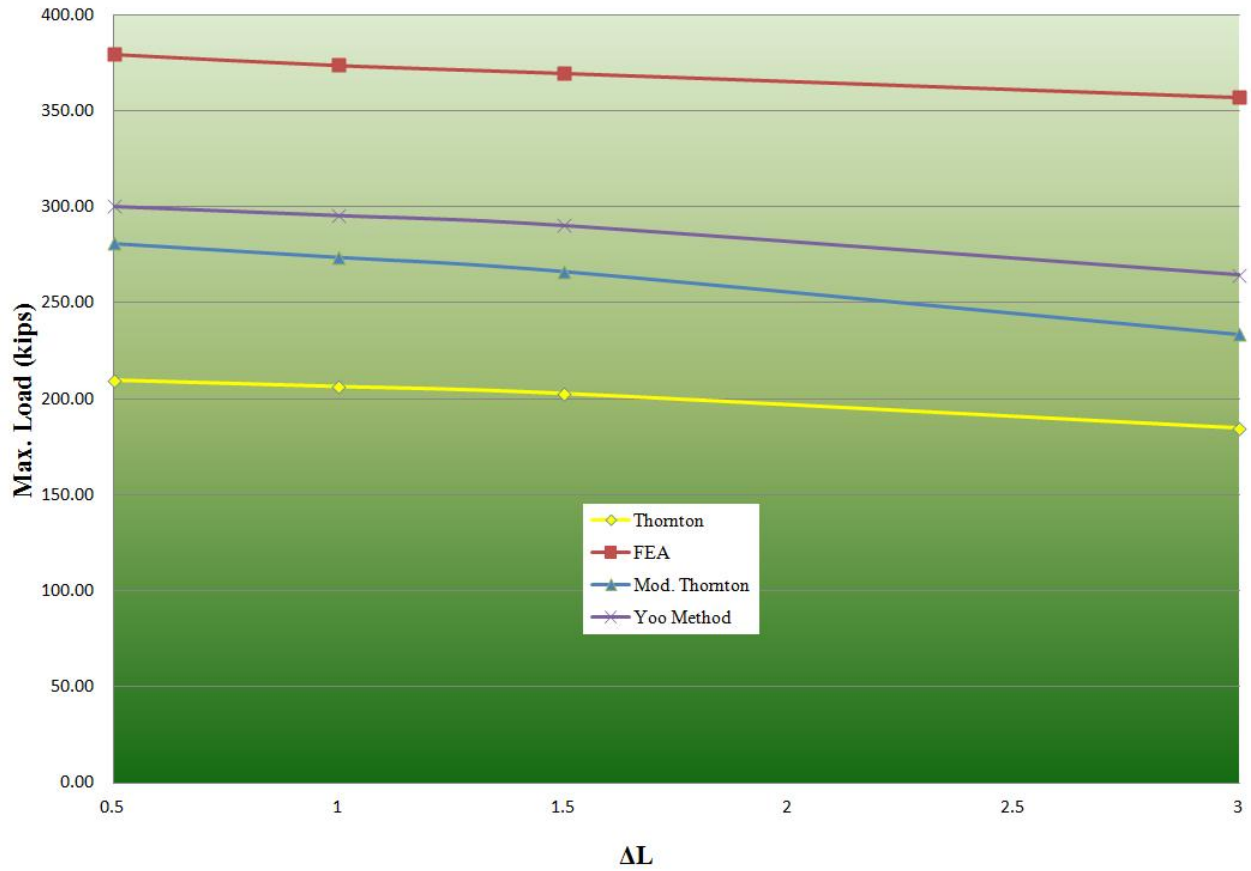


FIGURE 75: MAXIMUM LOAD VS LENGTH INCREMENT.

TABLE 23: MAXIMUM CRITICAL LOADS AND THEIR RATIO WITH RESPECT TO THE FEA RESULTS FOR UNBRACED LENGTH VARIATION.

Cases	Critical Load (FHWA) (kips)	Critical Load (Modified Thornton) (kips)	Critical Load (Yoo Method) (kips)	Critical Load (FEA) (kips)	P_{FEA}/P_{FHWA}	$P_{FEA}/P_{Mod.Thorn}$	P_{FEA}/P_{Yoo}
Case 1	209.60	280.85	300.2	379.55	1.81	1.35	1.26
Case 2	206.28	273.7	295.47	373.81	1.81	1.37	1.27
Case 3	202.61	266.34	290.22	369.70	1.82	1.39	1.27
Case 4	184.56	233.59	264.36	357.15	1.94	1.53	1.35

CHAPTER 6

6. CONCLUSION AND RECOMMENDATIONS

6.1. SUMMARY

This study aims to understand the structural behavior of steel gusset plate connections. Historical tragedies involving collapse of steel truss bridges have arisen questions regarding the design and assessment of these systems. Numerous investigations were carried out to study the current methodology used for design of steel connections. The principal gusset plate failures are shear and bearing in rivets and shear, tension, and buckling in gusset plates (GP).

This study address a target bridge located in Missouri, USA. It has GP connections commonly used in different steel truss bridges. A FEA was performed in the whole bridge using the loads specified in MBE (2011) to determine the capacity and obtain the critical loads. The critical connections were selected based on the results obtained from the analysis. These connections were obtained to analyze the following cases: i) load rating, ii) tension in the GP, iii) shear in rivets, and iv) buckling in the GP. These evaluations were performed using FEA with the program Abaqus and hand calculations. The conclusions and recommendations will be presented in the next sections.

6.2. CONCLUSIONS

The main conclusions of this thesis are the following:

- Results using the 3-D deformable solid rivets and “Fastener” rivet modeling techniques, demonstrated that both approaches predict similar stress distributions and magnitudes. The differences between the two techniques are that the 3-D deformable solid rivets take into account stresses generated in the rivets and the effect of the rivet hole in the gusset plate. The

fastener technique is 33% faster than the 3-D solid rivets in terms of computational time execution.

- The nonlinear tension analysis validates the current method used to determine the tensile capacity of a gusset plate. The maximum principal stresses were mainly in the area of the last rivet holes (inner region) as proposed by the Whitmore effective width. This effective width is used to evaluate yielding in the gross sections and fracture in the net sections. In addition, the local axial stress concentration is in accordance with the possible block shear rupture path.
- Rivets were analyzed to assess the effects produced by corrosion and by missing rivets in the critical connections. From results it seem that rivets could reduce as much as 7% its shear capacity if it experiences a reduction in diameter in the order of 6%. In addition, the loss in shear strength is not as sensitive as the FHWA equations suggests. Missing rivets could represent a potential problem in gusset plate connections since it seems that shear stresses in the remaining rivets could increase in the order of 18%.
- A buckling sensitivity analysis was the last task performed in this study. Two parameters were varied: i) reductions in the gusset plate thickness and ii) increments in the unbraced length. The results showed that the structural capacity of gusset plates can decrease in the order of 20 % in accordance to the FEA. This reduction is in close agreement with the equations used for buckling strength capacity. Furthermore, an increment of approximately 30 % in the unbraced length leads to a reduction in the order of 6% in the structural capacity, based on the FEA. The hand calculations showed a capacity reduction in the order of 13 %. Finally, the buckling study demonstrated that the Thornton method (used in the FHWA

guidance) yields significant conservative results. The approach recommended in this study for inelastic buckling capacity of non-slender gusset plates is the Yoo method since it is in very close agreement with the results obtained by computational FEA.

6.3. RECOMMENDATIONS

After the completion of this thesis, the following recommendations are proposed to continue the study of gusset plates. These are the following:

- The development of computational models for other gusset plate configurations to validate the results found in this investigation for the specific gusset plates used.
- Perform more experimental studies of large-scale gusset plate connections and rivets capable to obtain a realistic behavior and results.
- Study the effects of geometrical imperfections, cracks around the rivet holes, and load eccentricities in the gusset plates.
- Investigate the combined effect of the thickness and the unbraced length to compare the results with the methods adopted by standards and specifications for buckling capacity of gusset plates.

REFERENCES

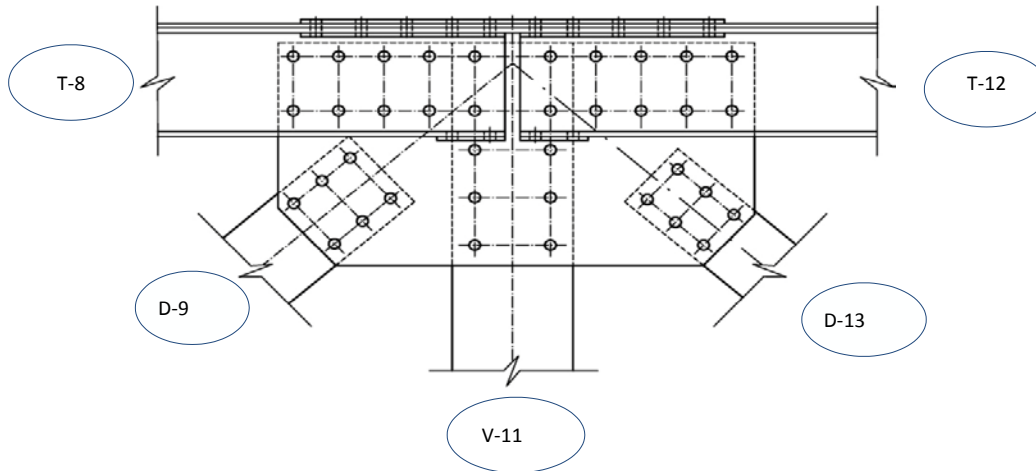
1. AASHTO LRFD Bridge Design Specifications. (2007). U.S. Customary and SI Units, 4th Edition, Washington, D.C., USA.
2. Abaqus 6.11 Dassault Systems Simulia Corp. (2011). Providence, RI, USA.
3. Berman, J., Wang B., Roeder, C., Olson, A., Lehman, D. (2010). “*Triagle Evaluation of Gusset Plates in Steel Truss Bridges*” WSDOT Research Report, WA-RD 757.1.
4. Bjorhovde, R. and Chakrabarti, S.K. (1985). “*Tests of Full-scale Gusset Plate Connections*” J. Struct. Eng., ASCE, 111(3), 667-684.
5. Chung, K., & Ip, K. (2000). “*Finite Element Modeling of Bolted Connections Between Cold-formed Steel Strips and Hot Rolled Steel Plates Under Static Shear Loading*” Engineering Structures , 22, 1271-1284.
6. Davis, C. (1967). “*Computer Analysis of the Stresses in a Gusset Plate*”. M.S. Thesis, University of Washington, Seattle, WA.
7. Goyal, V. (2011). “*Finite Element Analysis Official Lecture Notes.*” University of Puerto Rico at Mayaguez, Mayaguez, PR.
8. Gross, J.L. (1990). “*Experimental Study of Gusseted Connections.*” Eng. J., AISC, 27(3), 89-97.
9. Hu, S.Z., and Cheng, J.J.R. (1987). “*Compressive Behavior of Gusset Plate Connections.*” Struc. Eng. Report No. 153, University of Alberta, Canada.
10. Kay T. (2011). “*Numerical Modeling and Analysis of Steel Bridge Gusset Plate Connections*”. M.S. Thesis, Portland State University, Portland, OR.
11. Kulak, G., and GY, G. (2001). “*AISC LRFD Rules for Block Shear in Bolted Connections-A Review.*” AISC Eng. J. (Fourth Quarter), 199-203.

12. Liao, M., and Okazaki T. (2009). “*A Computational Study of the I-35W Bridge Failure*”
Report No. CTS 09-21
13. Liao, M., Okazaki, T., Ballarini, R., Schultz, A., Galambos, T. (2010). “*Nonlinear Finite Element Analysis of Critical Gusset Plates in the I-35W Bridge in Minnesota.*” J. of Struct. Eng., 137(1), 59-68.
14. National Transportation Safety Board (NTSB). (2008). “*Collapse of I-35W Highway Bridge Minneapolis, Minnesota, August 1, 2007.*” Accident Report NTSB/HAR-08/03.
15. National Transportation Safety Board (NTSB). (1967). “*Collapse of U.S. 35 Highway, Point Pleasant, West Virginia, December 15, 1967.*” Accident Report NTSB/HAR-71-1.
16. National Transportation Safety Board (NTSB). (1987). “*Collapse of Suspended Span of Route 95 Highway Bridge over Mianus River, Greenwich, Connecticut*” Accident Report NTSB/HAR-84/03.
17. Research Council on Structural Connections (RCSC). (2004). “*Specification for Structural Joints using ASTM A325 or A490 Bolts*”, Chicago IL, USA.
18. Richard, R.M., Rabern, D.A., Hornby, D.E., and William, G.C. (1983). “*Analytical Models for Steel Connections.*” Behavior of Metal Structures, Proceedings of the W.H. Munse Symposium, ASCE, edited by W.J. Hall and M.P. Gaus, 128-155.
19. Rossow, M. (2006). “*Bridge Inspection of Steel Superstructures-Part 1 (BIRM)*” Course No: S05-004.
20. SAP2000®. (2009). “*Integrated Software for Structural Analysis & Design*”, version 14, Computer and Structures, Inc.

21. The Manual for Bridge Evaluation Second Edition. (2011). American Association of State Highway and Transportation Officials. Washington, D.C. USA.
22. Thornton, W.A. (1984). "*Bracing Connections for Heavy Construction.*" Eng. J., AISC, 21(3), 139-148.
23. Vasarhelyi, D. (1971). "*Tests of Gusset Plate Models*". J. of the Structural Division, 97 (ST2), 665-678.
24. Walbridge S.S., Grondin G.Y., Cheng J.J.R. (2005). "*Gusset Plate Connections Under Monotonic and Cyclic Loading*". Canadian Journal of Civil Engineering, 32, 981-995.
25. Whitmore, R.E. (1952). "*Experimental Investigations of Stresses in Gusset Plates*". Bulletin No. 16, University of Tennessee Engineering Experiment Station.
26. Yam, M. C. H., and Cheng, J. J. R. (1993). "*Experimental Investigation of the Compressive Behavior of Gusset Plate Connections.*" Struct. Eng. Rep. No. 194, University of Alberta, Alberta, Canada.
27. Yam, M. C. H., and Cheng, J. J. R. (1994). "*Analytical Investigation of the Compressive Behavior and Strength of Steel Gusset Plate Connections.*" Struct. Eng. Rep. No. 207, University of Alberta, Alberta, Canada.
28. Yamamoto, K., Akiyama, N., and Okumura, T. (1988). "*Buckling Strengths of Gusseted Truss Joints*" J. Struct. Eng., ASCE, 114(3), 575-590.

APPENDIX A. LOAD RATING OF CRITICAL GUSSET PLATES

Gusset Plate Load Rating for Connection J-6 (LRFR)



Loads

Element	DC (Kips)	DW (Kips)	(LL+IM) (Kips)
D-9	41.6	0	14.11
D-13	18.9	0	9.85
V-11	15.8	0	6.9
T-8	97.4	0	25.49
T-11	138.5	0	34.62

Resistance of Rivets (J-6)

Data Rivet:		Material:			
Diameter	Area	F _y (ksi)	Tension :	45.00	(ksi)
3/4	0.442	33	Shear :	25.00	(ksi)

A) Rivets at Element D-9 (Compression)

Shear Resistance:

$$\phi R = \phi F_m A_r$$

* ϕF_v	m *	A _r	ϕR_n
21.00	1	0.442	9.28

* m: number of shear planes

*Table 1 FHWA(2009)

**Plate Bearing Resistance:

Clear distance between holes = 1.74

Clear end distance = 0.627 < 2d 1.52

$$\phi_{bb}R_n = \phi_{bb} \times 1.2 L_c t F_u$$

Φ_{bb}	L_c	t	F_u	$\phi_{bb}R_n$
0.80	0.6270	0.341	49.50	10.16

Therefore, shear resistance controls the resistance of fasteners.

Resistance of all rivets:

$P_r =$	55.692 kips
---------	--------------------

B) Rivets at Element D-13 (Tension)

Shear Resistance:

$$\phi R_n = 9.28$$

Plate Bearing Resistance:

Clear distance between holes = 1.74

Clear end distance = 0.62 < 2d 1.52

$$\phi_{bb}R_n = \phi_{bb} \times 1.2 L_c t F_u$$

Φ_{bb}	L_c	t	F_u	$\phi_{bb}R_n$
0.80	0.6200	0.341	49.50	10.05

Therefore, shear resistance controls the resistance of fasteners.

Resistance of all rivets:

$P_r =$	55.692 kips
---------	--------------------

C) Rivets at Element V-11 (Tension)

Shear Resistance:

$$\phi R_n = 9.28$$

Plate Bearing Resistance:

$$\text{Clear distance between holes} = 2.74 > 2d = 1.52$$

$$\text{Clear end distance} = 1.129 < 2d = 1.52$$

$$\phi_{bb} R_n = \phi_{bb} \times 1.2 L_c t F_u$$

ϕ_{bb}	L_c	t	F_u	$\phi_{bb} R_n$
0.80	1.1290	0.341	49.50	18.29

Therefore, shear controls the resistance of fasteners.

Resistance of all rivets:

$P_r =$	92.82 kips	185.64
---------	-------------------	--------

D) Rivets at Elements T-8 and T-12 (Compression)

Shear Resistance :

$$\phi R_n = 9.28$$

Plate Bearing Resistance:

$$\text{Clear distance between holes} = 2.24 > 2d = 1.52$$

$$\text{Clear end distance} = 0.62 < 2d = 1.52$$

$$\phi_{bb} R_n = \phi_{bb} \times 1.2 L_c t F_u$$

ϕ_{bb}	L_c	t	F_u	$\phi_{bb} R_n$
0.80	0.6200	0.341	49.50	10.05

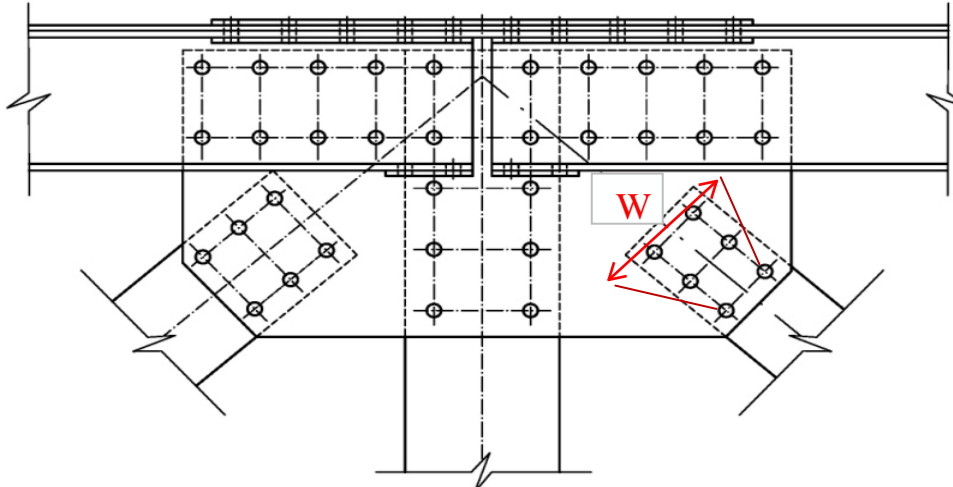
Therefore, shear resistance controls the resistance of fasteners. Resistance of all rivets:

$$P_r = \quad \mathbf{92.82 \text{ kips}} \quad 185.64$$

** Section 6.13.2.9 AASTHO LRFD Bridge Design Specification

Gusset Plate in Tension (J-6)

A) Tension at Element D-13 (Tension)



$$W = 8.774$$

Gross Section Yielding

$$\text{Resistance: } P_r = \phi_y F_y A_g$$

$$A_g$$

ϕ_y	F_y	A_g	P_r
0.95	33	2.992	93.80

kips

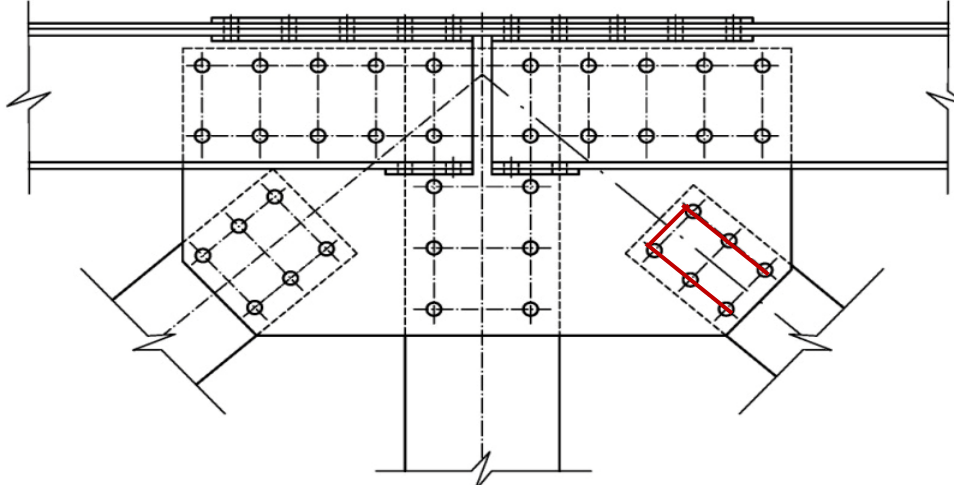
Net Section Fracture Resistance:

$$P_r = \phi_u F_u A_n U$$

ϕ_u	F_u	A_n	P_r
0.80	50	2.474	97.96

kips

Block Shear Rupture Resistance:



$$A_{tn} = 0.76384$$

$$A_{vn} = 2.7962$$

Check:

$$A_{tn} = 0.76384 \leq 0.58A_{vn} = 1.621796$$

Therefore:

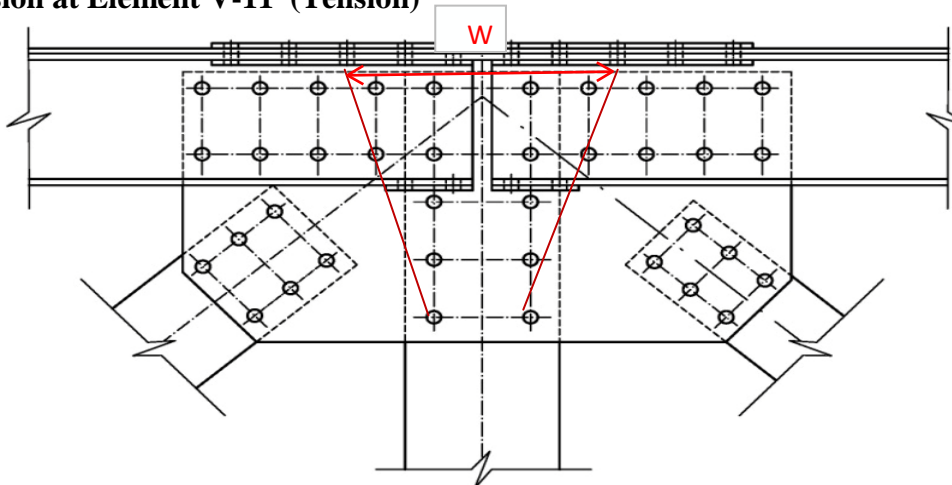
$$P_r = \phi_{bs} (0.58 * F_u A_{vn} + F_y A_{tg})$$

ϕ_{bs}	F_u	A_{vn}	F_y	A_{tg}	P_r
0.80	50	2.796	33.00	1.023	91.2303

Kips

*** Block Shear governs the capacity of the gusset plate for element D-9.**

B) Tension at Element V-11 (Tension)



$$W = 22.32$$

Gross Section Yielding

Resistance: $P_r = \phi_y F_y A_g$

$$A_g$$

ϕ_y	F_y	A_g	P_r
0.95	33	7.611	238.61

kips

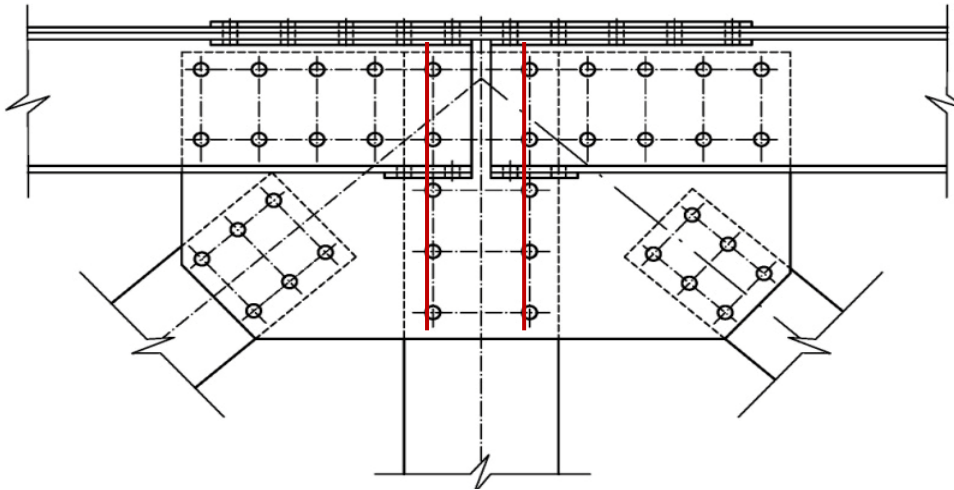
Net Section Fracture Resistance:

$$P_r = \phi_u F_u A_n U$$

ϕ_u	F_u	A_n	P_r
0.80	50	7.093	280.87

kips

Block Shear Rupture Resistance:



$$A_{tn} = 0$$

$$A_{vn} = 4.5012$$

Check:

$$A_{tn} = 0 \leq 0.58A_{vn} = 2.610696$$

$$P_r = \phi_{bs} (0.58 * F_u A_{vn} + F_y A_{tg})$$

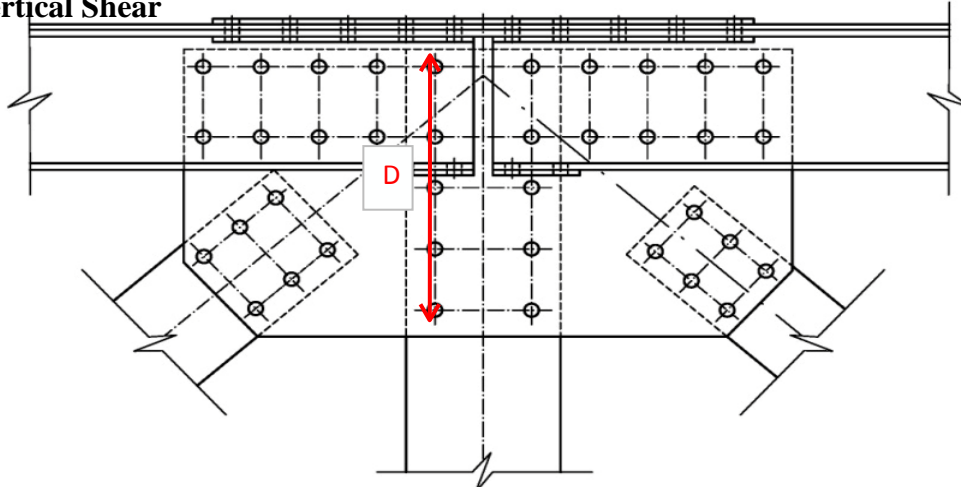
ϕ_{bs}	F_u	A_{vn}	F_y	A_{tg}	P_r
0.80	50	4.501	33.00	0	103.384

Kips

*** Block Shear governs the capacity of the gusset plate for element D-9.**

Shear Resistance (J-6)

A) Vertical Shear



Gross Section Shear Yielding Resistance :

$$D = 16.41$$

$$V_r = \phi_{vy} 0.58 F_y A_g \times \Omega$$

ϕ_{vy}	F_y	A_g	Ω	P_r
0.95	33	5.596	0.74	75.29397

kips

Net Section Shear Fracture Resistance

∴

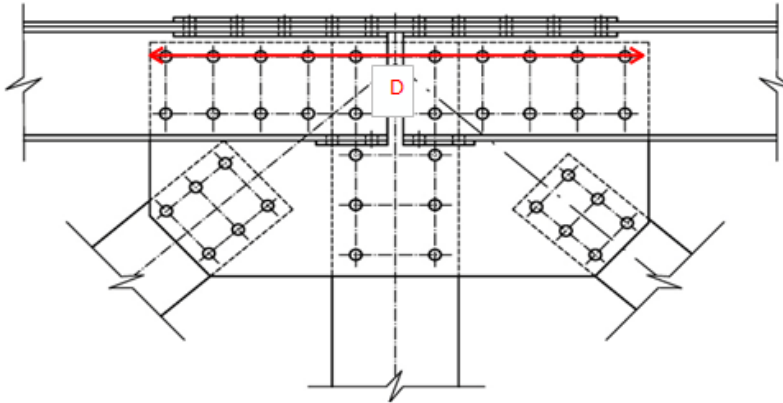
$$V_r = \phi_{vu} 0.58 F_u A_n$$

n

ϕ_{vu}	F_u	A_n	P_r
0.80	50	4.300	98.76263

kips

B) Horizontal Shear



Gross Section Shear Yielding Resistance:

$$D = 31.49$$

$$V_r = \phi_{vy} 0.58 F_y A_g \times \Omega$$

ϕ_{vy}	F_y	A_g	Ω	P_r
0.95	33	10.738	0.74	144.4855

kips

Net Section Shear Fracture Resistance:

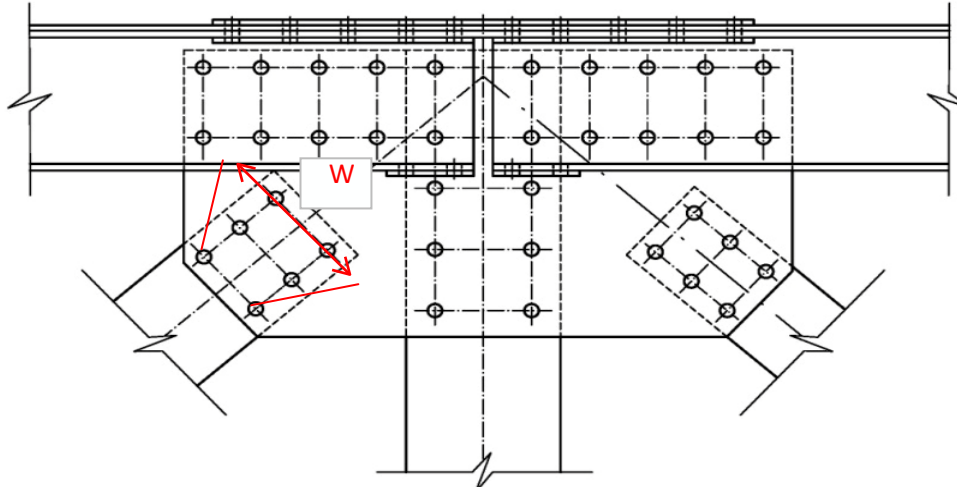
$$V_r = \phi_{vu} 0.58 F_u A_n$$

ϕ_{vu}	F_u	A_n	P_r
0.80	50	8.146	187.1086

kips

Gusset Plate in Compression (J-6)

A) Compression at Element D-9 (Compression)



$$W = 9.774$$

$$K = 0.65$$

I_g	A_g	r_s	l	F_y	E	λ
0.03	3.33	0.10	4.81	33	29000	0.116306919

$$\lambda = 0.116307 < 2.25$$

Therefore,

$$P_n = 0.66^\lambda F_y A_g$$

$P_n =$	104.798 kips
---------	---------------------

Load Rating J-6

A) Axial Resistance Summary

Elements	Axial Resistance of one Gusset Plate (Kips)					Controlling Axial Resistance (Kips)
	Resistance of Rivets (Kips)	Gross Section Yielding (Tension)	Net Section Fracture (Tension)	Block Shear Rupture	Compression Buckling	
D-9	55.7	-	-	-	104.8	55.7
D-13	55.7	93.8	98.0	91.2	-	55.7
V-11	92.8	238.6	280.9	103.4	-	92.8
T-8	92.8	-	-	-	-	92.8
T-11	92.8	-	-	-	-	92.8

B) Shear Resistance Summary

Orientation of Section	Shear Resistance of one Gusset Plate (Kips)		Controlling Shear Resistance (Kips)
	Gross Section Yielding in Shear	Net Section Fracture in Shear	
Vertical	75.3	98.8	75.3
Horizontal	144.5	187.1	144.5

C) Inventory and Operating Rating Factors

Element	1.25DC+1.50DW	(LL+IM)	Controlling Axial Resistance*	IRF*	ORF*
D-9	26	7.055	50.1	1.95	2.53
D-13	11.8125	4.925	50.1	4.44	5.76
V-11	9.875	3.45	83.5	12.20	15.82
T-8	45.65625	9.55875	83.5	2.26	3.93
T-11	64.921875	12.9825	83.5	0.82	1.80

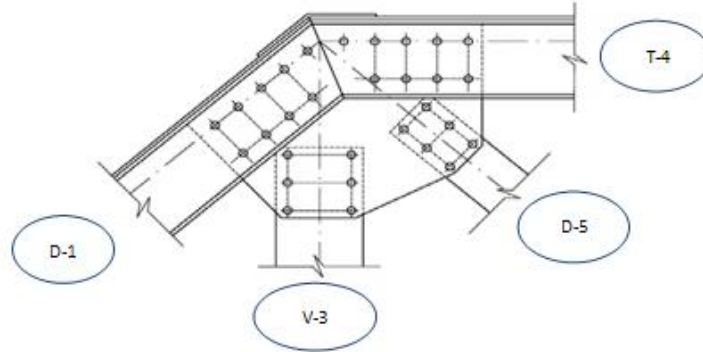
Orientation of Section	1.25DC+1.50DW	(LL+IM)	Controlling Axial Resistance*	IRF*	ORF*
Vertical	17.78125	6.745	67.8	4.234529	5.489205
Horizontal	28.09375	8.9	130.0	6.54531	8.484662

*Controlling Axial Resistance = $C = f_c \phi_s \phi R_n$

IRF = Inventory Rating Factor

ORF = Operating Rating Factor

Gusset Plate Load Rating for Connection J-2 (LRFR)



Loads

Element	DC (Kips)	DW (Kips)	(LL+IM) (Kips)
D-1	85.1	0	18.38
D-5	58	0	14.32
V-3	19.3	0	7.92
T-4	97.4	0	21.22

Resistance of Rivets

Data Rivet:		Material:			
Diameter	Area	F _y (ksi)	Tension :	45.00	(ksi)
3/4	0.442	33	Shear :	25.00	(ksi)

A) Rivets at Element D-1 (Compression)

Shear Resistance :

$$\phi R = \phi F_m A_r$$

* ϕF_v	m *	A _r	ϕR_n
21.00	1	0.442	9.28

* m: number of shear planes

*Table 1 FHWA(2009)

**Plate Bearing Resistance:

Clear distance between holes = 2.24

Clear end distance = 1.12 < 2d = 1.52

$$\phi_{bb}R_n = \phi_{bb} \times 1.2 L_c t F_u$$

* ϕ_{bb}	L_c	t	F_u	$\phi_{bb}R_n$
0.80	1.1200	0.341	49.50	18.15

* Section 6.5.4.2 AASTHO LRFD Bridge Design Specification

Therefore, shear resistance controls the resistance of

fasteners. Resistance of all rivets:

$P_r =$	83.538 kips
---------	--------------------

B) Rivets at Element D-5 (Tension)

Shear Resistance :

$$\phi R_n = 9.28$$

Plate Bearing Resistance:

Clear distance between holes = 2.24

Clear end distance = 0.625 < 2d = 1.52

$$\phi_{bb}R_n = \phi_{bb} \times 1.2 L_c t F_u$$

ϕ_{bb}	L_c	t	F_u	$\phi_{bb}R_n$
0.80	0.6250	0.341	49.50	10.13

Therefore, shear resistance controls the resistance of fasteners.

Resistance of all rivets:

$P_r =$	55.692 kips
---------	--------------------

C) Rivets at Element V-3 (Tension)

Shear Resistance:

$$\phi R_n = 9.28$$

Plate Bearing Resistance:

$$\text{Clear distance between holes} = 2.24$$

$$\text{Clear end distance} = 0.62 < 2d \quad 1.52$$

$$\phi_{bb} R_n = \phi_{bb} \times 1.2 L_c t F_u$$

Φ_{bb}	L_c	t	F_u	$\phi_{bb} R_n$
0.80	0.6200	0.341	49.50	10.05

Therefore, shear resistance controls the resistance of fasteners.

Resistance of all rivets:

$$P_r = 55.692 \text{ kips}$$

D) Rivets at Element T-4

(Compression) Shear Resistance :

$$\phi R_n = 9.28$$

Plate Bearing Resistance:

$$\text{Clear distance between holes} = 2.24$$

$$\text{Clear end distance} = 1.12 < 2d \quad 1.52$$

$$\phi_{bb} R_n = \phi_{bb} \times 1.2 L_c t F_u$$

Φ_{bb}	L_c	t	F_u	$\phi_{bb} R_n$
0.80	1.1200	0.341	49.50	18.15

Therefore, shear controls the resistance of fasteners.

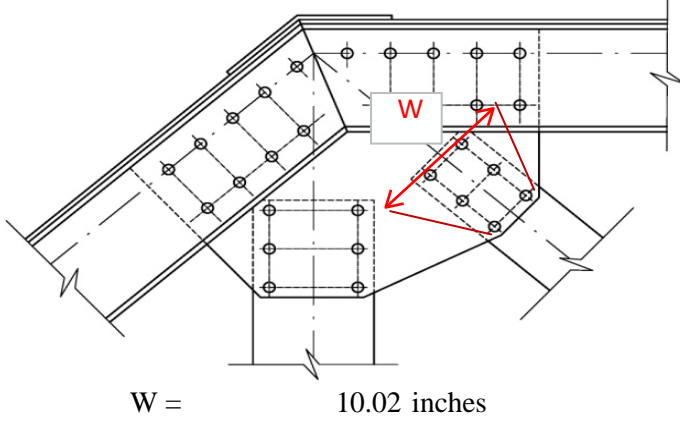
Resistance of all rivets:

$$P_r = 83.538 \text{ kips}$$

** Section 6.13.2.9 AASTHO LRFD Bridge Design Specification

Gusset Plate in Tension (J-2)

A) Element D-5 (Tension)



Gross Section Yielding

$$\text{Resistance : } P_r = \phi_y F_y A_g$$

A_g

ϕ_y	F_y	A_g	P_r
0.95	33	3.417	107.12

kips

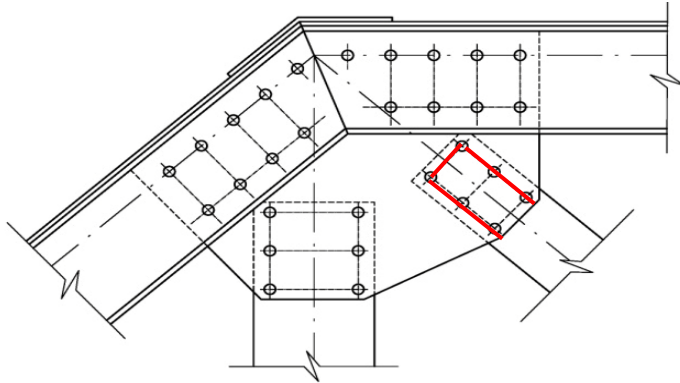
Net Section Fracture Resistance:

$$P_r = \phi_u F_u A_n U$$

ϕ_u	F_u	A_n	P_r
0.80	50	2.899	114.78

kips

Block Shear Rupture Resistance:



$A_{tn} = 0.76384$

$A_{vn} = 3.4782$

Check:

$A_{tn} = 0.76384 \leq 0.58A_{vn} = 2.017356$

Therefore:

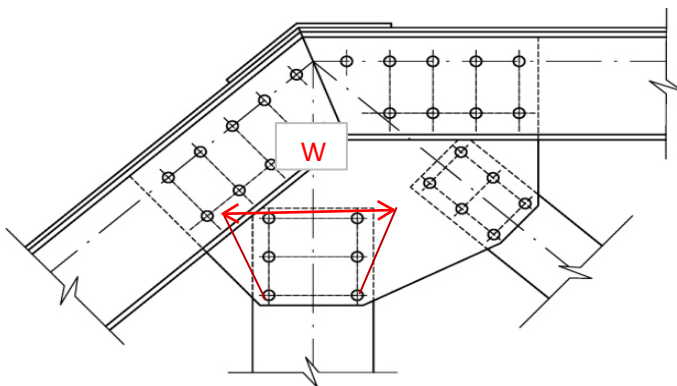
$P_r = \phi_{bs} (0.58 * F_u A_{vn} + F_y A_{tg})$

ϕ_{bs}	F_u	A_{vn}	F_y	A_{tg}	P_r
0.80	50	3.478	33.00	1.023	106.894

Kips

*** Block Shear governs the capacity of the gusset plate for element D-5.**

B) Element V-3 (Tension)



$W = 12.77$

Gross Section Yielding Resistance

:

$$P_r = \phi_y F_y A_g$$

ϕ_y	F_y	A_g	P_r
0.95	33	4.355	136.52

kips

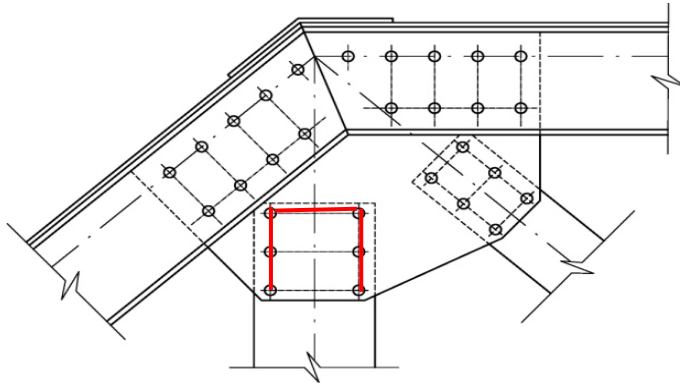
Net Section Fracture Resistance:

$$P_r = \phi_u F_u A_n U$$

ϕ_u	F_u	A_n	P_r
0.80	50	3.836	151.92

kips

Block Shear Rupture Resistance:



$$A_{tn} = 1.73228$$

$$A_{vn} = 3.4782$$

Check:

$$A_{tn} = 1.73228 \leq 0.58A_{vn} = 2.017356$$

Therefore:
:

$$P_r = \phi_{bs} (0.58 F_u A_{vn} + F_y A_{tg})$$

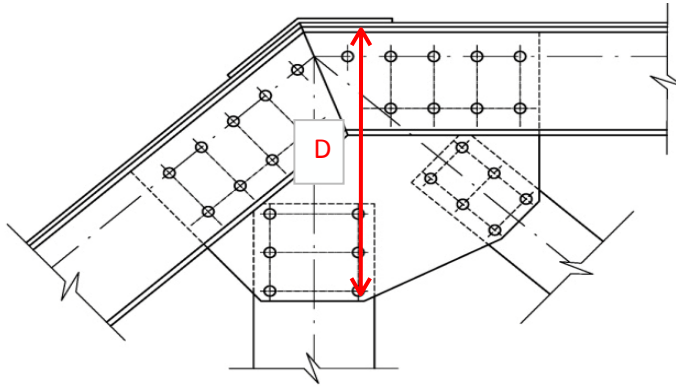
ϕ_{bs}	F_u	A_{vn}	F_y	A_{tg}	P_r
0.80	50	3.478	33.00	1.99144	132.461

Kips

*** Block Shear governs the capacity of the gusset plate for element V-3.**

Shear Resistance (J-2)

A) Vertical Shear



Gross Section Shear Yielding Resistance:

$$D = 21.08$$

$$V_r = \phi_{vy} 0.58 F_y A_g \times \Omega$$

ϕ_{vy}	F_y	A_g	Ω	P_r
0.95	33	7.188	0.74	96.72133

kip

Net Section Shear Fracture Resistance

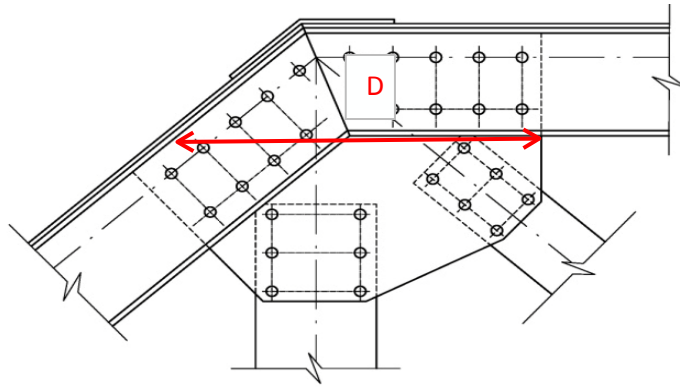
∴

$$V_r = \phi_{vu} 0.58 F_u A_n$$

ϕ_{vu}	F_u	A_n	P_r
0.80	50	6.411	147.2433

kip

B) Horizontal Shear



Gross Section Shear Yielding Resistance

∴

$$D = 24.5$$

$$V_r = \phi_{vy} 0.58 F_y A_g \times \Omega$$

ϕ_{vy}	F_y	A_g	Ω	P_r
0.95	33	8.355	0.74	112.4133

kips

Net Section Shear Fracture Resistance:

$$V_r = \phi_{vu} 0.58 F_u A_n$$

ϕ_{vu}	F_u	A_n	P_r
0.80	50	7.059	162.1242

kips

Load Rating J-2

A) Axial Resistance Summary

Elements	Axial Resistance of one Gusset Plate (Kips)					Controlling Axial Resistance (Kips)
	Resistance of Rivets (Kips)	Gross Section Yielding (Tension)	Net Section Fracture (Tension)	Block Shear Rupture	Compression Buckling	
D-1	83.5	-	-	-	-	83.5
D-5	55.7	107.1	114.8	106.9	-	55.7
V-3	55.7	136.5	151.9	132.5	-	55.7
T-4	83.5	-	-	-	-	83.5

B) Shear Resistance Summary

Orientation of Section	Shear Resistance of one Gusset Plate (Kips)		Controlling Shear Resistance (Kips)
	Gross Section Yielding in Shear	Net Section Fracture in Shear	
Vertical	96.7	147.2	96.7
Horizontal	112.4	162.1	112.4

C) Inventory and Operating Rating Factors

Element	1.25DC+1.50DW	(LL+IM)	*Controlling Axial Resistance	IRF*	ORF*
D-1	53.1875	9.19	75.2	1.37	1.77
D-5	36.25	7.16	50.1	1.11	1.44
V-3	12.0625	3.96	50.1	5.49	7.12
T-4	60.875	6.0477	75.2	1.35	1.75

Orientation of Section	1.25DC+1.50DW	(LL+IM)	*Controlling Axial Resistance	IRF*	ORF*
Vertical	36.33125	8.755	87.0	3.310301	4.29113
Horizontal	66.45625	12.15	101.2	1.632721	2.11649

Controlling Axial Resistance = $C = f_c \phi_s \phi R_n$

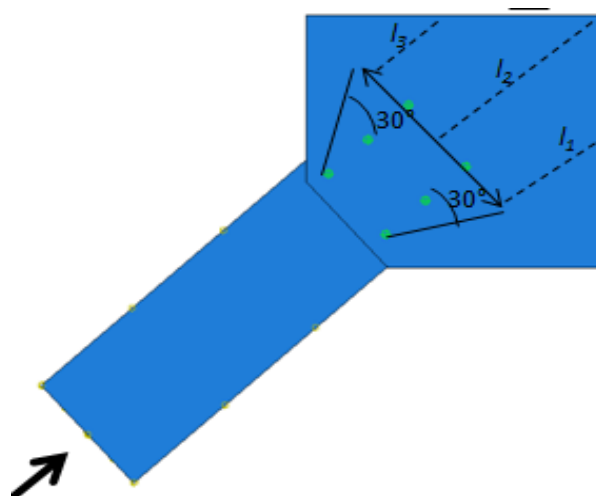
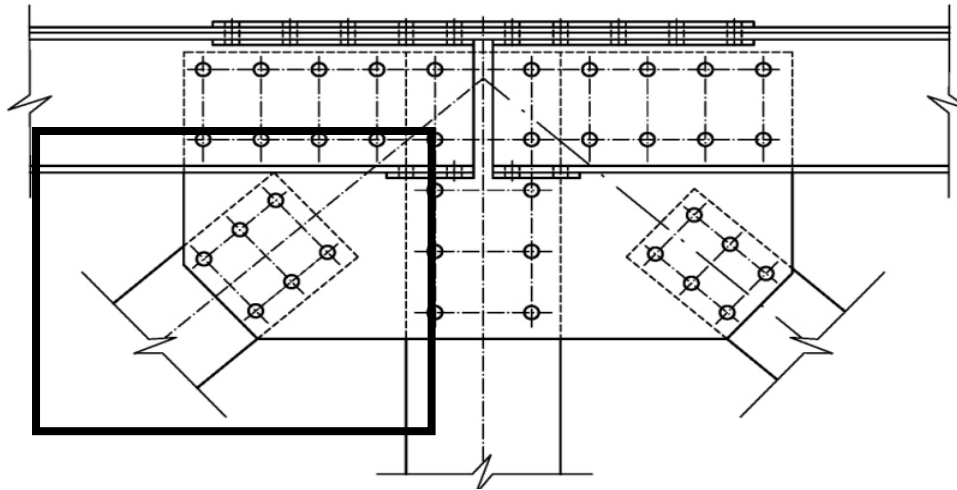
IRF = Inventory Rating Factor

ORF = Operating Rating Factor

APPENDIX B. HAND CALCULATIONS EXAMPLES FOR THE THREE METHODS USED TO DETERMINE BUCKLING CAPACITY OF GUSSET PLATE CONNECTIONS

Example for the Thornton (FHWA) Method (Original Case)

Compression at Element D-9 (J-6 Connection)



Hand Calculations (Original Case)(See Section 6.9.4.1 AASHTO):

Model Input Data:

Whitmore Effective Width (W) = 9.774 in
 Effective Length Factor (K) (See Table) 0.65
 Yield Stress (F_y) = 33 ksi
 Modulus of Elasticity (E) = 29000 ksi

	(a)	(b)	(c)	(d)	(e)	(f)
Buckled shape						
Theoretical K value	0.5	0.7	1.0	1.0	2.0	2.0
Design K value	0.65	0.80	1.0	1.2	2.1	2.0

Calculations:

$$\lambda = \left(\frac{kL}{r_s \pi}\right)^2 \frac{F_y}{E}$$

L = Average Unbraced Length (l₁, l₂, l₃) = 4.81 in
 Moment of Inertia (I_g) = 0.03 in⁴
 Area Gross (A_g) = 3.33 in²
 Radius of Gyration (r_s) = 0.098 in²

λ = 0.116307

Check:

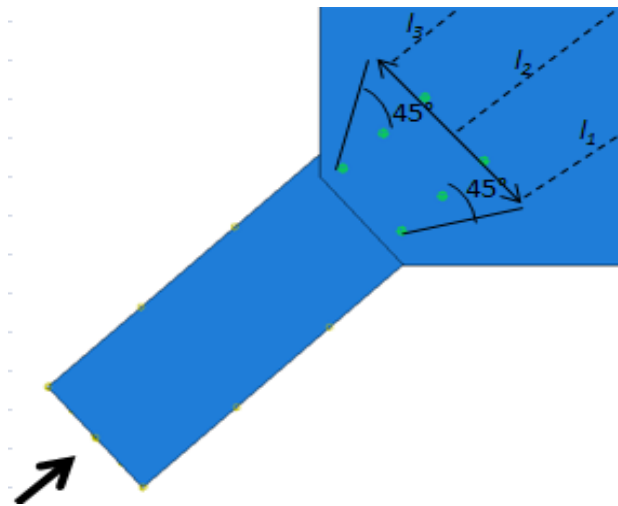
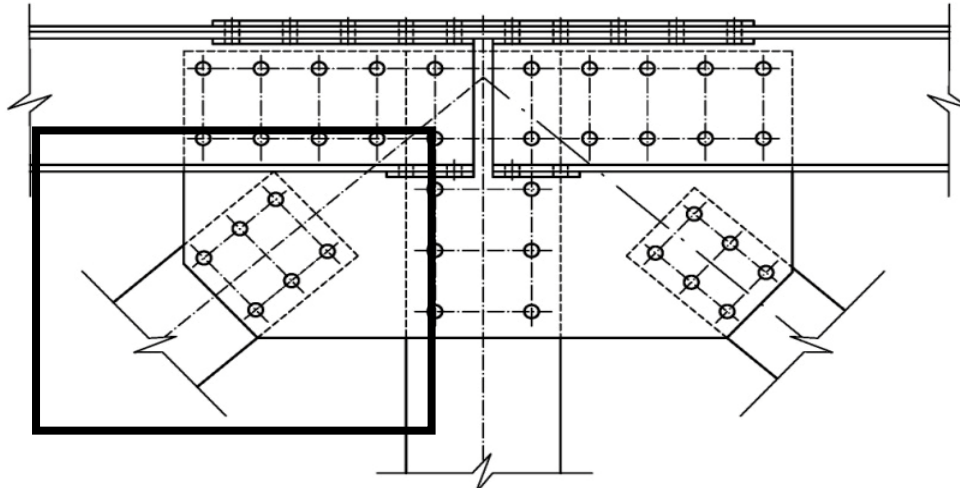
λ = 0.116 ≤ 2.25

P_n = .66^λ F_y A_g

P_n = 209.596 kips

Example for the Yoo Method (Original Case)

Compression at Element D-9 (J-6 Connection)



Hand Calculations (Original Case)(See Section 6.9.4.1 AASHTO):

Model Input Data:

Whitmore Effective Width (W) = 14 in
 Effective Length Factor (K) (See Table) 0.65
 Yield Stress (F_y) = 33 ksi
 Modulus of Elasticity (E) = 29000 ksi

	(a)	(b)	(c)	(d)	(e)	(f)
Buckled shape						
Theoretical K value	0.5	0.7	1.0	1.0	2.0	2.0
Design K value	0.65	0.80	1.0	1.2	2.1	2.0

Calculations:

$$\lambda = \left(\frac{kL}{r_s \pi}\right)^2 \frac{F_y}{E}$$

L = Average Unbraced Length (l₁, l₂, l₃) = 4.81 in
 Moment of Inertia (I_g) = 0.05 in⁴
 Area Gross (A_g) = 4.77 in²
 Radius of Gyration (r_s) = 0.098 in²

$\lambda = 0.116307$

Check:

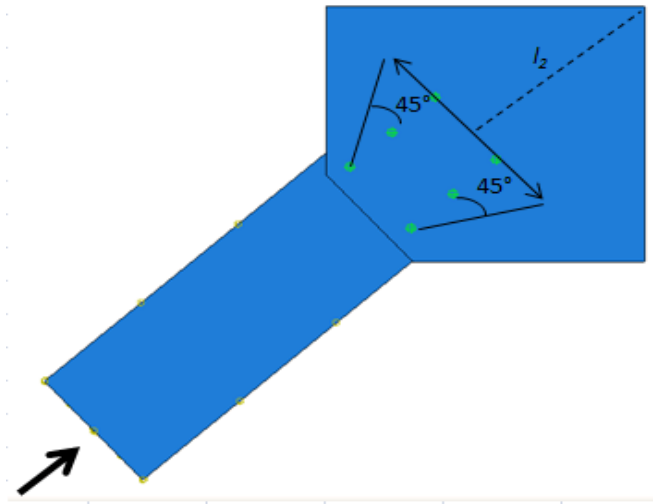
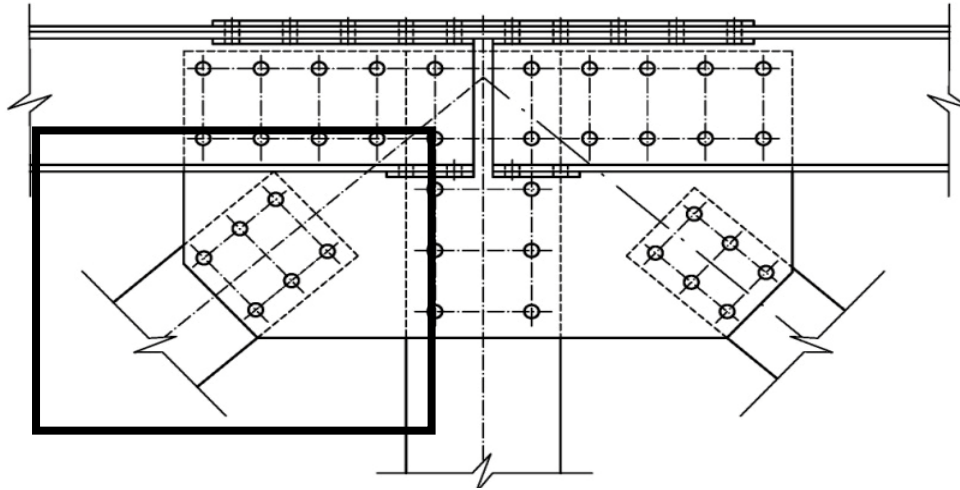
$\lambda = 0.116 \leq 2.25$

$P_n = .66^\lambda F_y A_g$

$P_n = 300.219$ kips

Example for the Modified Thornton Method (Original Case)

Compression at Element D-9 (J-6 Connection)



Hand Calculations (Original Case)(See Section 6.9.4.1 AASHTO):

Model Input Data:

Whitmore Effective Width (W) = 14 in
 Effective Length Factor (K) (See Table) = 0.65
 Yield Stress (F_y) = 33 ksi
 Modulus of Elasticity (E) = 29000 ksi

	(a)	(b)	(c)	(d)	(e)	(f)
Buckled shape						
Theoretical K value	0.5	0.7	1.0	1.0	2.0	2.0
Design K value	0.65	0.80	1.0	1.2	2.1	2.0

Calculations:

$$\lambda = \left(\frac{kL}{r_s \pi} \right)^2 \frac{F_y}{E}$$

L = Unbraced Length l₂ = 7.42 in
 Moment of Inertia (I_g) = 0.05 in⁴
 Area Gross (A_g) = 4.77 in²
 Radius of Gyration (r_s) = 0.098 in

λ = 0.276773

Check:

λ = 0.277 ≤ 2.25

P_n = .66^λ F_y A_g

P_n = 280.85 kips